# From fibre to function: are we accurately representing muscle architecture and performance?

James Charles[1,2†], Roger Kissane[2†], Tatjana Hoehfurtner[3] and Karl T. Bates[2*] 

[1]*Structure and Motion Lab, Comparative Biomedical Sciences, Royal Veterinary College, Hawkshead Lane, Hatfield, Hertfordshire, AL9 7TA, U.K.*
[2]*Department of Musculoskeletal & Ageing Science, Institute of Life Course & Medical Sciences, University of Liverpool, The William Henry Duncan Building, 6 West Derby Street, Liverpool, L7 8TX, U.K.*
[3]*School of Life Sciences, University of Lincoln, Joseph Banks Laboratories, Green Lane, Lincoln, LN6 7DL, U.K.*

## ABSTRACT

The size and arrangement of fibres play a determinate role in the kinetic and energetic performance of muscles. Extrapolations between fibre architecture and performance underpin our understanding of how muscles function and how they are adapted to power specific motions within and across species. Here we provide a synopsis of how this 'fibre to function' paradigm has been applied to understand muscle design, performance and adaptation in animals. Our review highlights the widespread application of the fibre to function paradigm across a diverse breadth of biological disciplines but also reveals a potential and highly prevalent limitation running through past studies. Specifically, we find that quantification of muscle architectural properties is almost universally based on an extremely small number of fibre measurements. Despite the volume of research into muscle properties, across a diverse breadth of research disciplines, the fundamental assumption that a small proportion of fibre measurements can accurately represent the architectural properties of a muscle has never been quantitatively tested. Subsequently, we use a combination of medical imaging, statistical analysis, and physics-based computer simulation to address this issue for the first time. By combining diffusion tensor imaging (DTI) and deterministic fibre tractography we generated a large number of fibre measurements (>3000) rapidly for individual human lower limb muscles. Through statistical subsampling simulations of these measurements, we demonstrate that analysing a small number of fibres ($n < 25$) typically used in previous studies may lead to extremely large errors in the characterisation of overall muscle architectural properties such as mean fibre length and physiological cross-sectional area. Through dynamic musculoskeletal simulations of human walking and jumping, we demonstrate that recovered errors in fibre architecture characterisation have significant implications for quantitative predictions of *in-vivo* dynamics and muscle fibre function within a species. Furthermore, by applying data-subsampling simulations to comparisons of muscle function in humans and chimpanzees, we demonstrate that error magnitudes significantly impact both qualitative and quantitative assessment of muscle specialisation, potentially generating highly erroneous conclusions about the absolute and relative adaption of muscles across species and evolutionary transitions. Our findings have profound implications for how a broad diversity of research fields quantify muscle architecture and interpret muscle function.

*Key words*: biomechanics, muscle, functional morphology, locomotion, modelling, physiology

## CONTENTS

\* Address for correspondence (Tel: +0151 794 9075; E-mail: k.t.bates@liverpool.ac.uk)
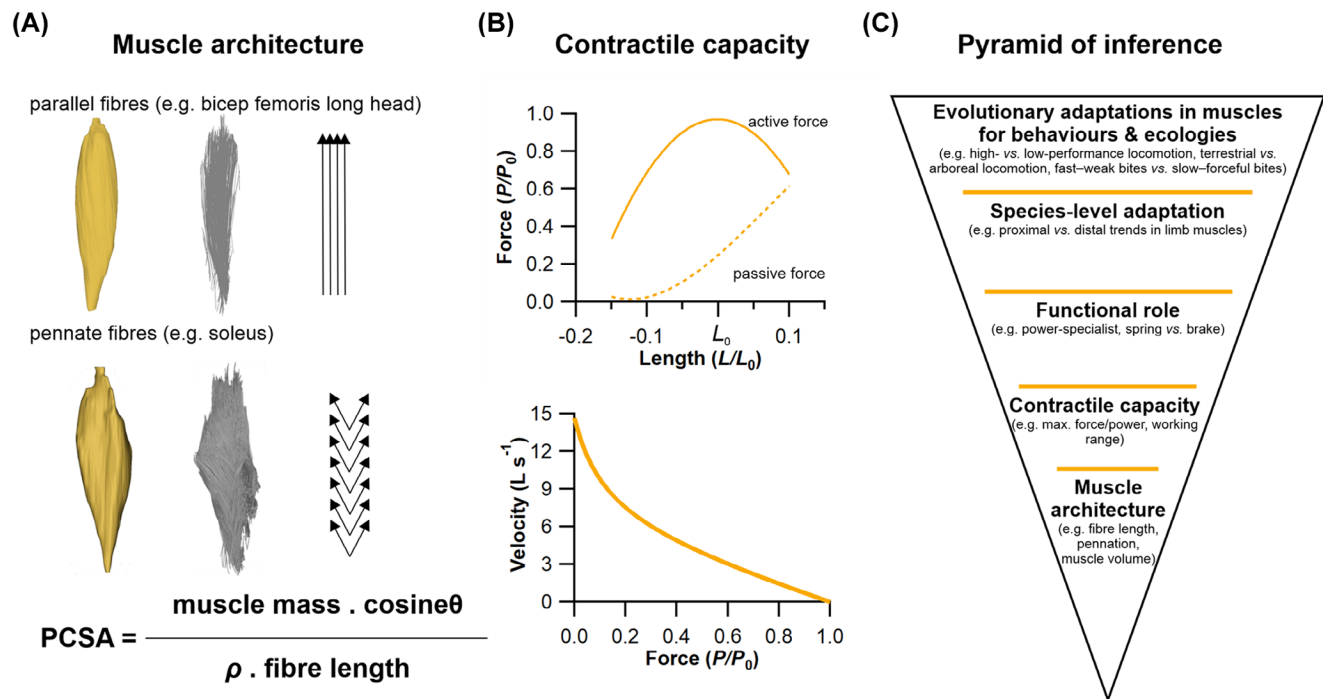† Joint first authors; these authors contributed equally to this work.

# I INTRODUCTION

Almost all animal motion is powered by striated muscle (Alexander, 2003). Skeletal muscle consists of cells known as fibres, which are bound in fascicle bundles usually considered functionally equivalent to a single muscle fibre (Bodine *et al.*, 1982). Since the seminal work of Nobel laureate A.V. Hill in the 1930s (Hill, 1938) it has been recognised that the macroscopic size and arrangement of these fibres, commonly collectively defined as muscle architecture (e.g. Lieber & Fridén, 2000), play a pivotal role in determining how a muscle functions. This functional capacity can be simplistically quantified using data on gross fibre properties through the calculation of its physiological cross-sectional area (PCSA), which is directly proportional to a muscle's maximum force-generating capacity (Lieber & Fridén, 2000) (Fig. 1A), as well as through more complex studies into relationships between the contractile force, length and velocities of its fibres (Luff, 1981) (Fig. 1B). With regard to the macroscopic arrangement of muscle fibres, different muscle structures exist that can directly impact how they function. For instance, fibres can, on a basic level, run in parallel from the origin of a muscle to its insertion (i.e. parallel fibred), or at an angle to the muscle's line of action and attach to an internal tendon or aponeurosis (i.e. pennate fibred) (Fig. 1A). Parallel-fibred muscles, often with long fibre lengths, are thought to be adapted to produce high-velocity contractions, while muscles with shorter and more pennate fibres are adapted for higher force output by virtue of their greater

fibre number (Fig. 1A). As such, the length of these fibres, along with their pennation angle and mass of the muscle belly, are crucial factors to measure accurately when assessing how a muscle functions during a dynamic movement.

The adaptation of skeletal muscle to function in a particular physiological niche is a complex process where remodelling may occur across the entire motor unit [i.e. changes in motor unit firing patterns (Sharples & Miles, 2021), in neuromuscular junction function (Padilla *et al.*, 2021), the muscle metabolome (O'Brien *et al.*, 2021) and in fibre architecture (Taylor *et al.*, 2009)], any or all of which can affect motor function. The mechanisms behind the temporal changes that occur across the central and peripheral nervous systems are much debated, however, it is logical to hypothesise that the varying functional properties afforded by different muscle architectures have been exploited to generate adaptations in muscles to power distinct motions and behaviours. This expectation has led researchers from research fields as diverse physiology (Luff, 1981; De Ruiter, De Haan & Sargeant, 1995; Talmadge *et al.*, 2002), zoology (Payne *et al.*, 2005a; Williams, Payne & Wilson, 2007a; Eng *et al.*, 2008; Williams *et al.*, 2008b; Allen *et al.*, 2010; Paxton *et al.*, 2010, 2014; Wareing *et al.*, 2011; Hudson *et al.*, 2011a,b; Lamas, Main & Hutchinson, 2014; Charles *et al.*, 2016a; Rose *et al.*, 2016a; Rose, Nudds & Codd, 2016b), anthropology (Payne *et al.*, 2006; Myatt, Crompton & Thorpe, 2011; Myatt *et al.*, 2012; O'Neill *et al.*, 2013), clinical and veterinary biomechanics (Steele *et al.*, 2010; Rankin, Rubenson & Hutchinson, 2016; Charles, Cappellari & Hutchinson, 2018; Ellis,

**(A)**
**Muscle architecture**

parallel fibres (e.g. bicep femoris long head)

pennate fibres (e.g. soleus)

$$PCSA = \frac{\text{muscle mass} \cdot \text{cosine}\theta}{\rho \cdot \text{fibre length}}$$

**(B)**
**Contractile capacity**

active force

passive force

**(C)**
**Pyramid of inference**

Evolutionary adaptations in muscles for behaviours & ecologies
(e.g. high- vs. low-performance locomotion, terrestrial vs. arboreal locomotion, fast–weak bites vs. slow–forceful bites)

Species-level adaptation
(e.g. proximal vs. distal trends in limb muscles)

Functional role
(e.g. power-specialist, spring vs. brake)

Contractile capacity
(e.g. max. force/power, working range)

Muscle architecture
(e.g. fibre length, pennation, muscle volume)

**Fig. 1.** The theoretical relationships between muscle fibre architecture, contractile capacity and functional inferences. (A) The architecture of skeletal muscle, also known as the arrangement of a muscle's fibres in relation to its axis of force generation, can be broadly classed as either parallel fibred, with long fibres and little to no pennation angle ($\theta$) or internal tendon/aponeurosis, or pennate, with shorter fibres orientated at an angle to an internal aponeurosis. This architecture can have a substantial impact on a muscle's ability to produce force, which is primarily determined by its physiological cross-sectional area (PCSA), the formulation of which depends on a muscle's mass, fibre length and density ($\rho$; which is considered relatively homogeneous in skeletal muscle). (B) These crucial architectural parameters have a large impact on a muscle's contractile capacity, often quantified by its force–length or force–velocity relationships, where $L$ = length, $L_0$ = optimal length, $P$ = force and $P_0$ = optimal force. (C) This forms the foundation of a pyramid of inference, similar to that of Witmer (1995), of muscle fibre to function, upon which predictions or observations of how a muscle functions in a dynamic context are subsequently used to infer species-level adaptations in a muscle's function, and finally to generate hypotheses surrounding potential adaptations of a muscle across species spanning major evolutionary and/or ecological transitions.

Rankin & Hutchinson, 2018; Stark et al., 2021), dentistry (Langenbach & Weijs, 1990), ageing research (Wilkinson, Piasecki & Atherton, 2018), sports and exercise science (Gonzales et al., 2019), biomimetic robotics (Jenkins & Bryant, 2019), and palaeontology (Bates & Schachner, 2012; Bates & Falkingham, 2018) to attempt to quantify the fibre architecture of muscles accurately to understand how they function at the most fundamental level (Luff, 1981; De Ruiter et al., 1995; Talmadge et al., 2002), how they are adapted to power key motions and behaviours that underpin the exploitation of specific ecological niches (Payne et al., 2005a; Carlson, 2006; Myatt et al., 2011; Hudson et al., 2011a,b; Bates & Schachner, 2012; Charles et al., 2016a; Bates & Falkingham, 2018), and how muscle performance can be maintained or improved in disease, dysfunction and sporting contexts (Steele et al., 2010; Wilkinson et al., 2018; Gonzales et al., 2019). This 'fibre to function' paradigm can be conceptualised as a pyramid of inference, similar to that of Witmer (1995), where higher-level interpretations based on the interaction between muscle design and function rest upon the

accurate founding characterisation of fibre architecture (Fig. 1C).

In this review, we provide a synopsis of how this fibre to function paradigm has been applied to understand muscle design, performance and adaptation in animals (Fig. 1C). We also review the different methods used in past studies to measure muscle architecture, with a specific focus on muscle fibre lengths, and briefly discuss the advantages and limitations of each method. As well as highlighting the widespread application of the fibre to function paradigm across a diverse breadth of biological disciplines, our review highlights a potential and highly prevalent limitation running through past studies. Specifically, we find that quantification of muscle architectural properties (fibre lengths, pennation angles and subsequently PCSA) is almost universally based on an extremely small number of fibre measurements. Despite the volume of research into muscle properties, across a diverse breadth of research disciplines, the fundamental assumption that a small proportion of fibre measurements can accurately represent the architectural properties of a muscle has never

been quantitatively tested. It therefore remains unknown whether potential inaccuracies in the representation of architectural properties derived from inadequate sample sizes impacts higher-level interpretations of basic muscle function and how muscles are (or are not) adapted to power specific motions within and across species (Fig. 1C). Herein, we subsequently apply a novel combination of state-of-the-art medical imaging, image and statistical analysis, and physics-based computer simulation of walking and jumping to address these fundamental issues for the first time. Our findings have profound implications for how a broad diversity of research fields quantify muscle architecture and utilise the fibre to function paradigm to interpret adaptive patterns in muscle function.

## II BACKGROUND

### (1) The fibre to function paradigm

As noted above, herein we adopt the definition of muscle architecture of Lieber & Fridén (2000, p. 1647), who described it as the "macroscopic arrangement of muscle fibres." Measurements of muscle architecture, specifically fibre lengths, pennation angles and PCSA, are widely used across a range of biological disciplines to understand functional morphology at different scales. Here we attempt to provide a concise overview of the range of analyses carried out across this extremely broad diversity of research fields by dividing the literature into four artificial but convenient categories. In particular, these categories attempt to capture the diversity of research at different levels of the fibre to function pyramid of inference (Fig. 1C) starting with smaller-scale analyses of the basic contractile behaviour of muscles ('muscle physiology'), followed by comparative studies that seek to quantify adaptive links between muscle architecture across muscles within ('musculoskeletal modelling') and across ('comparative anatomy and zoology') species, and finally high-level analyses of evolutionary adaptations in muscles that may represent key innovations underpinning the exploitation of specific behaviours or ecologies ('evolutionary biomechanics').

### (a) Muscle physiology

Measures of muscle architecture played a key role in determining some of the fundamental or qualitative contractile behaviours of muscles (Fig. 1A, B). At the base of the fibre to function pyramid of inference (Fig. 1C) it has been commonplace for measures of muscle architecture to be combined with other data (e.g. *in-vivo* contractile behaviour) to provide detailed assessments of the physiological and mechanical performance of muscles. In human muscles, for instance, Wickiewicz *et al.* (1984) tested a commonly used model of muscle dynamics (Hill, 1938) by relating the torque produced by specific lower limb muscle groups to the contraction velocity at which these torques were produced.

The experimental data showed a close match to the theoretical predictions, and the relationships between their measurements of fibre length and PCSA and these torque–velocity relationships indicated that these architectural parameters have a substantial influence on muscle contractile dynamics (Wickiewicz *et al.*, 1984).

Beyond this and a few other studies in humans (Barrett, 1962; Reeves & Narici, 2003), the majority of work into the relationships between muscle architecture, physiology and contractile capacity has been carried out in *ex vivo* experiments of rodent hindlimb muscles (Close, 1969; Baker & Hall-Craggs, 1978; Crow & Kushmerick, 1982; Roy *et al.*, 1985; De Ruiter *et al.*, 1995; James, Altringham & Goldspink, 1995; Askew & Marsh, 1997; Kissane, Egginton & Askew, 2018), and to a lesser extent, other animals (Rack & Westbury, 1969; Close, 1972; Loeb *et al.*, 1987; Lombardi & Piazzesi, 1990; Lieber & Brown, 1992; Pate *et al.*, 1995; Pellegrino *et al.*, 2003; Butcher *et al.*, 2010). For example, studies into the soleus (SOL) and extensor digitorum longus (EDL) muscles of the mouse found that power output can be increased by increasing the duration of shortening instead of increasing contractile velocity (Askew & Marsh, 1997) and that the cost of maintaining a tetanic contraction within fast-twitch muscle fibres is three times greater than in slow-twitch fibres, although this difference decreases to around 50% after 12 s of stimulation (Crow & Kushmerick, 1982). In rat muscles, Kissane *et al.* (2018) found a regional variation in mechanical performance and resistance fatigue in the EDL, suggesting that a differential recruitment pattern of these regions is possible during locomotion, while Roy *et al.* (1985) showed that overstimulation of the ankle plantarflexor muscles leads to increased muscle mass and proportion of slow-twitch muscle fibres, however these responses are ultimately governed by regional variation in fibre type and structure. Measures of muscle architectural properties were a key component of these analyses of contractile behaviour.

In other animals, Butcher *et al.* (2010) found strong relationships between the *in vivo* contractile behaviour of both the deep and superficial digital flexor of horses and their architecture (fibre lengths and pennation angle) and physiology and suggested that architecture may in fact have a greater influence on muscle function during locomotion than, for example, fibre type. Additionally, Lieber & Brown (1992) and Lieber & Shoemaker (1992) studied the relationships between sarcomere length and joint angles in the hindlimb muscles of frogs, which reflect the interaction between fibre length (or sarcomere number) and muscle moment arm. They found a high degree of variability in fibre length to moment arm ratio amongst the studied muscles, even within functional groups, suggesting that the lengths at which muscles produce their optimal force, and therefore their relative contribution to overall joint torques, is disparate even within muscles with a similar functional role.

Overall, these studies on isolated fibres or muscles, which rely heavily on the accurate characterisation of muscle architecture, have collectively provided a link between architecture, physiology and function which has underpinned

subsequent interpretations and predictions of muscle function on whole-system, within-species as well as cross-species scales.

## (b) Musculoskeletal modelling

Moving up the fibre to function pyramid of inference (Fig. 1C), musculoskeletal models are widely used to integrate measures of the architecture of individual muscles with experimental motion data to assess variations in muscle function and their absolute and relative contribution to a particular behaviour or movement task. In other words, such approaches examine the varying functional roles of muscles within a species and how disparate architectures within a structure (e.g. a limb) might facilitate efficient motion. These models provide a unique means to predict dynamic muscle functional parameters that are hard or often impossible to measure with purely experimental methods (Damsgaard et al., 2006; Seth et al., 2018).

Musculoskeletal models are computational representations of bone geometries, joint morphologies, musculotendon unit (MTU) attachments and force-generating properties. In human biomechanics, these models have traditionally been generic (constructed by merging anatomical data from multiple individuals, often cadavers) and subsequently scaled to match the anthropometry of a certain individual or participant in an experimental gait study (Arnold et al., 2010; Rajagopal et al., 2016). Such models have been used in clinical contexts to, for example, predict the muscle forces involved in crouch gait in children with cerebral palsy (Steele et al., 2012), to investigate contact forces at the knee in osteoarthritic patients (Richards et al., 2018) and to optimise the design of lower limb assistive devices such as prosthetics and exoskeletons through the prediction of muscle activation patterns and functions (Grabke, Masani & Andrysek, 2019). In sporting contexts, the mechanisms behind injuries (Bulat et al., 2019), individual muscle mechanics during sprinting (Schache et al., 2012) and the optimisation of strength training regimes (Plüss et al., 2018) have all been studied with these generic musculoskeletal models.

However, recent bodies of work have begun to develop optimised frameworks for developing accurate subject-specific models, where medical imaging techniques such as magnetic resonance imaging (MRI) or computed tomography (CT) are used in combination with model building tools such as NMSBuilder (Valente et al., 2017) to create models containing the musculoskeletal geometry and MTU force-generating properties from a specific individual (Charles et al., 2020). These models have been used to generate personalised predictions of anterior cruciate ligament forces during walking (Charles, Fu & Anderst, 2021) and to investigate knee contact forces after total knee arthroplasty (Hosseini Nasab et al., 2020).

Musculoskeletal models have also become a valuable tool to predict muscle dynamic behaviour in various animal species. These models can provide valuable insights into the muscle dynamics of species that are too small, large or rare to study extensively with in vivo methods. For instance, models of a mouse (Charles et al., 2018) and ostrich (Struthio camelus) (Rankin et al., 2016) constructed through medical imaging and manual dissection experiments to gather muscle architecture data (fibre lengths, pennation angles, and PCSAs), predicted that the lower limbs of small non-cursorial mammals may not possess the muscle adaptations for energetically efficient locomotion seen in larger vertebrates (i.e. a proximo-distal gradient of muscle function; Charles et al., 2018), while larger straighter limbed species likely make greater use of elastic energy storage in the distal hindlimb tendons to optimise locomotor economy (Rankin et al., 2016). Additionally, more complex predictive simulations have been used to predict the potential jumping performance of the tinamou (Eudromia elegans) (Bishop et al., 2021a). This work suggested that the strength of the distal lower limb muscles in this generalised bird are crucial in optimising jump height. Similar models have been used to examine muscular contributions to maximum bite force in a diverse array of animals (Curtis et al., 2010; Bates et al., 2010b; Bates & Falkingham, 2012; Watson et al., 2014; Broyde et al., 2021).

However, whether scaled-generic or subject-specific, human or non-human, how accurately these models reflect the dynamics of an individual is often dictated in part by the accuracy of the muscle architecture data that inform the dynamic behaviour of the MTUs within them. Indeed, various studies that have investigated the sensitivity of functional predictions from musculoskeletal measurements to changes in MTU force-generating properties have shown that fibre length is a particularly crucial parameter to measure accurately (Curtis et al., 2010; Bates et al., 2010b; Bates & Falkingham, 2012; Groning et al., 2013; Charles et al., 2016b, 2020; Broyde et al., 2021). Indeed, notable improvements in certain model outputs (e.g. maximal muscle torques) have been demonstrated when using subject-specific muscle architecture (fibre lengths, pennation angles, and PCSAs) data in musculoskeletal models (Charles et al., 2020) (Fig. 2). This study also highlighted the high sensitivity of musculoskeletal model outputs to their input values as well as, perhaps most significantly, the need to measure fibre lengths accurately to generate more reliable predictions of muscle functional performance.

## (c) Comparative anatomy and zoology

Moving beyond studies of individual species, muscle architecture data has been used to make higher level inferences about adaptations and constraints in muscle anatomy and function across species (Fig. 1C). The approach of linking similarities and differences in muscle architecture to behavioural and ecological specialisations across species is common in studies of locomotion (Anapol & Gray, 2003; Crook et al., 2008; Hudson et al., 2011a,b; Allen et al., 2014; Paxton et al., 2014; Rosin & Nyakatura, 2017; Bohmer et al., 2018, 2019; Leischner et al., 2018; Bribiesca-Contreras, Parslew & Sellers, 2019; Nyakatura et al., 2019) and mastication (Herrel et al., 2008; Taylor et al., 2009; Santana, Dumont &
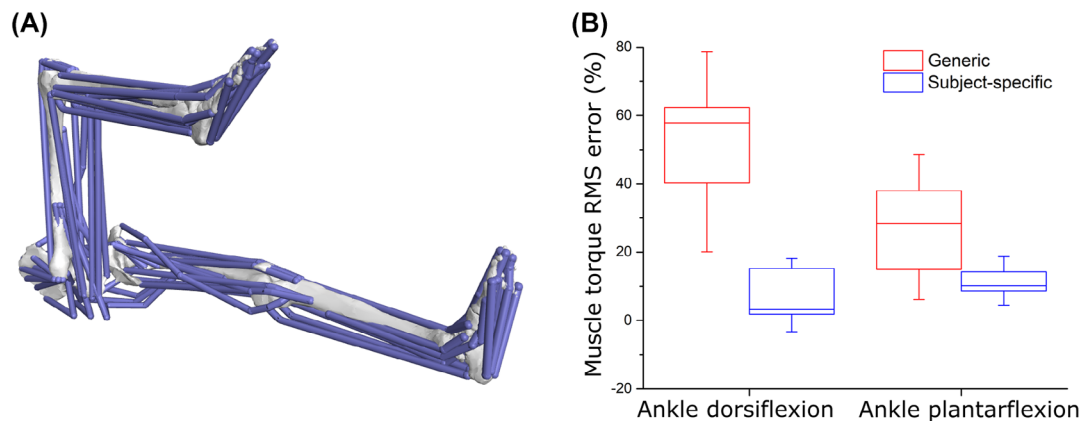
**Fig. 2.** The advantages of subject-specific muscle architecture for predicting muscle functional performance. (A) In a recent study, Charles *et al.* (2020) created 10 subject-specific lower limb musculoskeletal models which included individualised muscle architecture data obtained from medical imaging. Here, the accuracy of muscle torques around the hip, knee and ankle joints predicted from these models were compared to those predicted from the same models containing generic data from elderly cadaveric specimens. (B) The root mean squared (RMS) errors of the outputs from the subject-specific models were substantially lower than those from the generic models around all joints and through all movements tested, highlighting the importance of subject-specific muscle architecture to reflect *in vivo* muscle functional capacity accurately (B).

Davis, 2010; Becerra *et al.*, 2011; Perry, Hartstone-Rose & Wall, 2011; Hartstone-Rose, Perry & Morrow, 2012; Ginot *et al.*, 2018; Hartstone-Rose *et al.*, 2018; Meyers, Nishikawa & Herrel, 2018; Hartstone-Rose, Hertzig & Dickinson, 2019), but has been less frequently pursued in the axial system [for examples see Webster, Hudson & Channon (2014) and Cuff *et al.* (2016a)].

In locomotor studies, analyses of muscular adaptations of species capable of high-performance behaviours are particularly commonplace (Smith *et al.*, 2006; Williams *et al.*, 2007a, 2008a,b; Crook *et al.*, 2008; Lamas *et al.*, 2014), and provide insights into how feats such as exceptional running speeds are achieved by different animals. For example, Hudson *et al.* (2011a,b) explored the hypothesis that faster maximum running speeds in the cheetah (*Acinonyx jubatus*) *versus* the greyhound might be explained by differences in limb extensor muscle properties, including architectural parameters like fibre length, pennation angle, and PCSA. However, surprisingly, they found that while the hip extensor muscles of the cheetah have architectures and moment arms suitable for producing large joint torques, they were not systematically more powerful than in the greyhound. They suggest instead that the exceptional locomotor performance of the cheetah might be better explained anatomically by a range of skeletal features and functionally through greater power amplification generated through flexion–extension of the vertebral column (Hudson *et al.*, 2011a,b).

However, ecomorphological studies of muscle architecture in limbs are not restricted to celebrated high-performance animals. For example, a number of studies have examined the nature of functional modifications seen in limb muscles to facilitate flight (Bribiesca-Contreras *et al.*, 2019), arboreality (Anapol & Gray, 2003; Taverne *et al.*, 2018) and fossoriality (Nyakatura *et al.*, 2019). Allen *et al.* (2014)

compared both fore- and hind limb muscle architecture in Crocodylidae and Alligatoridae to assess the role it may play in the use of asymmetrical gaits in the former group. Based on this comparison, they hypothesise that relatively longer muscle fascicles and smaller PCSAs may facilitate asymmetrical gaits in Crocodylidae by enabling large, rapid limb motions (Allen *et al.*, 2014). Interestingly, these authors also note diverging ontogenetic trends in muscle architecture within these two groups. Ontogenetic changes in muscle architecture have also been studied in a range of other species [e.g. emu *Dromaius novaehollandiae* (Lamas *et al.*, 2014); ostrich (Channon *et al.*, 2019); eastern cottontail rabbit *Sylvilagus floridanus* (Butcher *et al.*, 2019); rat *Rattus norvegicus domestica* (Woittiez *et al.*, 1986)], including analyses of the contribution of differences in muscle properties to disparate gait, energetics and maximal performance in male *versus* female chickens across sexual maturity (Rose *et al.*, 2016a,b).

Adaptive changes in muscle architecture have also been studied in a range of other selectively bred animals. Webster *et al.* (2014) recovered differences in the architecture of the epiaxial musculature of Staffordshire bull terriers and greyhounds, which appeared to be functionally adaptive to their selective breeding for physical combat *versus* high-speed performance. Additionally, the impact of selective breeding practices in the meat industry on muscle architecture has been studied in chickens (Paxton *et al.*, 2010, 2014), where a decline in relative maximal force-generating capacity in meat-bred chickens relative to junglefowl (*Gallus sonneratii*) has been reported and hypothesised to contribute significantly to reduced locomotor performance in these domesticated breeds (Paxton *et al.*, 2010). Taylor, Vinyard & Payseur (2008) (see also Vinyard & Payseur, 2008) used selectively bred strains of mice to investigate plasticity and heritability in the architecture (fibre lengths, pennation angles, and

PCSAs) of jaw-closing muscles and correlated this with functional metrics such as maximum gape angle.

Comparative studies have also examined allometric patterns in muscle architecture, and the links between maximal
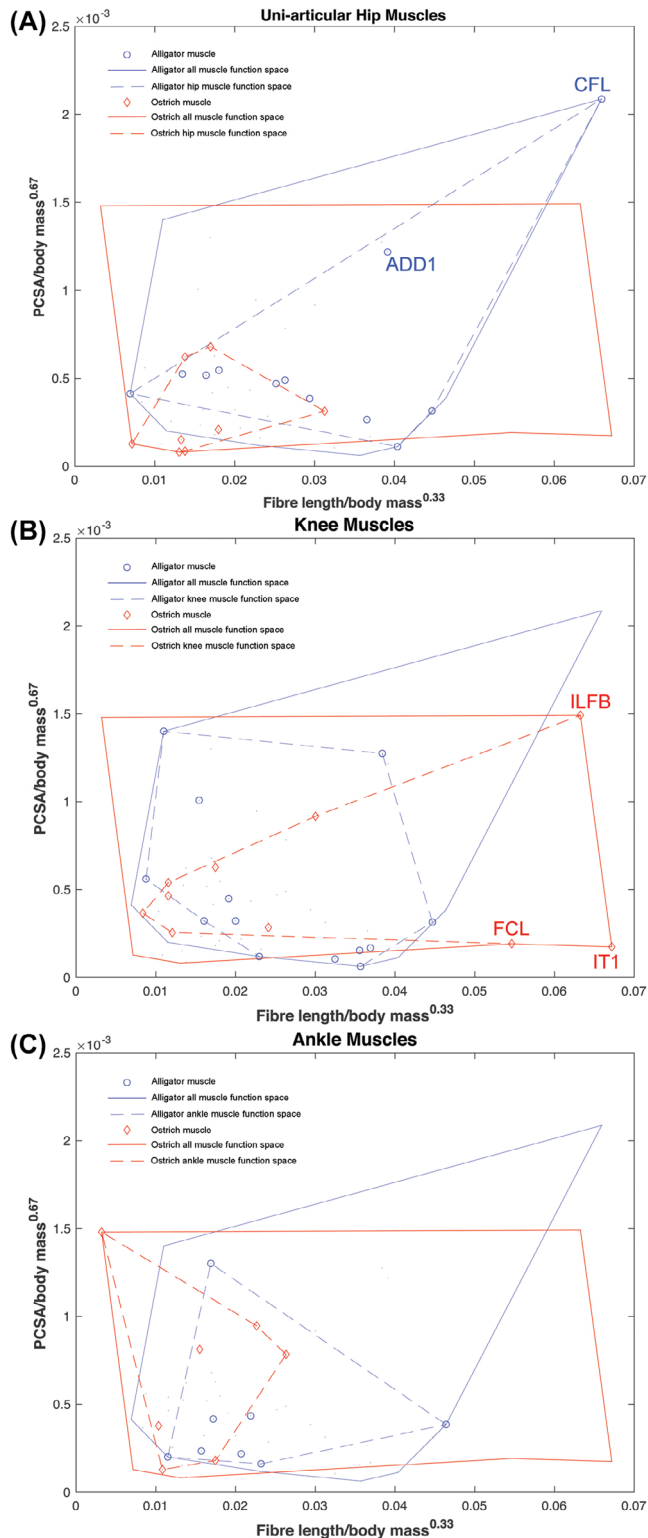


force-generating capacity and size-related changes in locomotor performance. Alexander *et al.* (1981) measured limb muscle masses and fibre lengths (and other properties) in a large sample of mammals, ranging in body size from shrews to elephants. While finding some statistical support for isometric scaling in muscle properties, these authors highlighted potentially important adaptive differences in taxonomic and ecological groups with different locomotor repertoires (Alexander *et al.*, 1981). By contrast, Maloiy *et al.* (1979) carried out a similar study of hind limb muscles in terrestrial birds and generally found allometric patterns consistent with elastic similarity, but noted wide confidence intervals in their regression analyses.

### (d) Evolutionary biomechanics

The use of muscle architecture data in evolutionary and palaeontological studies of functional morphology and biomechanics fall broadly into one of two categories; comparative studies that use measured data from extant taxa to infer evolutionary changes in muscle properties and functions in extinct lineages; and biomechanical simulations of function and behaviours in fossil taxa.

The rarity of soft tissue preservation in the fossil record makes reconstructing the form and function of extinct vertebrates a challenging practice and largely restricts morphological analyses to the most durable skeletal materials (i.e. bone). The Extant Phylogenetic Bracket (EPB) approach was proposed by Witmer (1995) as a systematic means of inferring soft tissue features in extinct taxa and has been widely employed by researchers interested in understanding functional transitions documented in the fossil record. Stated explicitly, the development of soft tissue attributes in extinct taxa is judged by the presence of the same features in extant outgroups that phylogenetically bracket the fossil taxon of interest (Witmer, 1995). The EPB principle has also been

**Fig. 3.** The concept of functional morphospace to examine muscle architectural functional specialisations. By relating the fibre length to the physiological cross-sectional area (PCSA) of a muscle, it can be classified as either force specialised (short fibres, high PCSA), displacement specialised (long fibres, low PCSA), or power specialised (moderate to long fibres, moderate to high PCSA). Bates & Schachner (2012) found that the hip muscles of the alligator *Alligator mississippiensis* occupy a wider area of functional morphospace, and thus contain a wider range of architectural specialisations, than those in the ostrich *Struthio camelus*, (A). This pattern is reversed at the knee joint however, with the ostrich muscles displaying more adaptations for power and displacement specialisation than the alligator muscles (B). At the ankle, muscles are more force specialised in the ostrich compared to the more displacement specialised muscles of the alligator (C). Overall, these differences hint at possible adaptations of muscle architecture throughout evolutionary lineages. ADD, adductor femoris; CFL, caudofemoralis longus; FCL, flexor cruris lateralis; ILFB, iliofibularis; IT, iliotibialis.

used to gain insight into evolutionary changes in muscle architecture by quantitively comparing measured muscle properties in the first or most immediate outgroups of the fossil group of interest. For example, the differences in muscle architecture measured in representatives of extant crocodilians and birds have been used to constrain changes that might have occurred during the evolution of bipedalism in bird-line dinosaurs (Bates & Schachner, 2012). This work used the muscle functional morphospace concept to examine specialisations in the architecture (fibre lengths and PCSAs specifically) of key muscles that might underpin the way extant groups habitually move (Fig. 3). The data highlights, among other things, that hip-driven locomotion in the alligator *Alligator mississippiensis* is associated with hip muscles occupying a much larger area of total functional morphospace than those of the ostrich (Fig. 3A), which uses considerably less hip motion and powers the stride predominantly from the knee and ankle (Gatesy, 1990, 1991a,b). Particularly notable among hip muscles are the much greater specialisation for power (long fibres and large PCSAs) in the caudofemoralis longus (CFL) and adductor femoris muscles (particularly ADD1) in the alligator, which play prominent roles in propulsion and three-dimensional limb control in the abducted limb postures used by crocodilians (Gatesy, 1991a; Hutchinson & Gatesy, 2000). This pattern of muscle specialisation is reversed at the knee joint, with the ostrich knee muscles occupying a greater area of functional morphospace and possessing a number of muscles with much higher levels of power and displacement (long fibres) specialisation than in the alligator (Fig. 3B). This is again consistent with the knee showing a greater range of motion and contribution to overall stride length during *in-vivo* behaviours in birds compared to crocodilians (Gatesy, 1990, 1991a,b). Most ankle muscles show relatively weak specialisation in both the ostrich and alligator (Fig. 3C). However, the individual muscles and overall ankle muscle functional morphospace are noticeably more force specialised in the ostrich compared to the more general (and some instances extreme) displacement specialist architectures seen in the alligator (Fig. 3C). Greater force specialisation in the ostrich may be associated with digitigrade posture and an enhanced role of tendons in modulating MTU length change *in vivo*, such that ostriches (and other birds; Roberts *et al.*, 1997) are able to generate greater stance-phase mechanical power *via* the storage and release of elastic energy from the tendons of ankle muscles (Rubenson *et al.*, 2011). Collectively, these relationships between muscle specialisation and joint contributions to gait provide qualitative insights into muscular adaptations that might have occurred during the evolution of bipedalism in dinosaurs (Hutchinson & Gatesy, 2000; Bates & Schachner, 2012; Allen, Kilbourne & Hutchinson, 2021). For example, basal theropod dinosaurs likely retained large (power specialised) tailed-based femoral retractors similar to crocodilians, but as digitigrade bipeds may have already utilised more force-specialised musculature and amplified elastic energy generation through tendons at the ankle (Bates & Schachner, 2012). Similar hypotheses regarding evolutionary changes in

muscle mechanics in early mammals (Fahn-Lai, Biewener & Pierce, 2020) and hominids (Payne *et al.*, 2006; Strait *et al.*, 2009; Myatt *et al.*, 2011, 2012) have also been made based on comparisons of muscle architecture and function in EPB groups.

With the more widespread availability and affordability of digitisation approaches over the past two decades (Bates *et al.*, 2010a; Falkingham, 2012), biomechanical modelling and simulation has become an increasingly popular means of quantitatively testing hypotheses about the functional capabilities of extinct animals, and how morphological change seen in the fossil record translates to changing mechanical performance. The major benefit of these models is the ability to derive absolute quantitative predictions of performance (e.g. bite force, running speed, metabolic costs of movement) by analysing all the major causative factors that underpin animal motion. As such, they require numerical values for anatomical and physiological factors that govern muscle force production, including muscle architecture (Fig. 1A, B). For this reason, palaeobiologists have used a variety of approaches and assumptions to derive quantitative values for muscle architecture (fibre lengths, pennation angles, and PCSAs) in biomechanical models of fossil taxa.

A popular approach, particularly in biomechanical evaluations of skull mechanics in extinct taxa, has been to reconstruct all muscles as parallel fibred with fibre lengths equal to the total length of the MTU at a specific length or joint posture (Button, Barrett & Rayfield, 2016; Gignac & Erickson, 2017; Adams *et al.*, 2019; Chambi-Trowell *et al.*, 2020), and subsequently use these values in the calculation of PCSA (Fig. 1A). Other studies have also assumed uniform parallel-fibre architecture across muscles but have used a variety of different data from extant animals to derive mean fibre length for their reconstructed muscles in extinct taxa. For example, in an analysis of limb biomechanics in fossil theropod dinosaurs, Hutchinson (2004b) set fibre lengths as the same proportion of the relevant segment length (thigh, shank etc.) measured in extant EPB taxa. Another approach, popular in studies of hominid evolution, is to scale fibre lengths (e.g. by body mass) directly from measured values in closely related extant taxa like humans or chimpanzees (Sellers *et al.*, 2005; Strait *et al.*, 2009, 2010; Crompton *et al.*, 2012). Other studies have set fibre lengths to the proportion, or proportions, of total MTU measured in extant animals, and additionally examined the functional consequences of assuming parallel-fibred *versus* pennate muscle architecture on hypothesis testing (Bates & Falkingham, 2012, 2018; Cost *et al.*, 2020).

Conceptual or theoretical models of animal movement also require numerical values for muscle architecture, and given the generalised nature of these models (i.e. not specific to any particular real animal) researchers have often used functional principles based on the expected force–length characteristics of muscles (Fig. 1B) to derive values for fibre lengths. For example, Alexander (1995) used a generalised model to investigate the over-arching mechanics of bipedal jumping and set resting fibre lengths as a proportion of the

length change that each muscle would be expected to experience. Sellers *et al.* (2009) extended the same functional rationale to their reconstruction of limb muscles in the ornithischian dinosaur *Edmontosaurus*. Specifically, these authors set muscle fibre lengths to the value of MTU length change experienced when joints were rotated through their maximum flexion–extension ranges. They considered this a means of objectively generating fairly optimal fibre lengths for muscles since vertebrate muscles are typically able to generate force from approximately 60% to 160% of their resting length and would therefore be expected to work within this range *in vivo* (Fig. 1B). These authors later tested this assumption by examining the relationships between measured fibre length and total MTU length change in chimpanzees, greyhounds, ostrich and horses (Sellers *et al.*, 2013). Overall, they found a modal value of between 0.4 and 0.6 for MTU extension/fibre length in these four species but noted that many muscles appeared to fall above and below this range (Sellers *et al.*, 2013). This study was later extended by Bishop *et al.* (2021b) who carried out a similar assessment of the hind limb muscles of the tinamou and similarly suggested that simply setting fibre length as directly equal to MTU length change may not be strictly appropriate for most muscles.

The obvious implication of these different subjective choices about muscle architecture reconstruction is that longer fibre lengths and parallel-fibred architecture will lead to lower maximal isometric forces (by yielding lower PCSAs; Fig. 1A) and different force–length and force–velocity profiles to muscles reconstructed with shorter fibre lengths and pennate architectures (Fig. 1B). However, despite the obvious impact on muscle force-generating capacities, relatively few studies have examined how these subjective choices impact biomechanical predictions for extinct taxa (Bates *et al.*, 2010b; Bates & Falkingham, 2012, 2018; Cost *et al.*, 2020; Broyde *et al.*, 2021). Where sensitivity analyses or direct comparisons of different approaches to architecture reconstruction have been carried out, they have tended to suggest the potential for relatively large uncertainty in predictions for parameters like muscle and bite force (Bates & Falkingham, 2012, 2018) and bone stress (Cost *et al.*, 2020) within individual extinct species, which might limit the capacity of models to predict evolutionary patterns correctly (Broyde *et al.*, 2021). The clear implication of these studies is a need to understand, through quantitative data, how muscle architecture is adaptively tuned in extant animals to better inform soft tissue and biomechanical reconstructions of fossil taxa (Bates & Falkingham, 2018; Broyde *et al.*, 2021; Bishop *et al.*, 2021b).

## (2) Methods of measuring muscle architecture

Muscle architecture, as defined by (Lieber & Fridén, 2000), can be gathered from individual muscles from a variety of species with two primary methods: traditional manual dissection of cadaveric specimens, or newer *in situ* or *in vivo* medical imaging-based techniques, which each have distinct advantages and limitations.

### (a) Manual dissection

Manual dissection has been the most common method to study anatomical form and function for over 1000 years, with pioneering anatomists such as Leonardo da Vinci using this approach as the foundation for detailed drawings of the human body. In more recent years, these dissection-based approaches have been the basis of many seminal research papers detailing the architecture of human (Wickiewicz *et al.*, 1983; Ward *et al.*, 2009) and animal muscles (Sacks & Roy, 1982; Lieber & Blevins, 1989), as well as developing novel predictive models of how muscle fibres produce force (Hill, 1938; Zajac, 1989).

The process of measuring these muscle data from both human and animal cadaveric specimens can be broadly sub-divided into two approaches: fresh *versus* fixed dissections. Fresh dissection typically involves removal of individual muscles from fresh/unfrozen specimens, followed by direct and immediate manual measurement of fibre properties by the investigator (e.g. using a ruler or callipers). Fixed dissection measurement typically involves a standardised set of procedures described by Sacks & Roy (1982) and Lieber, Fazeli & Botte (1990). Initially, the specimen is often immersed in a phosphate-buffered formal saline solution to fix the muscle tissue. During this process, the joints can be locked at certain angles to ensure that any data measured from the muscles is specific to a physiologically appropriate pose. After fixation, the muscle or muscles of interest are carefully removed from the specimen and, if necessary, stored in phosphate-buffered saline until measurement. Each muscle is then weighed to determine muscle mass ($M_m$) and measured from origin to insertion to determine total muscle length ($L_m$). Any external tendon is often removed prior to this step. To measure the lengths of individual muscle fascicles (bundles of 5–50 fibres), the muscles are then placed in a sulfuric acid solution partially to digest the connective tissue surrounding the muscle belly and fascicles. After digestion, the pennation angle ($\theta$) of the muscle fibres can be measured from the surface of the muscle; multiple measurements are usually taken from different regions of the muscle (i.e proximal, middle, distal) to generate an average value. Individual muscle fascicles (considered to be functionally equivalent to individual muscle fibres) can then be isolated and measured to estimate muscle fibre length ($L_f$). Similar to $\theta$, these are taken from various regions of the muscle belly to generate an average value. For larger specimens (i.e. humans), these are usually measured using callipers, while for smaller animals the fascicles can be mounted on slides and measured under magnification (Burkholder *et al.*, 1994; Charles *et al.*, 2016a). For human muscles, it is then common to adjust these measured fibre length values to an optimal fibre length to account for any discrepancies between the measured fibre length and the length at which it produces its optimal force. This can be done by measuring the length of the sarcomeres within each extracted fibre bundle through laser diffraction (Lieber *et al.*, 1990), which are then compared to an accepted optimal sarcomere length for skeletal muscle and used to

generate $L_f$' for each muscle. All these data gathered for each muscle are then used to calculate their PCSA (Fig. 1A).

Arguably the principal limitation of these manual approaches is that gathering a large volume of muscle data can be time consuming and doing so in an accurate manner can require a high level of dissection skill. Furthermore, ensuring measurements, particularly of $L_f$ and θ, are taken at either a resting or physiologically appropriate length is difficult (particularly if measuring from unfixed tissue), and there is a high probability of *post-mortem* artefacts or damage to specimens if not stored correctly. For human muscle architecture data, the frequent use of cadavers biases these data towards being mostly obtained from elderly individuals, which somewhat reduces the applicability of the data to the wider population, particularly if the data are being used to infer muscle function in younger individuals.

### (b) Imaging

These limitations of traditional dissection methods to measure muscle architecture, along with advances in technology, have led to the formulation of alternative frameworks to gather these data. These primarily involve using various medical imaging modalities such as ultrasound, MR or CT imaging to visualise muscles *in vivo* or *in situ*, which allows for the non-destructive measurement of crucial muscle architectural properties.

Ultrasound imaging has been used extensively in humans to image the fibre arrangements *in vivo* within prominent muscle groups such as the quadriceps (Seymour *et al.*, 2009; Noorkoiv, Nosaka & Blazevich, 2010) and triceps surae (Barber, Barrett & Lichtwark, 2009; Dick, Biewener & Wakeling, 2017), which have tested assumptions of the Hill-type model of muscle force production (Dick *et al.*, 2017) and investigated the tendency for pennate muscles to optimise θ to produce maximal force, known as 'muscle gearing' (Randhawa, Jackman & Wakeling, 2013). However, despite the low relative cost of ultrasound imaging, the small field of view and ability to only image the more superficial muscles of the musculoskeletal system limit its utility in fully characterising the muscle architecture within an individual.

Recent studies have shown that a combination of MRI sequences can be used to obtain detailed muscle force-generating properties from every muscle within a large field of view in a valid and repeatable way and thus overcomes many of the limitations associated with ultrasound imaging (Bolsterlee, D'Souza & Herbert, 2019; Charles, Moon & Anderst, 2019a; Charles *et al.*, 2020). The most important of these sequences is diffusion tensor imaging (DTI), which images different structures based on the relative diffusion of water through them and therefore allows for the visualisation and measurement of a large number of muscle fibres within a range of muscles (Froeling *et al.*, 2012, 2015; Bolsterlee *et al.*, 2015, 2018, 2019; Damon *et al.*, 2016; Sieben *et al.*, 2016; D'Souza *et al.*, 2019; Charles *et al.*, 2019a). When combined with an anatomical sequence to allow for the measurement of muscle volumes (e.g. T1 turbo spin echo), this MRI-based

framework can be used to gather extensive muscle architecture data from an individual *in vivo* (Charles, Suntaxi & Anderst, 2019b). However, while this framework has been validated for gathering muscle architecture data from healthy human muscle, it is unclear how effectively it could be used to gather similar data from pathological or dysfunctional tissue, which may contain damaged fibres or otherwise disrupt the diffusion of water, which would make the interpretation of such images somewhat unclear. Furthermore, while this methodology could theoretically be applied to other large animals, it is currently unclear how well the approach will scale down to smaller animals.

Instead, several studies have used iodine-based contrast-enhanced CT scanning (also known as diceCT; Gignac *et al.*, 2016) to gather these data from smaller animals. This framework involves submerging a specimen in an iodine potassium-iodide ($I_2KI$) solution for an appropriate amount of time to optimise soft tissue contrast but minimise shrinkage artefacts (Vickerton, Jarvis & Jeffery, 2013) prior to CT or microCT scanning. This staining process enhances the contrast of soft tissue structures thus rendering individual muscles visible in these CT scans, from which various important anatomical variables (muscle volumes and fibre lengths) can be measured (Kupczik *et al.*, 2015). This method has been used to quantify the muscle architecture and musculoskeletal geometry of, among others, the jaw musculature of the crab-eating macaque (*Macaca fascicularis*) (Dickinson, Stark & Kupczik, 2018), the pectoral muscles of the European starling (*Sturnus vulgaris*) (Sullivan *et al.*, 2019), various species of bat (Santana, 2018), as well as the hindlimbs of the mouse (Charles *et al.*, 2016a) and the red-legged running frog (*Phlyctimantis maculatus*) (Collings & Richards, 2019). Some of these frameworks (Dickinson *et al.*, 2018; Sullivan *et al.*, 2019) were able to produce estimates of muscle fibre lengths from imaging alone through a form of digital fibre tracking, which generated a sample size of fibre lengths equivalent to that produced from DTI. However, while diceCT has been successful for investigating the muscle architecture of many small species and specimens, it is limited to *in situ* staining and imaging of cadaveric tissue which has been shown to undergo a potentially substantial degree of shrinkage during the staining process (Vickerton *et al.*, 2013), and the time needed to stain each tissue successfully also reduces its ease of applicability to larger specimens.

Overall, these medical imaging-based methods of measuring muscle architecture hold several advantages compared to dissection methods, including the ability to automate imaging protocols to ensure repeatability both within and across studies within different specimens. The non-destructive nature of these methods also eliminates the possibility of damaging important structures through human error, a common drawback of more manual methods. Additionally, particularly with regard to MR scanning, they are methods that can be used in the context of humans to measure muscle architecture from a wider range of demographics than is possible with dissection methods, including in young, healthy individuals (Charles *et al.*, 2019b, 2020), and theoretically

could be applied in more a comparative sense to rare or endangered animal species from which cadaveric specimens are difficult to obtain. However, it should be noted that these techniques often require the use of often prohibitively expensive equipment. For example, a 3T MRI scanner can cost around $3 million USD to purchase, with additional funds required for infrastructure and maintenance, and so are not as ubiquitously available as other methods. Furthermore, creating and optimising imaging protocols, if needed, can be time-consuming and requires an expert in radiography or medical physics to achieve (particularly for MRI and CT), and is a crucial step in the process given how much the quality of the muscle data gathered from these methods is dependent on the quality of the initial images.

### (c) Sample size

Ultimately, the method chosen to measure muscle architecture (e.g. dissection *versus* medical imaging) will be dictated by the goals of the study and equipment available, accounting (where possible) for the advantages and disadvantages of each method. However, certain experimental considerations apply universally to all methods, with one such important consideration being sample size. Throughout the literature reviewed above, studies have sought to quantify and compare mean values for muscle architectural parameters, such as $L_f$ and $\theta$ (Fig. 1A, B) to make inferences of muscle function and adaptation within and across animals (Fig. 1C). For example, for fibre lengths, this involves measuring a number of fascicles within a muscle belly to generate a single representative value (e.g. a mean fibre length). The fundamental assumption, therefore, is that the sub-sample of individual fibres measured is sufficient in number to characterise the central tendency of fibre lengths within that muscle accurately, and subsequently other gross properties like PCSA.

Here, we surveyed 243 studies into vertebrate skeletal muscle (see online Supporting Information, Table S1) and found that the number of fibres used to generate mean values for architectural properties is usually extremely small (Fig. 4). We did not carry out a systematic review, rather we sought to sample as many papers as possible (prior to 2021) from across the research areas reviewed in the previous sections. Where studies reported the number of fibres measured, only 1.8% measured 250 fibres or more per muscle and only 17.4% used 25–250 measurements per muscle to generate a mean value. Thus the vast majority of studies (more than 80%) characterised muscle architectural properties based on less than 25 fibre measurements, with nearly 40% using 5 fibre measurements or fewer (Fig. 4A). In humans, it has been suggested that large muscles can contain up to ∼400000 fibres (or ∼600 fascicles) (Henriksson-Larsen, Lexell & Sjostrom, 1983; Lexell, Downham & Sjostrom, 1986). Therefore, most studies have derived and analysed mean architectural properties for muscles based on a tiny fraction of the total number of fibres within those muscles (potentially <1% in some cases). It is also notable that of these 243 studies, only three calculated the median value of the initial fibre sample as a

representation of a muscle's fibre length instead of the mean, despite the likelihood that fibre lengths are not normally distributed throughout a muscle (Young, Scott & Loeb, 1993; Schenk *et al.*, 2013; Kupczik *et al.*, 2015).
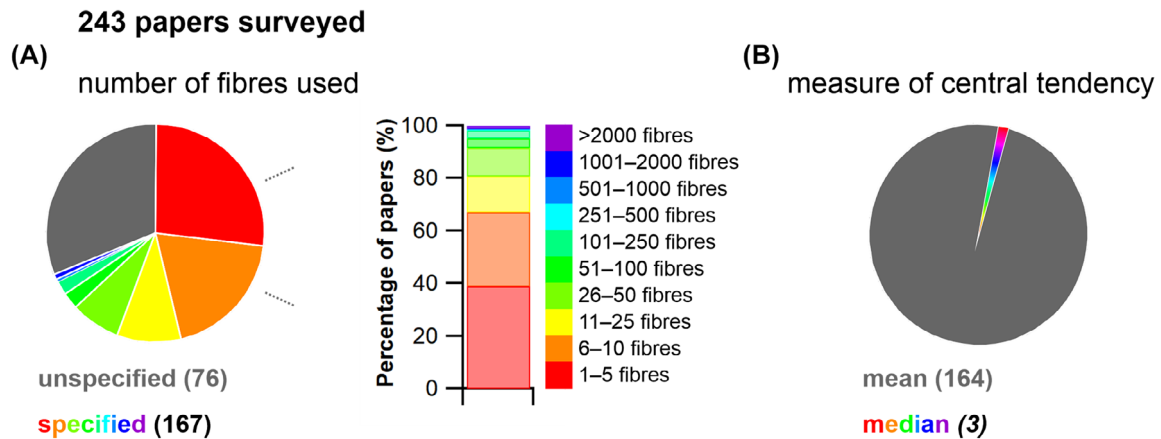
Breaking studies down by method reveals that both automated imaging and manual dissection-based approaches have been used to measure relatively large numbers of fibres per muscle. For example, Rosin & Nyakatura (2017) measured up to 1754 fibres per muscle using manual dissection of fixed muscles. At least two other studies (Kim *et al.*, 2007; Rosatelli, Ravichandiran & Agur, 2008) have taken more than 1000 measurements per muscle using the same manual approaches. On the other hand, it is surprising that approaches based on medical imaging data have not measured such high fibre numbers despite the potential for more rapid measurement using automated imaging tools, with Sullivan *et al.* (2019) and Dickinson *et al.* (2018) measuring a maximum of only 218 and 603 fibres, respectively. In fact, all methodological approaches for measuring muscle architecture have been used to measure only a small number of fibres, with zoological studies utilising fresh manual dissection almost always measuring fewer than 25 fibres per muscle (Table S1).

## III ASSESSING RELIABILITY ACROSS THE FIBRE TO FUNCTION PYRAMID OF INFERENCE

### (1) Framework and hypotheses

Measurements of muscle architecture are widely used across a range of biological disciplines to understand functional morphology at different scales. The near-universal assumption that the mean value of a small proportion of fibre measurements can accurately represent the architectural properties of a muscle (Fig. 4; Table S1) has never been quantitatively tested. It therefore remains unknown whether potential inaccuracies in the representation of architectural properties derived from inadequate sample sizes impacts higher-level interpretations of basic muscle function and how muscles are (or are not) adapted to power specific motions within and across species (Fig. 1C). In other words, it is presently unclear whether much of the biomechanics and muscle physiology literature over the past 80 years has made accurate interpretative leaps from fibre to function when analysing skeletal muscle.

To address these fundamental issues, we apply a novel combination of state-of-the-art medical imaging, image and statistical analysis, and physics-based computer simulation of human walking and jumping (Fig. 5) to quantify the potential errors in fibre length measurements, and the potential impacts of these errors on muscle functional predictions. First, we used DTI and deterministic fibre tractography (Bolsterlee *et al.*, 2019; Charles *et al.*, 2019a) to derive the architectural properties of a sample of human lower limb muscles using a large number of fibre measurements per muscle [approximately two and half times more than the

**243 papers surveyed**

**(A)**
**number of fibres used**



Percentage of papers (%)

>2000 fibres
1001–2000 fibres
501–1000 fibres
251–500 fibres
101–250 fibres
51–100 fibres
26–50 fibres
11–25 fibres
6–10 fibres
1–5 fibres

unspecified (76)
specified (167)

**(B)**
**measure of central tendency**



mean (164)
median *(3)*

**Fig. 4.** A review of the number of fibres per muscle measured to calculate mean architectural properties in 243 published studies. (A) From the studies that reported the number of muscle fibres used to calculate mean fibre length, 80.8% measured fewer than 25 fibres per muscle, with 38.9% measuring 5 fibres or fewer per muscle. Only 1.8% of the papers that reported their totals used over 250 fibres. (B) In addition, 99% of the 243 papers reported the mean fibre length, while only 1% reported the median.
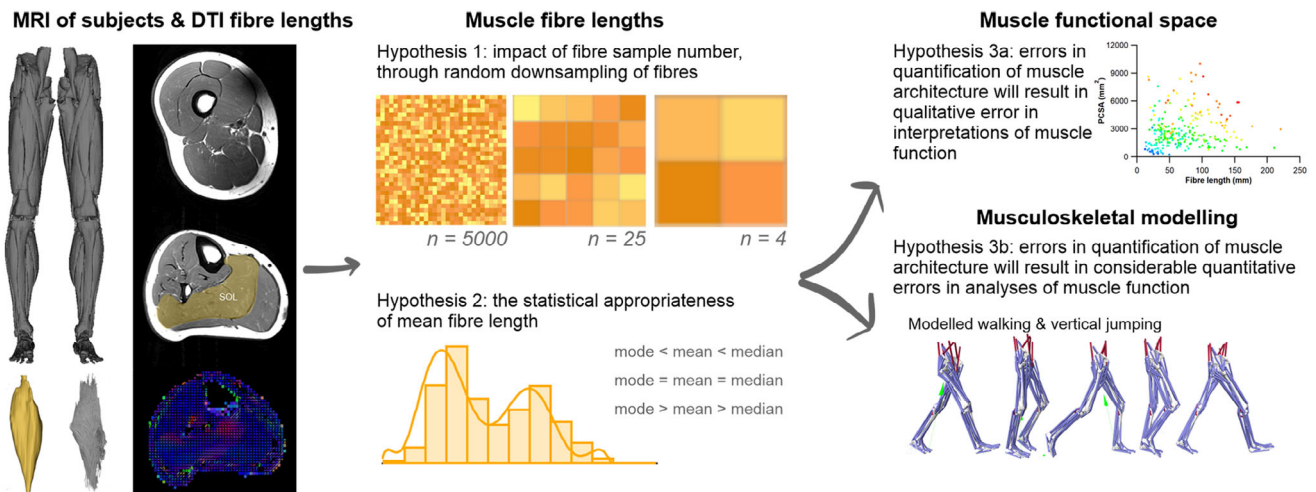


**Fig. 5.** Overview of our experimental approach. T1 magnetic resonance imaging (MRI) was used to generate three-dimensional meshes of 25 muscles of the lower limb of 10 subjects, and diffusion tensor imaging (DTI) was used to generate a sample of up to 5000 fibres from each of these muscles. To address Hypothesis 1, 1000 random subsamples of 5, 10, 50, 100, 250, 500, 1000 and 2000 fibres from the full sample were taken to assess the effect of fibre sample size on calculations of mean muscle fibre length and interpretations of functional specialisations. To address Hypothesis 2, the distributions of fibres within each muscle were assessed to quantify the statistical appropriateness of calculating mean or median fibre lengths to generate a single representative value. The functional implications of these two major assumptions often made during the collection of muscle architecture data, were tested using muscle function plots (Hypothesis 3a) to compare human and chimpanzee muscles, and musculoskeletal modelling and simulations (Hypothesis 3b), where muscle fibre dynamics during walking and jumping movements were predicted, and the potential errors introduced by these assumptions on these output metrics were calculated. PCSA, physiological cross-sectional area; SOL, soleus.

highest used in previous studies (Rosin & Nyakatura, 2017)]. Second, using statistical analysis we determined the central tendency and distribution of fibre lengths and examined its vulnerability to sample size using subsampling simulations. Finally, we quantified the implications of inaccuracies in fibre architectures due to low sample sizes using a combination of dynamic simulations of human walking and jumping (to assess within-species effects) and muscle function plots (to assess across-species effects). We applied these approaches

to test three hypotheses. First (HYP1), we hypothesise that measuring a small number of fibres (e.g. <25) per muscle may result in a substantial error in quantification of the central tendency of fibre architecture (i.e. an inaccurate mean value). Second (HYP2), based on the irregular and complex design of many muscles, as well as some previous muscle architecture studies (Young *et al.*, 1993; Schenk *et al.*, 2013; Kupczik *et al.*, 2015), we theorise that the central tendency of muscle architectural properties is mostly, and perhaps

always, more appropriately represented by the median value, rather than the mean, which has been used in 99% of studies surveyed here (Fig. 4B; Table S1). Finally, our third hypothesis proposes that the errors in the quantification of muscle architecture identified in HYP1 and HYP2 will result in considerable qualitative (HYP3a) and quantitative (HYP3b) error in higher-level interpretations of muscle functional capacity, fibre dynamics and overall interpretations of muscle specialisation (Fig. 4C).

## (2) Methods

Data were gathered from 10 human subjects [Table S2; 5 male, 5 female; mean $\pm$ SD age 29 $\pm$ 3.7 years; body mass 67.9 $\pm$ 9 kg; height 175 $\pm$ 7 cm; body mass index (BMI) 21.9 $\pm$ 1.6 kg m$^{-2}$] who gave informed consent prior to participating in the study in accordance with ethical approval from the University of Liverpool's Central University Research Ethics Committee for Physical Interventions (Reference number: 3757). A previously validated framework (Charles *et al.*, 2020) was used to estimate subject-specific muscle architecture data from 25 muscles of the right lower limb from each subject (Fig. 5A). This involved the use of two MRI sequences: T1-weighted anatomical turbo spin-echo (TSE) to estimate muscle volumes and visualise muscle attachment points, and DTI to estimate muscle $L_f$, $\theta$ and PCSA (see Appendix S1 for sequence parameters and details regarding image analysis and processing). The validity and accuracy of this and similar 3D techniques has been established previously (Kupczik *et al.*, 2015; Bolsterlee *et al.*, 2019; Charles *et al.*, 2019a, 2020), and it carries the advantage of allowing the *in vivo* measurement of a large number of individual fibres (>3000 per muscle). The general framework is described in detail in Appendix S1 and in Charles *et al.* (2020).

### (a) Muscle fibre subsampling

To assess the range of both mean and median fibre length values possible from measuring only a subsample of muscle fibres (HYP1), 1000 random subsamples of 5, 10, 50, 100, 250, 500, 1000 and 2000 fibres from the full initial sample were obtained for each lower limb muscle from each subject (Figs 5B, 6B, C). The ranges of possible mean and median fibre length values obtained from each random subsample were calculated for each subject (Fig. 6B). The 'accuracy' of these values, here reported as these values relative to the 'true' mean and median value (from the full sample of fibres) and expressed as a ratio, were also calculated (Fig. 6C).

### (b) Means versus medians

To test whether fibre lengths were normally distributed within a muscle belly (HYP2), Shapiro–Wilk tests were performed on the post-processed fibre lengths to assess the
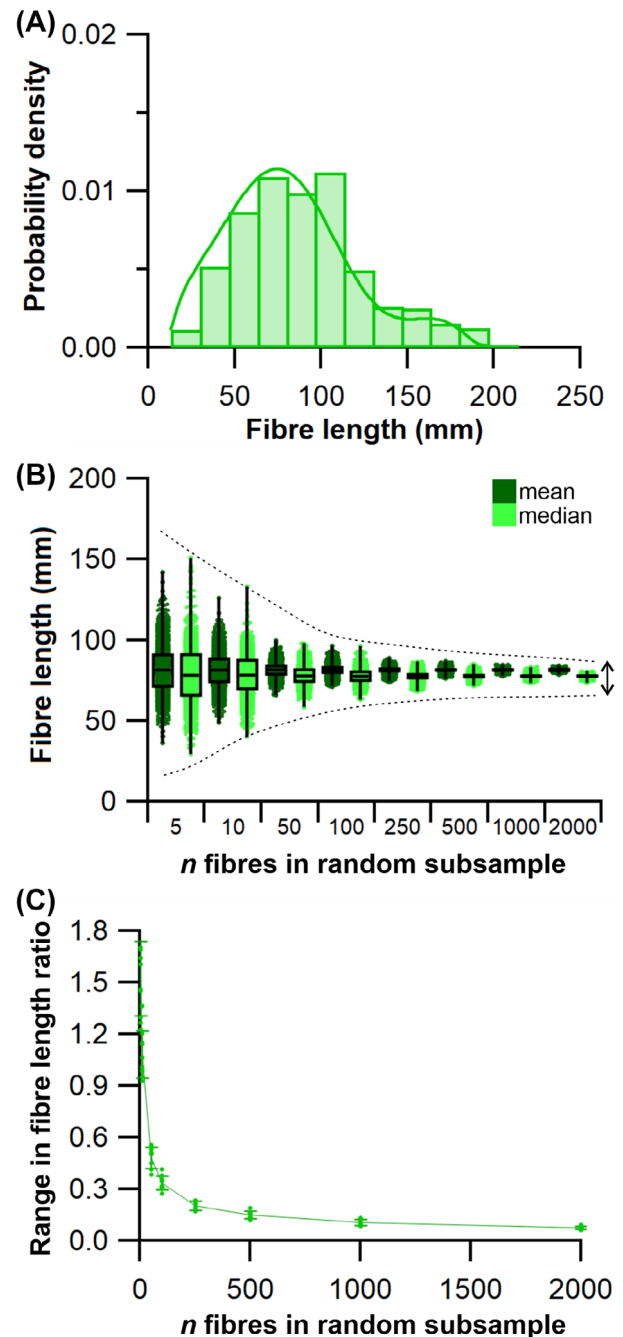


**Fig. 6.** An example of the approach used to quantify potential errors in fibre length measurements due to sample size. (A) Example distribution of fibre lengths within a single muscle. The distributions of fibre lengths within each muscle were studied to assess the appropriateness of calculating mean or median of these measured fibres and address Hypothesis 2 (HYP2). (B, C) Random subsamples of the full set of muscle fibres generated from diffusion tensor imaging were used to study the possible range of mean and median fibre lengths obtainable from different initial sample sizes, expressed as a fraction of the 'true' mean or median value, to address Hypothesis 1 (HYP1).
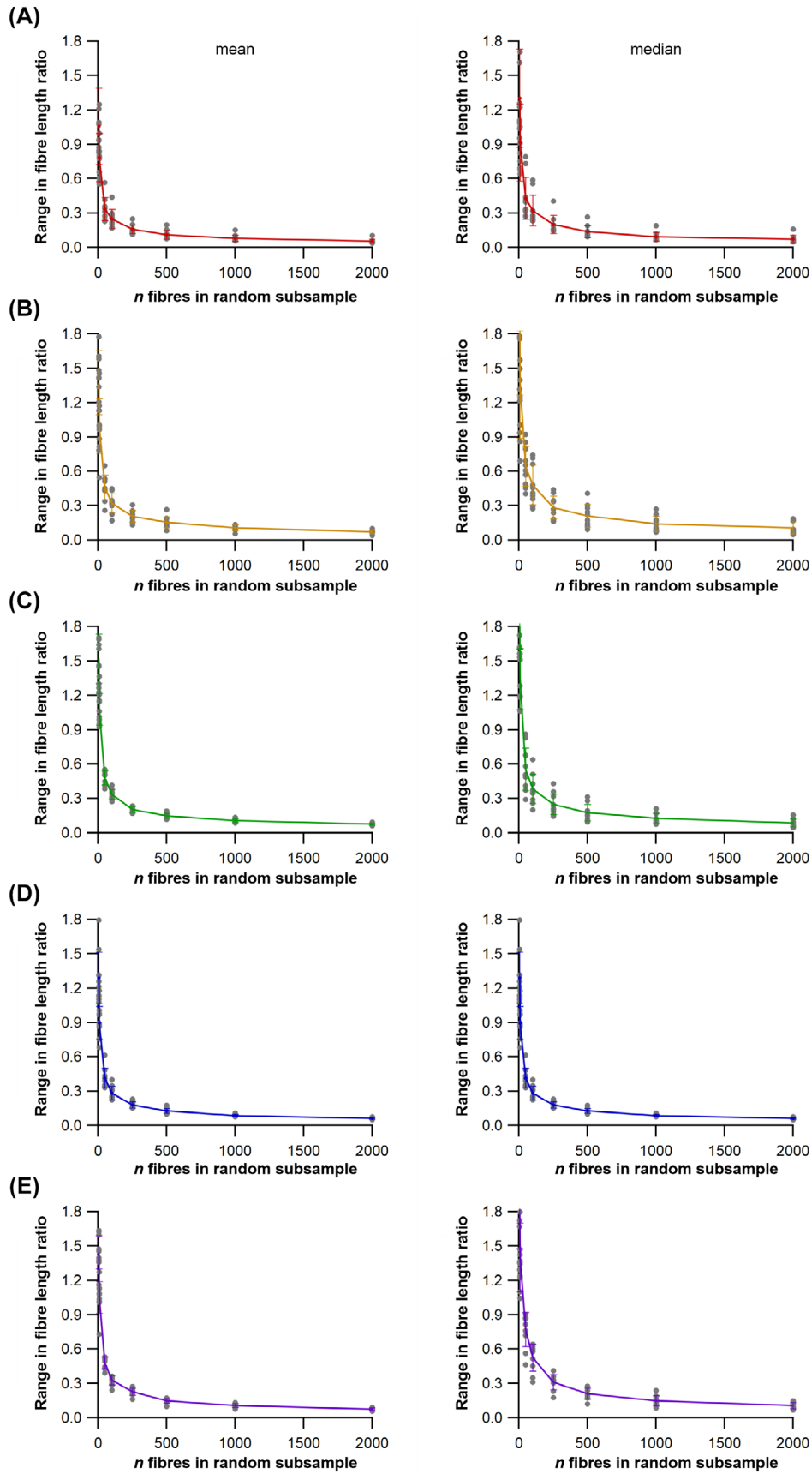
distribution of fibre lengths within each muscle of the lower limb (e.g. Fig. 6A). Here, $P \leq 0.05$ indicates that the distribution of fibres within a muscle is significantly different from a normal distribution and would suggest that mean values are not appropriate to represent the fibres within a particular muscle. Statistical tests were carried out in SPSS software (IBM Corp. IBM SPSS Statistics for Windows, Version 25.0).

### (c) Climbing the pyramid of inference: from fibre to function

To examine the impact of results from HYP1 and HYP2 on quantitative predictions of muscle kinetics and energetics (HYP3b) within humans we used subject-specific musculoskeletal modelling within the Opensim 4.1 (Seth et al., 2018) framework (Fig. 5). A previously constructed 92 MTU actuated personalised lower limb musculoskeletal model (Charles et al., 2020) (male, age 35 years, body mass 68 kg, height 176 cm, BMI 21.95 kgm$^{-2}$) was used to predict muscle fibre lengths, forces and velocities throughout one stride of level walking (self-selected speed of 1.4 m s$^{-1}$) and one vertical jump (height 39 cm) using static optimisation. In this model, $L_f$ and $\theta$ for each muscle actuator were defined by mean values from the fibres tracked from DTI (Model$^{mean}$), with the $L_f$ values then normalised to sarcomere length to generate an optimal fibre length [see Charles et al. (2020) for further details regarding normalisation]. The muscle actuator force-generating properties within this musculoskeletal model were then edited to create three additional model conditions, where actuator properties were informed by: (i) the maximum possible mean fibre length values from the subsamples of 5 fibres [$L_f^{max5}$; Model$^{max5}$ (HYP1)], (ii) the minimum possible mean fibre length values from the subsamples of 5 fibres [$L_f^{min5}$, Model$^{min5}$ (HYP1)] and (iii) the median fibre length values from the full sample of muscle fibres [$L_f^{median}$, Model$^{median}$ (HYP2)]. For the Model$^{max5}$ and Model$^{min5}$ conditions, maximum isometric force values [$F_{max}$, which is directly proportional to PCSA; see Charles et al. (2020) for more details] were recalculated based on these new $L_f$ values in five muscles of the lower limb [gluteus maximus (Gmax); adductor magnus (AM); vastus lateralis (VL); tibialis anterior (TA); and soleus (SOL)], and tendon slack length ($L_{ts}$) values for each muscle were recalculated using the same optimisation algorithm (Manal & Buchanan, 2004). In the Model$^{median}$ condition, these properties were changed for all lower limb MTUs. Kinematic and kinetic data for walking and jumping performed by the human subject were collected using a 12-camera motion capture system (Qualisys Inc.) and embedded force plates (Kistler).

The changes in functional outputs of each MTU in each model condition were quantified in two ways. Firstly, the root mean squared errors (RMSE) of the predicted MTU contractile dynamics (fibre force and normalised fibre length) were calculated during walking and jumping for Model$^{mean}$, Model$^{max5}$ and Model$^{min5}$ relative to Model$^{median}$,

$$\mathrm{RMSE} = \sqrt{\left(\mathrm{Model}^{median} - \mathrm{Model}^x\right)^2}, \qquad (1)$$

where Model$^x$ refers to outputs from either Model$^{mean}$, Model$^{max5}$ or Model$^{min5}$. As it was hypothesised that median fibre length would be more appropriate than means (HYP2) and this hypothesis was supported (see Section IV.2), the outputs from Model$^{median}$ were assumed to be the 'gold standard' outputs against which errors were calculated from the other model conditions.

Secondly, from the positive and negative mechanical work generated by the fibres of each MTU in each model condition, their functional roles were quantified through the calculation of four dimensionless functional indices: strut, spring, motor and brake (Qiao & Jindrich, 2016; Lai, Biewener & Wakeling, 2019). Calculating these functional indices and the relative mechanical work generated by a muscle provides an approximation of their contribution to the flow of mechanical energy through the musculoskeletal system during dynamic movements. Comparing these values provides an overview of the influence of fibre length on inferred muscle function and changes in contribution to walking and jumping movements (see Appendix S1 for more details). These indices were calculated through both walking and jumping for each MTU with altered force-generating properties ($L_f^{max5}$, PCSA$^{max5}$, $L_f^{min5}$, PCSA$^{min5}$) as well as each MTU with unaltered properties ($L_f^{mean}$, PCSA$^{mean}$), in order to observe the effect that uncertainties in the measurement of the muscle architecture of a particular MTU have on the predicted functional capacity of another MTU.

We supplemented these within-species (human) analyses with simple calculations of muscle function specialisation (as reviewed in Fig. 3), and this analysis was also extended to examine the impact of sample size ($n$ fibres) on comparative (across species) inferences of muscle function, thereby assessing the implications of findings from HYP1 and HYP2 on the highest levels of the fibre to function pyramid of inference (Fig. 1C). First, we recalculated the PCSA of the Gmax, AM, VL, TA and SOL muscles in subject 1 using

**(Figure legend continued from previous page.)**
**Fig. 7.** The effect of fibre number ($n$ fibres) on mean and median fibre length. The effects on mean and median fibre length calculations from measuring random subsamples of 5, 10, 50, 100, 250, 500, 1000 and 2000 fibres from the full sample of fibres from the gluteus maximus (Gmax; A), adductor magnus (AM; B), vastus lateralis (VL; C), tibialis anterior (TA; D) and soleus (SOL; E) from all 10 subjects (lines represent data set means). For all muscles, the range of mean or median fibre lengths, expressed as a fraction of the 'true' mean or median value, was high in random subsamples of 5 fibres, but substantially lower in subsamples of >500 fibres.
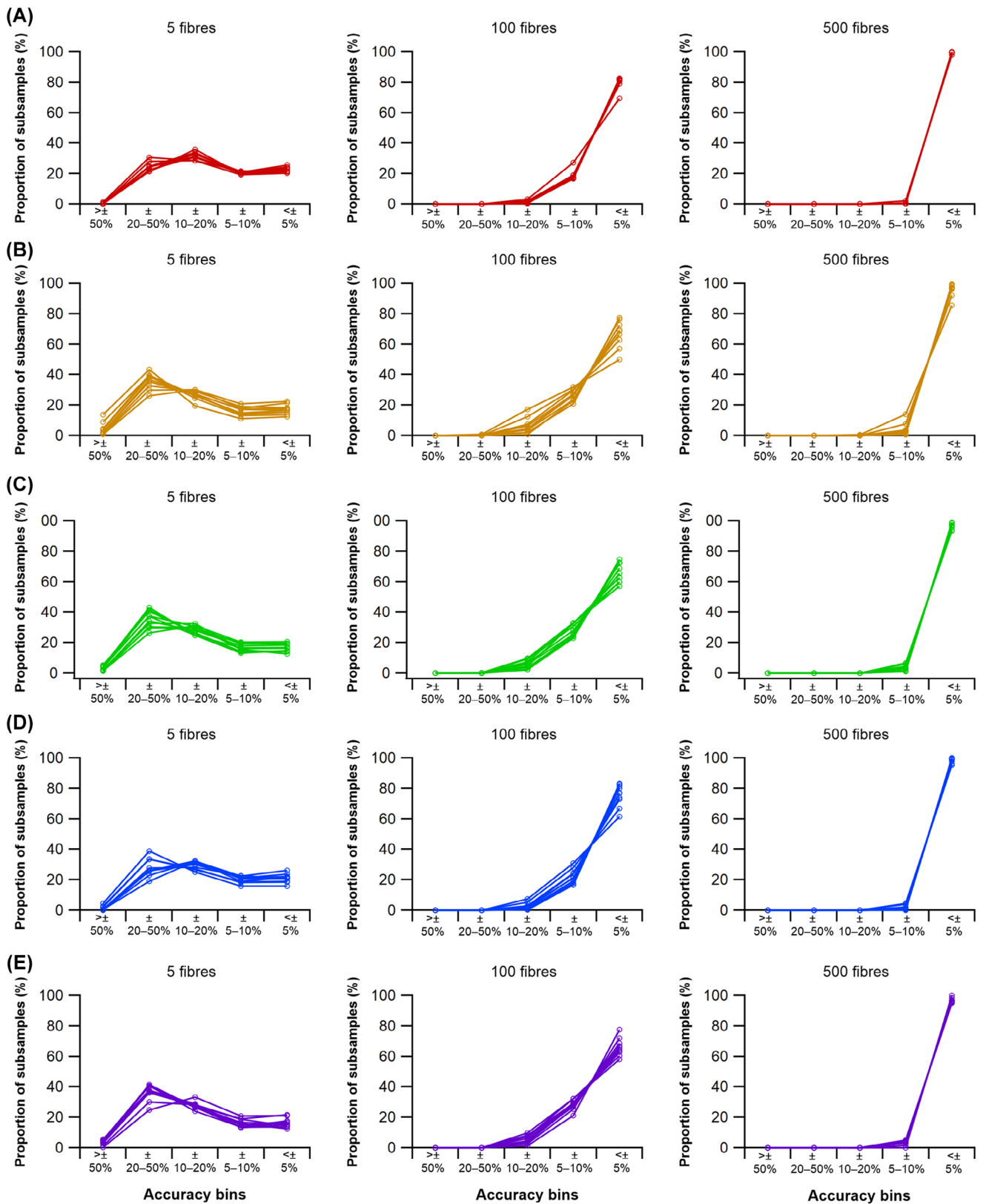
**Fig. 8.** The influence of fibre sample numbers on mean fibre length across 10 subjects. The percentage of mean fibre length values within random subsamples of 5, 100 and 500 fibres for the gluteus maximums (A), adductor magnus (B), vastus lateralis (C), tibialis anterior (D) and soleus (E) muscles relative to the mean value from the full set of fibres, i.e. falling within 'accuracy bins' indicating how close the randomly subsampled values were to the 'true' mean.
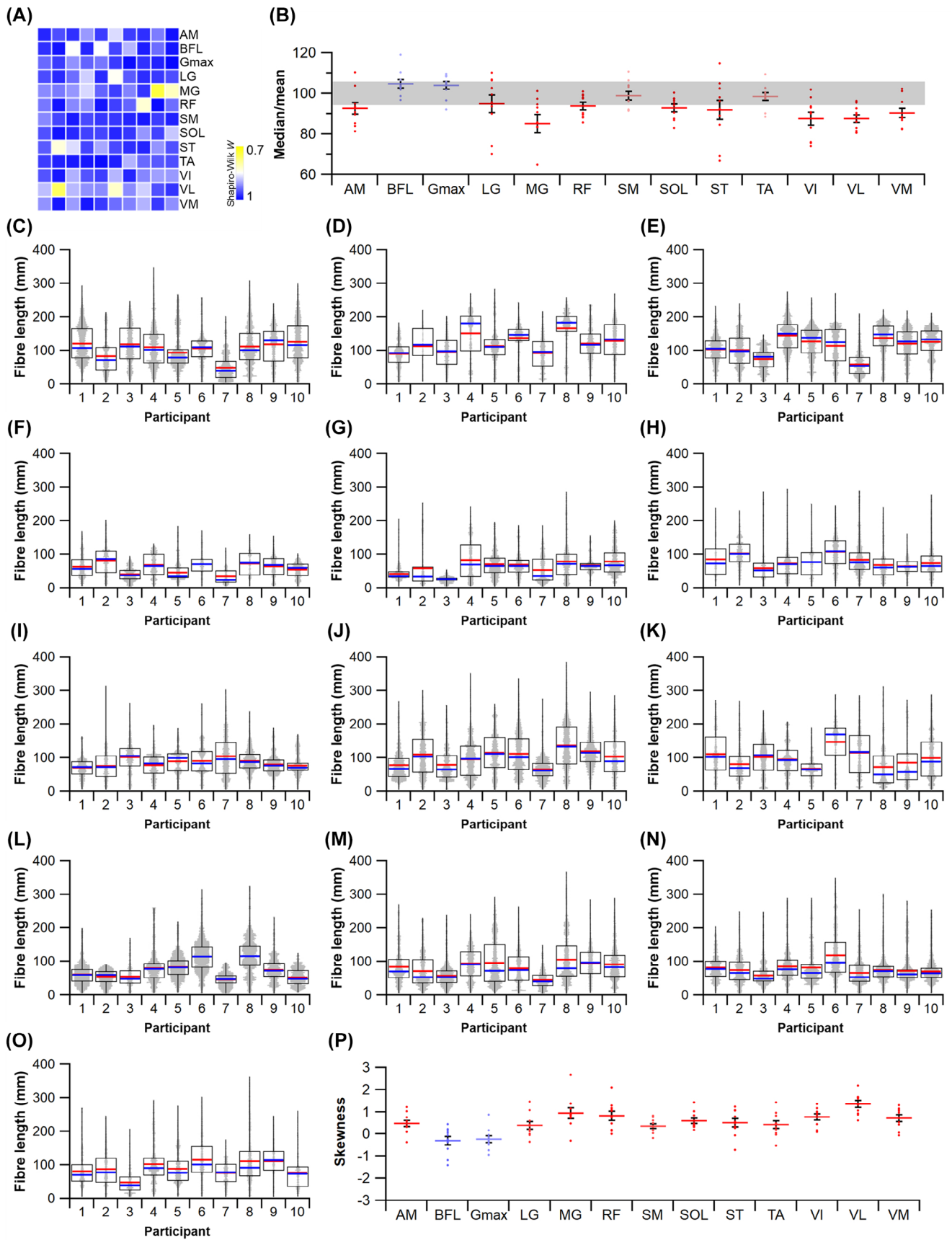
*(Figure legend continues on next page.)*

both the maximum mean fibre length values from subsamples of 5 fibres ($L_f^{max5}$, PCSA$^{max5}$) and the minimum mean fibre length values from subsamples of 5 fibres ($L_f^{max5}$, PCSA$^{min5}$). From the relationship between $L_f$ and PCSA and the $L_f$:PCSA ratio, it was possible to infer the functional specialisations of these five muscles and how this changed depending on initial $L_f$ sample size using muscle function plots, similar to previous studies (Wickiewicz *et al.*, 1983). Here, muscles with long $L_f$ and low PCSA (high $L_f$:PCSA ratio) were classed as displacement specialised, short $L_f$ and high PCSA (low $L_f$:PCSA ratio) as force specialised and long $L_f$ and high PCSA as power specialised. To place these values in a comparative context, these relationships were compared to those from a common chimpanzee (*Pan troglodytes*) (O'Neill *et al.*, 2013). This provided a between-species comparison of the functional specialisations of lower limb muscles and allowed the exploration of potential errors in these comparisons that could be introduced by measuring only a small subset of a muscle's fibres.

## IV  RESULTS AND DISCUSSION

Tables S3–S12 provide data on the fibre architecture and distributions for each of the study participants. Table S13 shows these data averaged across all subjects. Table S14 provides all-subject averages and percentage differences in fibre length and PCSA between the mean and median values of the full sample of fibres, and the maximum and minimum possible mean and median values from random subsamples of 5 fibres.

### (1)  How does fibre sample size influence mean architectural properties?

This analysis shows that the range in both mean and median fibre lengths within the 1000 randomly generated subsamples remains narrowly distributed around the values given by the full sample of fibres in all muscles tested when *n* fibres is above 1000 per muscle (Figs 6, 7; Tables S15–S25). At *n* fibres <250 the range in mean and median fibre lengths increased considerably in an approximately exponential fashion, indicating that the values used to represent

the fibre length of a muscle are highly sensitive to the particular fibres included within any measured sample (Figs 6, 7; Tables S15–S25). These patterns were consistent across all muscles of the lower limb and in all subjects, with a wide range of errors (expressed as percentage error) potentially attainable by measuring only a small sample of fibres from all muscles tested. For instance, the maximum mean or median fibre length values from samples of 5 fibres ($L_f^{max5}$) across all muscles in all subjects were on average 82% and 66% longer than the respective value from the full sample (Table S14), while taking the minimum possible mean fibre length value from these small subsamples ($L_f^{min5}$) led to fibre lengths that were on average 63% and 74% shorter than the original mean or median value. This degree of error varied between muscles however, with the more distal muscles of the limb showing higher potential errors (e.g. ankle dorsiflexors; mean = 123%/−57%; median = 155%/−69%) than the more proximal groups (e.g. knee extensors; mean = 57%/−69%; median = 94%/−76%). On an individual muscle level, the largest potential errors in attainable fibre length values were within the flexor digitorum longus (FDL), which ranged from −64 to 128% of $L_f^{mean}$ and −68 and 203% of $L_f^{median}$. The smallest errors were in the Gmax, which ranged from −62 to 33% of $L_f^{mean}$ and −75 to 40% of $L_f^{median}$ (Table S14).

These potential errors in estimates of fibre length translated to substantial differences in PCSA (PCSA$^{max5}$, PCSA$^{min5}$). The largest errors from PCSA$^{max5}$ relative to PCSA$^{mean}$ and PCSA$^{median}$ were both in the EDL (mean = −60%; median = −66%), while the largest errors from PCSA$^{min5}$ values were seen in the SOL (274%) and biceps femoris – long head (BFL; 628%) relative to PCSA$^{mean}$ and PCSA$^{median}$ values respectively. For the absolute ranges in these potential errors in both $L_f$ and PCSA for each muscle, see Tables S3–S14.

To quantify the probability by which different *n* fibres sample sizes generated certain levels of error in mean fibre lengths we calculated the frequency with which error magnitudes across the 1000 randomly generated samples fell within a range of 'error bins' at each *n* fibres size (Fig. 8). Here, the probability that the mean fibre length value obtained from a sample of measured fibres is within an 'error bin' closer to the mean value from the full sample of fibres increases substantially with increasing sample size. For instance, for the

*(Figure legend continued from previous page.)*
**Fig. 9.** Statistical appropriateness of the use of mean fibre length. (A) Every muscle tested in this study violated the Shapiro–Wilk test for normality, indicating that no distribution of sampled fibres was normally distributed, despite a wide range of W statistics for these samples. (B) Dividing the median fibre length by the mean highlights the gross overestimation of fibre lengths when the mean is used, with data points falling outside the grey bar indicating ±5% difference from the mean. (C–O) Distributions of fibre lengths for all 10 participants across the adductor magnus (C), biceps femoris (long head) (D), gluteus maximus (E), lateral gastrocnemius (F), medial gastrocnemius (G) rectus femoris (H), semimembranosus (I), soleus (J), semitendinosus (K), tibialis anterior (L), vastus intermedius (M), vastus lateralis (N) and vastus medialis (O). Mean fibre length (red horizontal line) and median fibre length (blue horizontal line) are presented for each boxplot. (P) Skewness for each individual across each muscle. AM, adductor magnus; BFL, biceps femoris (long head); Gmax, gluteus maximus; LG, lateral gastrocnemius; MG, medial gastrocnemius; RF, rectus femoris; SM, semimembranosus; ST, semitendinosus; SOL, soleus; TA, tibialis anterior; VI, vastus intermedius; VL, vastus lateralis; VM, vastus medialis.
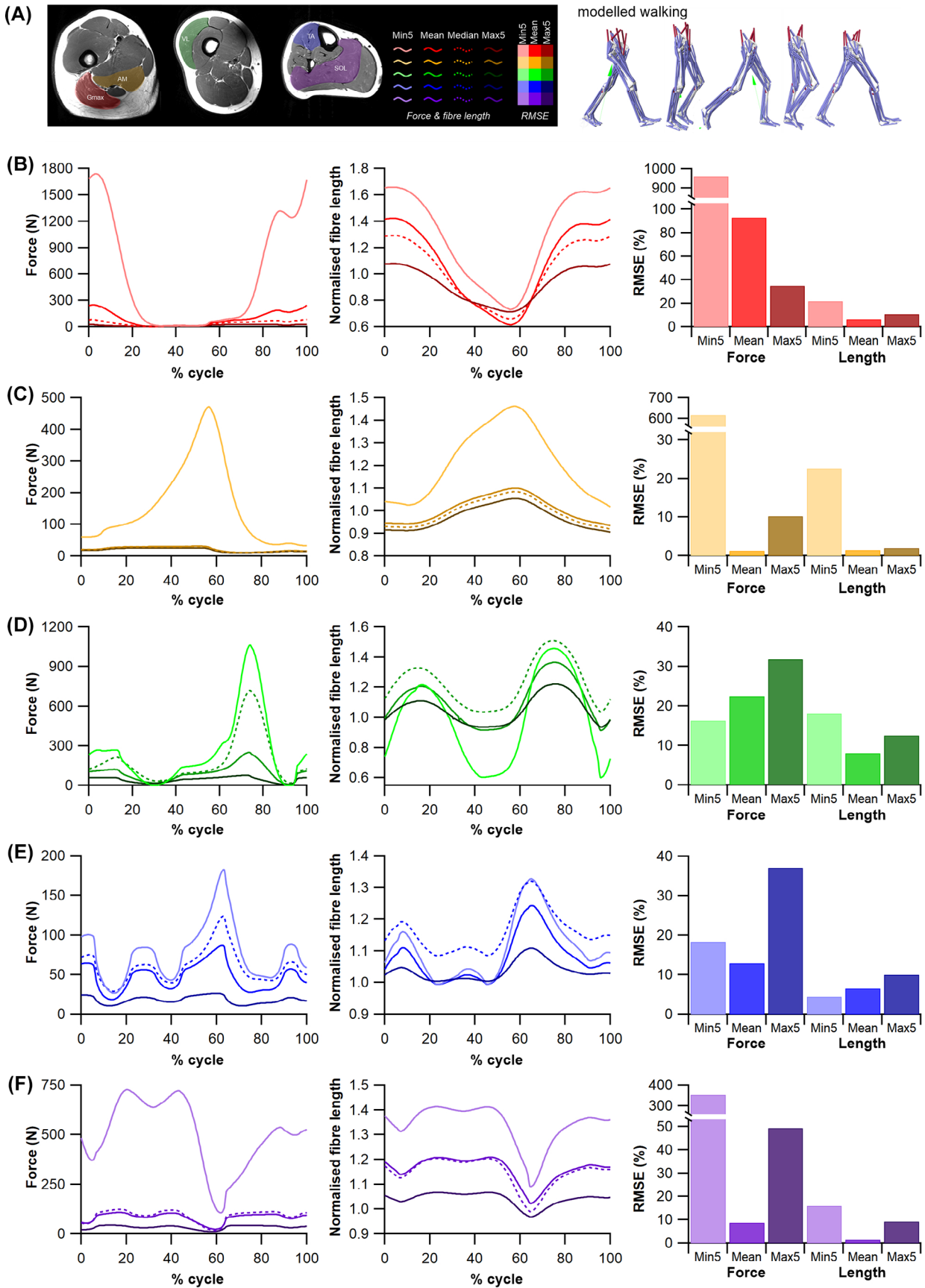
*(Figure legend continues on next page.)*

1000 subsamples of 5 fibres, 34.1% of the possible mean values fell within 20–50% of the 'true' mean when averaged across all muscles within all subjects. However this probability fell to 0.2% with samples of 100 fibres, and was 0% for samples ≥500 fibres (Fig. 8; see Tables S15–S24 for these data from individual subjects, and Table S25 for all-subject and all-muscle averages). Conversely, the probability of generating a fibre length value within 5% of the full mean was 100% with samples of 2000 fibres for all muscles, although this fell gradually with sample size to a probability of 17.4% on average over all muscles with samples of 5 fibres. The highest probability of obtaining a mean value within 5% of the true mean from these small samples was in the Gmax (22.9%), while the lowest probability was in the tibialis posterior (TP; 14.1%).

Collectively, these data provide strong support for the hypothesis (HYP1) that using small samples of muscle fibres may not accurately characterise the architecture of a muscle. Using samples as small as 5 fibres to generate either a mean or median fibre length value for the entire muscle decreases the probability of obtaining a value close to the 'true' value considerably and also potentially introduces degrees of error high enough to change estimations of a muscle's PCSA substantially. Only in subsamples of >500 fibres were ~100% of the mean fibre length values within ±5% of this 'true' mean. This number is more than 20× the *n* fibres that are usually measured in muscle architecture studies (Fig. 4A, Table S1). Our data also suggest that even measuring 100 fibres per muscle (e.g. Baker & Hall-Craggs, 1978; Gollnick *et al.*, 1981; Hermanson & Hurley, 1990), i.e. ~5–10 times more than the number measured in most studies with a few exceptions, may not be sufficient to obtain a representative mean or median fibre length value.

### (2) Are the central tendencies of muscle architectural properties typically more appropriately represented by the median or mean value?

Shapiro–Wilk tests were carried out on the fibre length distributions within 25 muscles from each of the 10 subjects to test for normality. The results indicate that none of these 250 muscles showed a normal distribution of fibre lengths (Fig. 9; Tables S3–S12). Therefore, using medians to obtain a single representative value of a muscle's fibre length has more statistical support than using a mean value. Across all muscles in all 10 subjects, median fibre lengths were on average 4 mm shorter than mean fibre lengths, which

translates on average to a 10% increase in PCSA (266 mm$^2$) when using median fibre lengths to calculate muscle force-generating properties relative to using mean values (Tables S3–S13). This discrepancy was variable between muscle groups, with an average difference of −10 mm/541 mm$^2$–10%/13%) in the knee extensors, but only <1 mm/29 mm$^2$ (−1%/3%) in the hip extensors (Table S14). In individual muscles, the largest average error was seen in the iliacus muscles, where a 9% error in $L_f$ (4 mm) by measuring the mean value resulted in a 31% lower PCSA (916 mm$^2$) relative to median values (Table S14). Collectively, this represents strong statistical support for the hypothesis (HYP2) and that the central tendency of muscle architectural properties is more appropriately represented by the median value rather than the mean, although the potential effects on fibre lengths and PCSA are much less than those of sample size.

### (3) How do fibre sample size-related errors impact upon higher-level interpretations of muscle function within a species?

Potential errors in the quantification of muscle architecture due to (HYP1) low sample size (*n* fibres) and (HYP2) the use of mean instead of median values also have significant impacts on the quantitative aspects of muscle function derived from musculoskeletal simulations of dynamic movements (Figs 10–13). Here, four different musculoskeletal models of one individual, which differed only in the muscle fibre lengths used to inform their muscle actuator force-generating properties, were used to predict *in vivo* muscle fibre lengths, forces and mechanical work generation during walking (Fig. 10) and vertical jumping movements (Fig. 11). The root mean squared errors (RMSEs) of these outputs of the models which included MTU actuators with the maximum possible fibre length from a sample of 5 fibres (Model$^{max5}$), the minimum possible fibre length from a sample of 5 fibres (Model$^{min5}$) and the mean fibre lengths from the full sample of fibres (Model$^{mean}$) were calculated relative to a model including MTU actuators with the median fibre lengths from the full sample of fibres (Model$^{median}$) (Table S26). The largest errors relative to Model$^{median}$ were seen in Model$^{min5}$, where there were RMSEs in fibre length of 16.2 ± 5.2% (0.20 ± 0.07 mm) during walking (Fig. 10) and 13.7 ± 5% (0.19 ± 0.06 mm) during jumping (Fig. 11) when averaged across the tested muscles. Errors were substantially higher in terms of fibre force, with average errors of 401 ± 299% (337 ± 262 N) during walking (Fig. 10) and

*(Figure legend continued from previous page.)*
**Fig. 10.** The influence of inaccurate fibre length measurements on simulations of walking. (A) Musculoskeletal modelling for walking. (B–F) Muscle fibre lengths and forces of the gluteus maximus (mid portion) (B), adductor magnus (hamstring part) (C), vastus lateralis (D), tibialis anterior (E) and soleus (F) predicted by static optimisation simulations of walking in models informed by the full mean value (Model$^{mean}$, mid-tone line), median value (Model$^{median}$; mid-tone dashed line), and the maximum (Model$^{max5}$; darkest line) and minimum (Model$^{min5}$; palest line) possible values from random subsamples of 5 fibres. The root mean squared errors (RMSEs) of these variables relative to Model$^{median}$ are shown expressed as a percentage of the maximum Model$^{median}$ value.
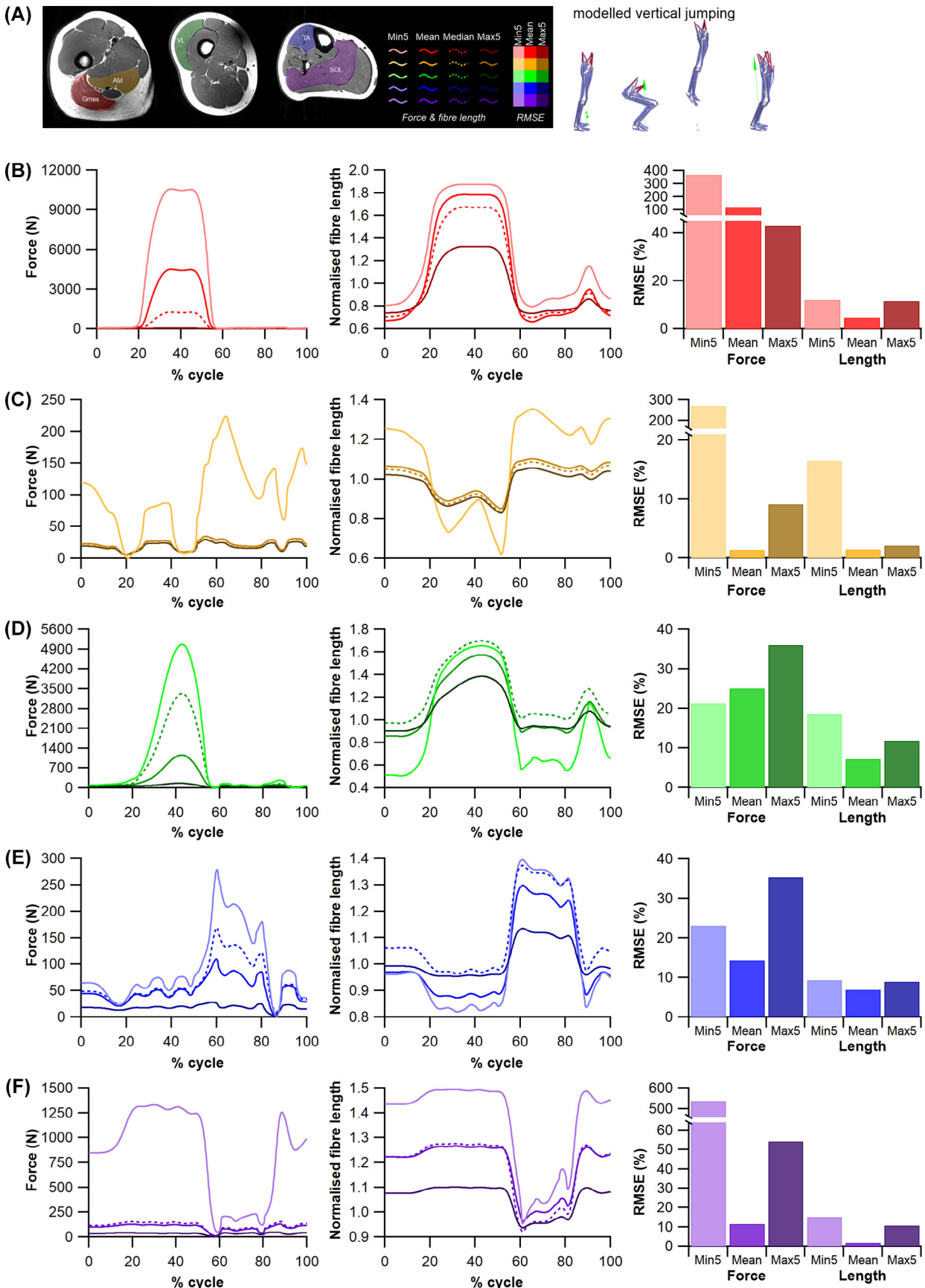
*(Figure legend continues on next page.)*

$266 \pm 177\%$ ($1845 \pm 2098$ N) during jumping (Fig. 11). The muscle actuators that showed the largest error in Model[min5] were Gmax, with errors in fibre force of 530% (579 N), 962% (797 N) and 502% (502 N) in the anterior, middle and posterior portions of this muscle respectively during walking (Fig. 10A; Table S26), and SOL, where there were errors of up to 537% (837 N) in fibre force during jumping (Fig. 11F; Table S26). The errors in both Model[max5] and Model[mean] were lower across all variables and all muscles. The largest error in the Model[max5] outputs was a 54% (85 N) error in fibre force in SOL during jumping (Fig. 10F), while the largest error in the Model[mean] outputs was a 121% (1526 N) error in fibre force in Gmax (mid portion) during jumping (Fig. 11A).

In terms of the functional indices, using median (Model[median]) instead of mean (Model[mean]) fibre lengths to inform muscle force-generating properties results in different inferred fibre functions for several muscles during both walking (Fig. 12) and jumping (Fig. 13). During walking, these changes were most apparent in the flexor hallucis longus (FHL) and psoas (PMA) MTUs, where their fibres appeared to act as springs (equal positive and negative work; 76%) or motors (high force, positive work; 97%) respectively in Model[mean], but motors (94%) or struts (high force, low work; 49%) respectively in Model[median] (Fig. 12J, K). During jumping, the TA showed the greatest change in fibre function, with a primary motor function (92%) in Model[mean] but a spring function (61%) in Model[median] (Fig. 13E).

Similarly, the functions inferred from the Model[max5] and Model[min5] conditions also showed large changes relative to Model[mean] through walking and jumping in the MTUs with altered force-generating properties (Figs 12B–F, 13B–F) as well as the MTUs with unchanged properties (Figs 12G–L, 13G–L). For instance, the Gmax showed a shift from a spring-like function (80%) to a spring/brake function (51%/48%) in Model[min5] during walking (Fig. 12B), and from a brake function (high force, negative work; 79%) to a spring function (76%) in Model[max5] during jumping (Fig. 13B). The SOL fibres also showed a large change in function in Model[min5], with a switch from a spring/motor (59%/40%) to a strut/spring function (36%/58%) during walking (Fig. 12F), and from a spring/brake (49%/50%) to a primarily braking function (84%) in jumping (Fig. 13F). Interestingly, it was not solely the muscles in which the fibre length values were altered in the Model[min5] and Model[max5] conditions that showed substantial changes in functional roles, with the fibres of the FHL having a more
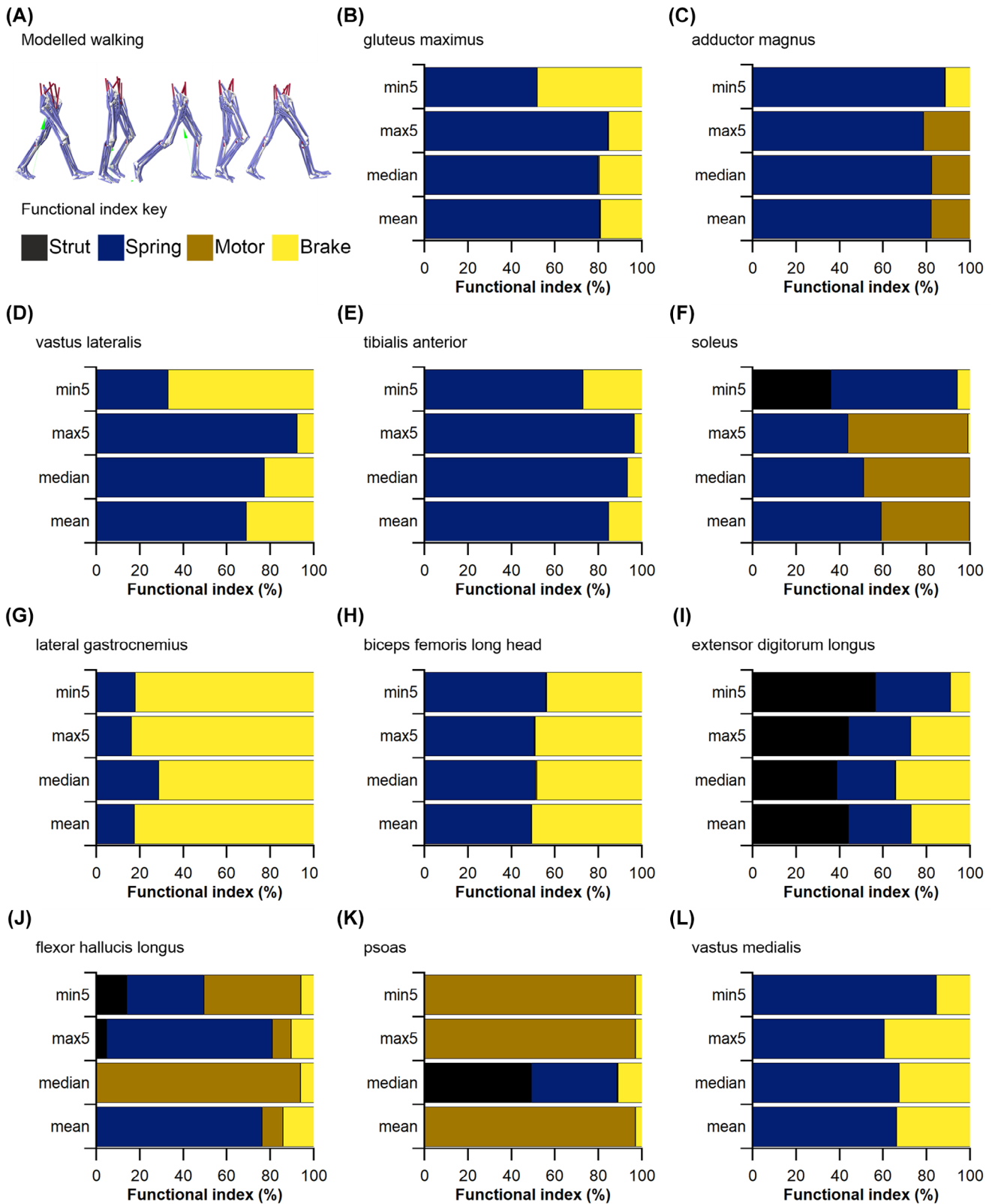
motor-like (9 to 44%) function in Model[min5] during walking (Fig. 12J), and the vastus medialis (VM) becoming slightly more spring-like (65 to 84%) (Fig. 12L), despite no change in their own force-generating properties from Model[mean]. This demonstrates that even the qualitative functional role predicted for muscles with 'accurate' data (i.e. those provided by measuring a large number of fibre lengths) can be substantially affected by inaccurate architecture data in other muscles.

It should also be noted that measurements of muscle fibres entered into our models are influenced by other potential sources of error not considered fully here. In particular, this includes measurements of sarcomere length, which in this study were taken from previous work (Ward *et al.*, 2009) and used to adjust the mean and median fibre lengths measured from DTI to an 'optimal' length. This was necessary as gathering *in vivo* sarcomere lengths from each muscle in each subject was outside the scope of this study. The use of these data was considered valid as they were gathered from tissue fixed in the anatomical position, which is how each subject was positioned during MR image acquisition. However, published sarcomere lengths vary both within and between previously published data sets, with Ward *et al.* (2009) reporting large standard deviations associated with their mean values, and Cutts (1988) reporting substantially different values despite specimens in both studies being fixed in the same anatomical position. Using the maximum mean ± standard deviation value from Ward *et al.* (2009) to optimise the fibre lengths reported here resulted in maximum errors of 17% in the VM MTU, while the maximum error introduced by using data from Cutts (1988) was 13% in the rectus femoris (RF) MTU (Table S27). However, it has been shown that sarcomere lengths vary considerably within a muscle, as well as among individuals, so eliminating this error even with primary individualised data is unlikely (Lichtwark *et al.*, 2018). Ultimately, using previously published sarcomere length data to optimise subject-specific fibre length data from DTI did introduce some degree of error into the derivation of the optimal fibre length values reported here. However, these errors were small compared to those potentially introduced by measuring a small initial sample size of fibres (up to 203% in the FDL).

It should also be noted that biomechanical models and simulations, as used here, provide estimates or approximations of skeletal muscle function during locomotor tasks. While the models used here were based on individualised muscle properties and musculoskeletal geometry, many

*(Figure legend continued from previous page.)*
**Fig. 11.** The influence of inaccurate fibre length measurements on simulations of vertical jumping. (A) Musculoskeletal modelling for vertical jumping. (B–F) Muscle fibre lengths and forces of the gluteus maximus (mid portion) (B), adductor magnus (hamstring part) (C), vastus lateralis (D), tibialis anterior (E) and soleus (F) predicted by static optimisation simulations of jumping in models informed by the full mean value (Model[mean], mid-tone line), median value (Model[median]; mid-tone dashed line), and the maximum (Model[max5]; darkest line) and minimum (Model[min5]; palest line) possible values from random subsamples of 5 fibres. The root mean squared errors (RMSEs) of these variables relative to Model[median] are shown expressed as a percentage of the maximum Model[median] value.

**(A)** Modelled walking

Functional index key

Strut | Spring | Motor | Brake

**(B)** gluteus maximus

**(C)** adductor magnus

**(D)** vastus lateralis

**(E)** tibialis anterior

**(F)** soleus

**(G)** lateral gastrocnemius

**(H)** biceps femoris long head

**(I)** extensor digitorum longus

**(J)** flexor hallucis longus

**(K)** psoas

**(L)** vastus medialis

*(Figure legend continues on next page.)*

simplifications remained, such as limited rotational and translational degrees of freedom at the joints, simplified muscle lines of action and generic human values for certain physiological properties (Charles *et al.*, 2020). These simplifications will undoubtedly have introduced some error in our model output predictions (Figs 10–13), but it is unlikely that this influenced the conclusions drawn from our models with respect to HYP3.

### (4) How do fibre sample size-related errors impact upon higher-level interpretations of muscle function across species?

Errors in the quantification of muscle architecture due to (HYP1) a low *n* fibres measured and (HYP2) the use of mean instead of median values also had a significant impact upon interpretations of muscle specialisation in humans *versus* chimpanzees (Fig. 14). When the full samples of fibres were used to calculate muscle properties, each muscle in which force-generating properties were changed (Gmax, AM, VL, SOL and TA) showed different qualitative specialisations within human lower limbs (Fig. 14A). Gmax is recovered as the most power-specialised lower limb muscle, capable of generating very high absolute forces across a relatively large working (length) range (Fig. 14A). Proportionally long fibres and a relatively small PCSA means that the AM is recovered as by far the strongest displacement-specialist muscle, adapted to maintaining modest force output across a large working range (Fig. 14A). The TA shows little specialisation among surrounding lower limb muscles, having both modest PCSA and fibre length values, while both the VL and SOL are similar in showing a moderate degree of power-specialisation (Fig. 14A).

However, the high variability in mean fibre lengths (and subsequently PCSA values) that are potentially possible when only measuring 5 fibres (Figs 6–8) means that an extremely broad continuum of specialisations (spanning the functional space occupied by a very large portion of all human lower limb muscles) become possible for all of these muscles (Fig. 14A). As a result, there is clearly significant potential qualitatively to misclassify the adaptive specialisation of muscles within a species both in absolute and relative terms when small fibre numbers are used. For example, at 5 fibres there is considerable potential to lose the displacement-specialisation of AM, erroneously interpret TA, VL and SOL as
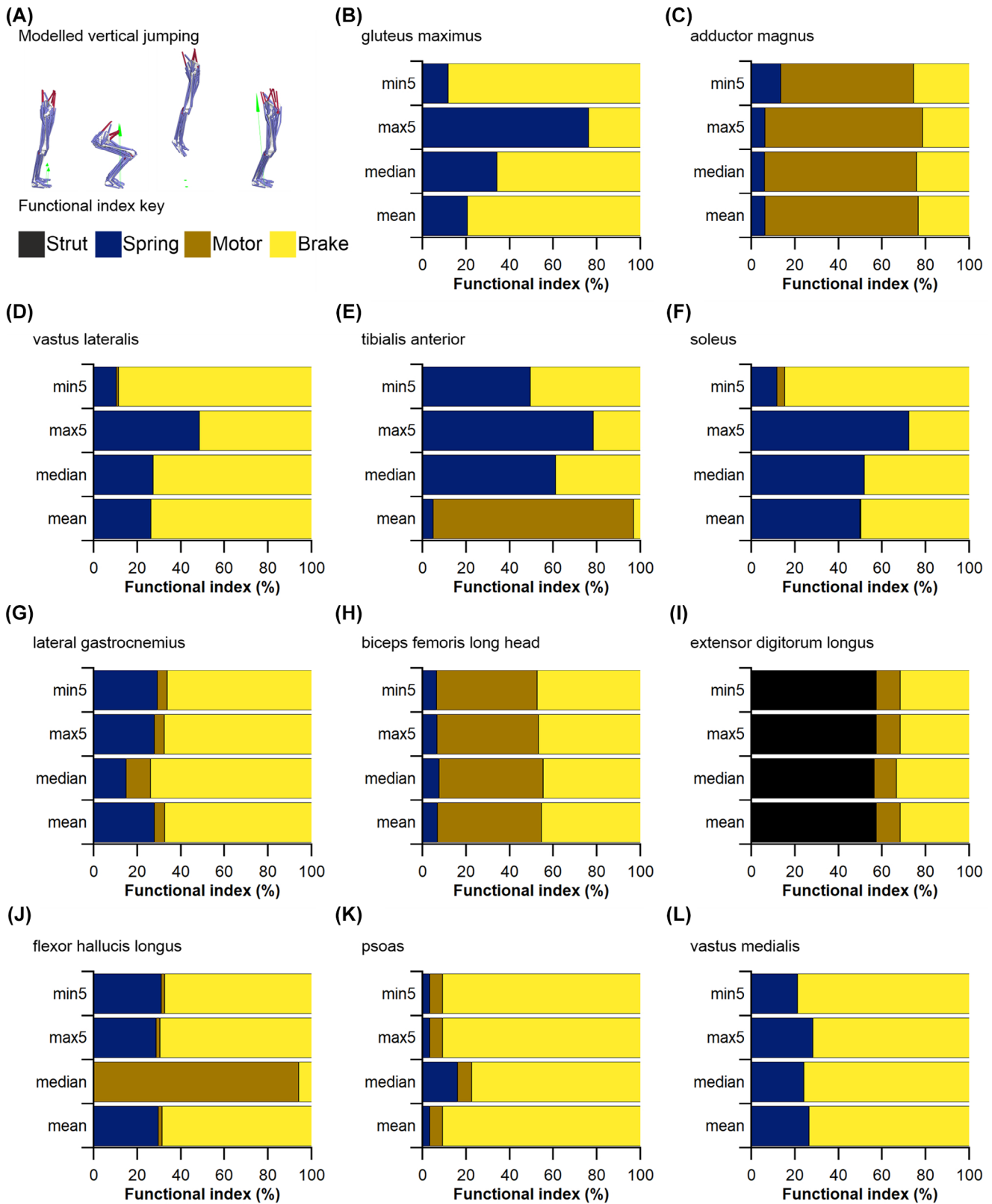
displacement or force-specialised muscles, and to recover any of Gmax, VL, SOL or AM as the most force, displacement or power-specialised lower limb muscle in humans (Fig. 14A). In other words, the magnitude of potential inaccuracy seen at *n* = 5 fibres means that any combination of specialisation across all muscles might be recovered depending on the specific fibres measured.

Studies of muscle specialisation (Fig. 14) are common not only in zoological studies (Payne *et al.*, 2005a; Allen *et al.*, 2010) but also in palaeontology where the extant phylogenetic approach (Witmer, 1995) is used to identify transitions in muscle architecture and function that must have occurred in fossil lineages that bridge extant groups, such as human and non-human great apes (Bramble & Lieberman, 2004) (human evolution) and birds and crocodilians (Bates & Schachner, 2012) (dinosaur evolution). In both contexts, differences in the location of homologous muscles within function plots (Fig. 14A) are often interpreted as functional adaptations that have evolved to facilitate different locomotor characteristics of the species under study (Payne *et al.*, 2005a; Allen *et al.*, 2010; Bates & Schachner, 2012). For example, in primatology and human evolution, such an approach has been used to hypothesise adaptive changes in muscle design that enabled the evolution of efficient upright walking and enhanced running ability in modern humans (Bramble & Lieberman, 2004; Carlson, 2006; Myatt *et al.*, 2011). To optimise the efficiency of striding bipedalism, the muscle groups of the human lower limb have functional specialisations organised in a somewhat proximo-distal gradient (Wickiewicz *et al.*, 1983; Daley, Felix & Biewener, 2007; Ward *et al.*, 2009), in which proximal muscle groups such as the hip extensors are thought to be more displacement specialised, with long parallel muscle fibres and relatively low PCSAs, and distal muscle groups such as the ankle plantarflexors having relatively shorter fibres and higher PCSA for more force specialisation. This gradient of muscle function is a feature of many cursorial mammals (Payne *et al.*, 2005a; Williams *et al.*, 2007a, 2008b), but is less strongly pronounced in animals using more flexed-limb postures such as the primarily knuckle-walking chimpanzee (*Pan troglodytes*) (O'Neill *et al.*, 2013). There are therefore thought to be significant muscle architectural differences between the lower limb muscles of humans and *P. troglodytes* which highlight adaptations for different locomotor repertoires. Here we show the scale of
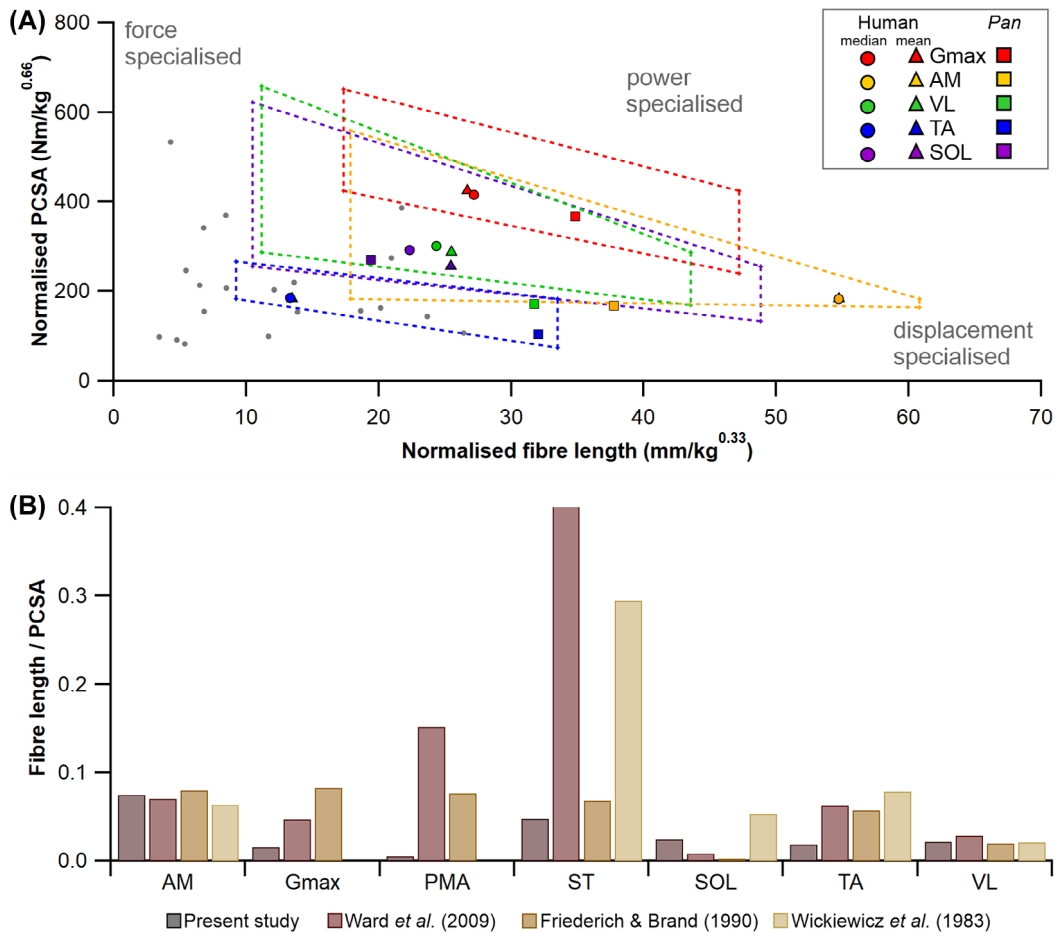
*(Figure legend continued from previous page.)*
**Fig. 12.** Functional implications of fibre length sample size as predicted by a musculoskeletal model and simulation of walking. In four different model interactions containing muscles with optimal fibre length and maximum force values informed by the full mean value (Model^mean), median value (Model^median), and the maximum (Model^max5) and minimum (Model^min5) possible values from random subsamples of 5 fibres, all muscles were characterised as acting as struts, springs, motors or brakes depending on the level and timing of force and power generation. In Model^mean and Model^median, all muscles were informed by the appropriate values, while in Model^max5 and Model^min5, results are shown for only five muscles (B–F) informed by these properties, with the properties of all other muscles (e.g. G–L) determined by their Model^mean values. The vastus lateralis (D) and soleus (F) showed substantial changes in function relative to Model^mean due to reductions in fibre sample size (Model^min5), while the flexor hallucis longus (J) showed a similarly large change in function in Model^min5 despite no change in muscle force-generating properties from Model^mean.

**(A)** Modelled vertical jumping

Functional index key

■ Strut ■ Spring ■ Motor ■ Brake

**(B)** gluteus maximus

**(C)** adductor magnus

**(D)** vastus lateralis

**(E)** tibialis anterior

**(F)** soleus

**(G)** lateral gastrocnemius

**(H)** biceps femoris long head

**(I)** extensor digitorum longus

**(J)** flexor hallucis longus

**(K)** psoas

**(L)** vastus medialis

*(Figure legend continues on next page.)*

**Fig. 14.** Interpretations of muscle function and specialisation based on fibre architecture. (A) Relationship between normalised muscle fibre length and normalised physiological cross-sectional area (PCSA) across human (●, ▲) and chimpanzee (■) lower limb muscles. Median fibre lengths are in grey (●) with selected muscle-specific data points highlighted in colour, and with a colour-matched mean data point (▲). Dashed quadrilaterals depict potential error in fibre length and PCSA dependent on the number of fibres used to calculate fibre length. These uncertainties yield large potential error on inferences of muscle functional specialisations (inferred from the relationship between fibre length and PCSA), where random subsamples of 5 fibres can predict a muscle to either be displacement specialised or force specialised, depending on the mean value used. (B) Muscle fibre length to PCSA ratio in human muscles derived from data in this study and previously published work. The ratios of muscle fibre length to PCSA in selected muscles of the lower limb for the data presented here compared to those from previous studies highlight the range of functional behaviours inferred for certain muscles, particularly the semitendinosus (ST), which may be interpreted as resulting from measurements of only a small subset of fibres in past literature. AM, adductor magnus; Gmax, gluteus maximum; PMA, psoas; SM, semitendinosus; SOL, soleus; TA, tibialis anterior; VL, vastus lateralis.

these differences can be removed, exaggerated, or reversed by potential errors in functional inferences brought about by measuring small samples of muscle fibres (Fig. 14A). It

is therefore clear that the large range of fibre lengths and PCSA values possible at low *n* fibre numbers (Figs 7, 8) creates significant potential for qualitatively incorrect

---

*(Figure legend continued from previous page.)*
**Fig. 13.** Functional implications of fibre length sample size as predicted by a musculoskeletal model and simulation of vertical jumping. In four different model interactions containing muscles with optimal fibre length and maximum force values informed by the full mean value (Model$^{mean}$), median value (Model$^{median}$), and the maximum (Model$^{max5}$) and minimum (Model$^{min5}$) possible values from random subsamples of 5 fibres, all muscles were characterised as acting as struts, springs, motors or brakes depending on the level and timing of force and power generation. In Model$^{mean}$ and Model$^{median}$, all muscles were informed by the appropriate values, while in Model$^{max5}$ and Model$^{min5}$, results are shown for only five muscles (B–F) informed by these properties, with the properties of all other muscles (e.g. G–L) determined by their Model$^{mean}$ values. The tibialis anterior (E) and soleus (F) showed substantial changes in function relative to Model$^{mean}$ due to reductions in fibre sample size (Model$^{min5}$), while changes in function in muscles with unchanged force-generating properties from Model$^{mean}$ were much less than those seen during walking.

interpretations of evolutionary adaptations in muscles across major functional transitions (Fig. 14).

The potential for significant quantitative and qualitative error in muscle function analysis at low $n$ fibre numbers (Fig. 14) is not surprising given that high magnitudes of error in mean or median fibre lengths synchronously translate into large errors for muscle PCSA (e.g. 73% error in mean fibre length yielding 274% error in SOL; Figs 7, 8; Table S14). Indeed, this effect of fibre sample size may have resulted in some of the functional specialisations inferred here from muscle architecture alone to be different from those reported in previous studies (Wickiewicz *et al.*, 1983; Friederich & Brand, 1990; Ward *et al.*, 2009) (Fig. 14B). Functional specialisations of muscles have also been quantified using the $L_f$:PCSA ratio, where a high value indicates a tendency for the muscle to be displacement specialised, and a low value suggesting it is force specialised. In previous studies of human lower limbs (where only 10–20 fibres were measured), muscles such as the PMA were predicted to be more suited for velocity in contraction (i.e. displacement specialised) than they were in this study, where they appeared more suited for force generation (Fig. 14B). Additionally, the data from Ward *et al.* (2009) and Wickiewicz (1983) suggested that

the semitendinosus (ST) muscle is a displacement specialist, whereas the data from Friederich & Brand (1990) (where up to 200 fibres were measured from each muscle) showed this muscle to be more of a force specialist, which is in line with the inferences recovered here (Fig. 14B). Of course, these discrepancies could be due to factors other than fibre number, such as anatomical variation, but the large range of possible fibre length values attainable from only a small sample of fibres suggests it is likely to be a primary cause behind variations in the data presented in previous muscle architecture studies.

## (5) Future perspectives

We recover a clear tendency for certain muscles to show greater variation in mean and median $L_f$ at small sample sizes than others. One possible explanation for this is systematic variation in error magnitude *versus* sample size is overall muscle size and total fibre number. As a preliminary assessment of size-based variation in error, we investigated the statistical relationships between muscle volume, maximum fibre $n$ and the maximum potential percentage errors in both $L_f$ and PCSA in all lower limb muscle
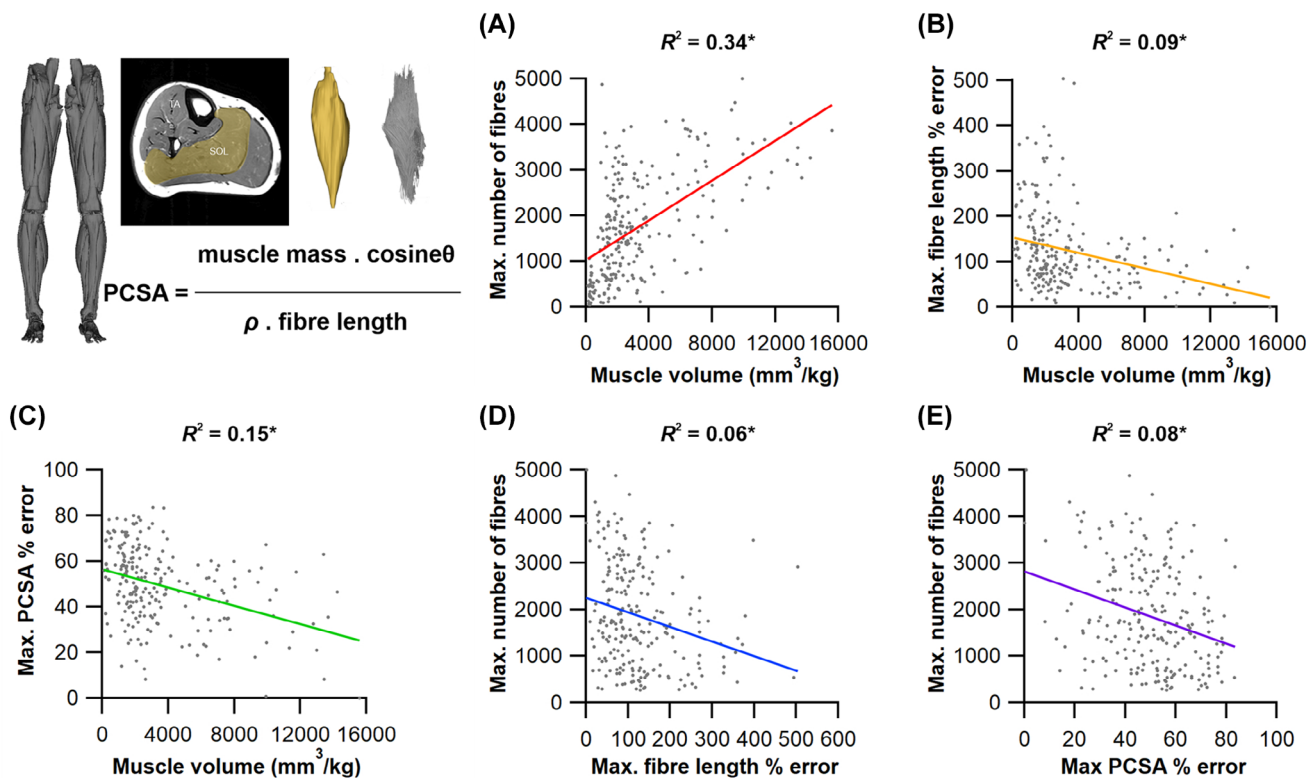


**Fig. 15.** The relationships between muscle volume, maximum fibre number and percentage error in the lower limb muscles. (A) There was a moderately strong positive relationship between normalised muscle volume and the maximum number of fibres present, as measured using diffusion tensor imaging and deterministic fibre tractography. Neither of these metrics were strongly correlated with the maximum recovered percentage errors in either fibre length (B, D) or physiological cross-sectional area (PCSA; C, E). This suggests that other factors, such as muscle architectural complexity, could instead explain the variation in fibre length, PCSA and contractile capacity errors seen here for the muscles of the lower limb. *$P < 0.01$. SOL, soleus.

across all our subjects (Fig. 15). As expected, while the larger muscles of the lower limb tend to contain more fibres than the smaller muscles ($R^2 = 0.32$; Fig. 15B), there was little evidence for a relationship between either muscle volume or maximum fibre number and the % error in either $L_f$ ($R^2 = 0.09, 0.06$, respectively; Fig. 15C, E) or PCSA ($R^2 = 0.15, 0.08$, respectively; Fig. 15D, F) resulting from a small fibre $n$.

It is therefore possible that this variation in recovered $L_f$ and PCSA error within the muscles of the lower limb is due to differences in their fibre architectural arrangements. For instance, recent work using DTI has shown that the SOL
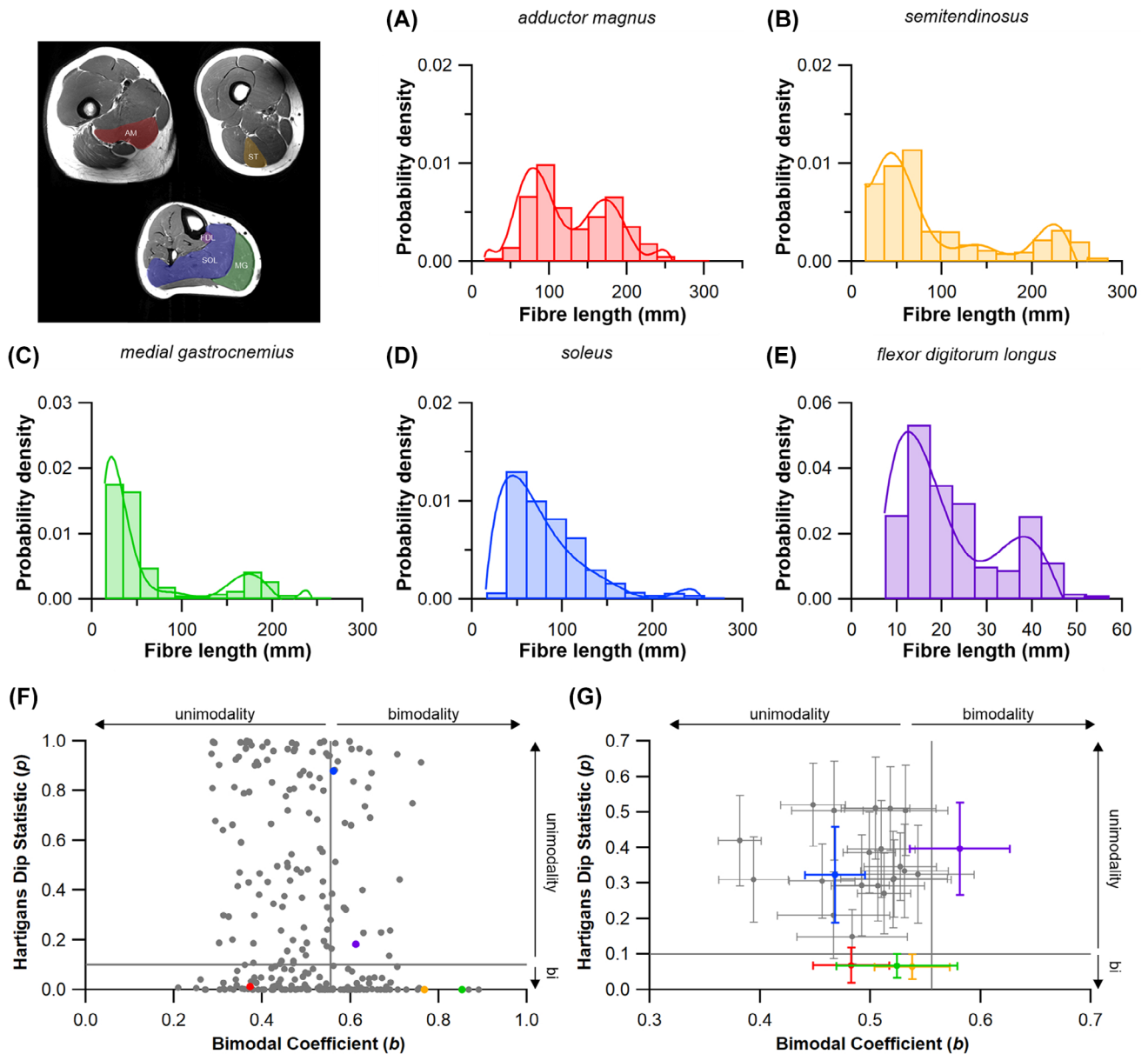


**Fig. 16.** Statistical measures of bimodality in fibre length distributions. Data from all 250 muscles sampled were assessed using Hartigan's Dip statistic and the Binomial Coefficient equation to assess if the distribution of muscles fibres presented as a uni- or bimodal distribution. (A–E) Example distributions taken from the adductor magnus (A), semitendinosus (B), medial gastrocnemius (C), soleus (D) and flexor digitorum longus (E) highlight the variability in fibre distribution. (F) Of the 250 individual muscles sampled, 153 were considered bimodal in distribution. 77 were identified only by Hartigans Dip statistic, 30 were considered multi-modal only by the Binomial Coefficient, with 46 considered multi-modal by both statistical tests. (G) Presented as a muscle average across the 10 participants the adductor magnus (A, G), semitendinosus (B, G) and medial gastrocnemius (C, G) were classified as statistically bimodal by the Hartigans Dip Statistic only ($p$) while the flexor digitorum longus (E, G) was classified as bimodal by the Binomial Coefficient only. The soleus (D) was classified as unimodal by both statistical tests. AM, adductor magnus; FDL, flexor digitorum longus; MG, medial gastrocnemius; SOL, soleus; ST, semitendinosus.

muscle, which showed some of the largest $L_f$ errors due to small fibre $n$ (up to 78%) and was assumed here to be one homogeneous muscle, is actually composed of multiple compartments with substantially different fibre lengths and functional capabilities (Bolsterlee *et al.*, 2018). This could also explain the relatively large $L_f$ errors also seen in the AM muscle (also up to 78%), which was also assumed to be one whole muscle during the architecture measurements but is well known to include functionally distinct adductor and hamstring parts with separate insertions onto the femur.

Interestingly however, statistical analyses carried out here in association with HYP2 revealed that this compartmentalisation may be present in more muscles of the lower limb. In studying the distribution of fibre lengths throughout each muscle of each subject (250 muscles), 44% and 30% were identified as being multimodal in distribution using the Hartigan's Dip Statistic and Binomial Coefficient (BC) respectively (Fig. 16; see Appendix S1 for further details). This was most significant in the AM, ST, MG and FDL muscles amongst those studied here, with a potential error in $L_f$ of up to 203% recovered from the FDL due to a small initial $n$ (Table S14). This proposes interesting issues not only when predicting the functional behaviour of these muscles where whole muscle outputs are often informed by a single fibre length value, but also somewhat questions the conceptualisation of the muscle as a single actuator in general. Ultimately, the relatively low resolution ($2.96 \times 2.96 \times 6.5$ mm$^3$) and large field of view (proximal aspect of the iliac crest to the dorsal aspect of the foot) of the DT images in this study [particularly compared to Bolsterlee *et al.* (2018) who used a resolution of $1.875 \times 1.875 \times 5$ mm$^3$ to image the lower leg only] prevented the accurate separation of the different compartments of these muscles here. However elucidating the extent of architectural compartmentalisation within skeletal muscle and the potentially disparate functions of these compartments represents an important area of future research. This could build on current studies by combining different imaging and analysis methods such as higher resolution diffusion tensor imaging, fibre tractography, functional *in vivo* muscle imaging (i.e. shear wave elastography; Vigotsky, Rouse & Lee, 2020), high-density electromyography (Rojas-Martinez *et al.*, 2020) and musculoskeletal modelling fully to investigate the functional consequences of unique muscle architecture distributions within skeletal muscle.

## V CONCLUSIONS

(1) Extrapolations between fibre architecture and performance underpin our understanding of how muscles function and how they are adapted to power specific motions within and across species (Fig. 1). Here we provide a synopsis of how this fibre to function paradigm has been applied to understand muscle design, performance and adaptation in animals. Our review highlights the widespread application of the fibre to function paradigm across a diverse breadth of biological disciplines but also reveals a potential and highly prevalent limitation running through past studies. Specifically, we find that quantification of muscle architectural properties is almost universally based on an extremely small number of fibre measurements. Despite the volume of research into muscle properties, across a diverse breadth of research disciplines, the fundamental assumption that a small proportion of fibre measurements can accurately represent the architectural properties of a muscle has never been quantitatively tested.

(2) By combining DTI and deterministic fibre tractography (Bolsterlee *et al.*, 2019; Charles *et al.*, 2019a) we were able rapidly to generate a large number of fibre lengths for human lower limb muscles; more than 3500 in many muscles, which represents approximately two and a half times the highest number in any previous muscle study (Rosin & Nyakatura, 2017), and between 200 and 1666 times higher than the current standard observed in more than 80% of previous literature (Fig. 4A; Table S1). With this large data set were able to test, for the first time, the most basic assumptions commonly made when measuring muscle fibre lengths to calculate muscle force-generating properties, which are subsequently used to understand muscle functional behaviour in both qualitative (comparative) and quantitative contexts following the fibre to function paradigm (Fig. 1C).

(3) Through statistical subsampling simulations of our large fibre data sets, we demonstrate that the measurement of only a small number of fibres ($n < 25$) typical in previous studies may potentially realise extremely large errors in the characterisation of overall muscle architectural properties such as mean fibre length and physiological cross-sectional area (Figs 6–8), which are key determinants of muscle force production and function.

(4) Through dynamic musculoskeletal simulations of human walking and jumping, we demonstrate that the recovered errors in fibre architecture characterisation have significant implications for quantitative predictions of *in-vivo* dynamics and muscle function within a species (Figs 10–13).

(5) By applying data subsampling simulations to comparisons of muscle function in humans and chimpanzees, we demonstrate that error magnitudes significantly impact both qualitative and quantitative assessment of muscle specialisation, potentially generating highly erroneous conclusions about the absolute and relative adaption of muscles across species and evolutionary transitions (Fig. 14).

(6) These data and analyses demonstrate the importance of accurate fibre architecture measurements and the benefits of DTI and fibre tractography over more traditional dissection methods in allowing the relatively

rapid and automated measurement of a large set of muscle fibres in order to predict muscle functional behaviour. Future developments of MR imaging and tractography, and integration with *in-vivo* experimental measures and modelling approaches, will likely provide deeper insights into the functional consequences of complex and heterogenous muscle architecture distributions within skeletal muscle.

(7) The level of accuracy or reliability required for any analysis depends on the goals of the experiment or the specific hypotheses being tested. The effects of the number of fibres analysed per muscle derived herein provide general guidance in this respect for a number of metrics in healthy mammalian skeletal muscle that could be used to guide power analyses in future studies, alongside other data sets where high fibre numbers have been measured. Ideally, future work in this area will formally incorporate sample size considerations into experimental design.

## ACKNOWLEDGEMENTS

## VI. REFERENCES

References identified with an asterisk (*) are used only in the supporting information.

1. *ABOURACHID, A. (1993). Mechanics of standing in birds: functional explanation of lameness problems in giant turkeys. *British Poultry Science* **34**, 887–898.
2. *ABRAMS, G. D., WARD, S. R., FRIDÉN, J. & LIEBER, R. L. (2005). Pronator teres is an appropriate donor muscle for restoration of wrist and thumb extension. *The Journal of Hand Surgery* **30**, 1068–1073.
3. *ABRAMS, R. A., TSAI, A. M., WATSON, B., JAMALI, A. & LIEBER, R. L. (2000). Skeletal muscle recovery after tenotomy and 7-day delayed muscle length restoration. *Muscle & Nerve* **23**, 707–714.
4. ADAMS, N. F., RAYFIELD, E. J., COX, P. G., COBB, S. N. & CORFE, I. J. (2019). Functional tests of the competitive exclusion hypothesis for multituberculate extinction. *Royal Society Open Science* **6**, 181536.
5. *AL-AMOOD, W. S. & POPE, R. (1972). A comparison of the structural features of muscle fibres from a fast-and a slow-twitch muscle of the pelvic limb of the cat. *Journal of Anatomy* **113**, 49–60.
6. *ALEXANDER, R. M. (1974). The mechanics of jumping by a dog (*Canis familiaris*). *Journal of Zoology* **173**, 549–573.
7. *ALEXANDER, R. M. (1977). Allometry of the limbs of antelopes (Bovidae). *Journal of Zoology* **183**, 125–146.
8. ALEXANDER, R. M. (1995). Leg design and jumping technique for humans, other vertebrates and insects. *Philosophical Transactions of the Royal Society B-Biological Sciences* **347**, 235–248.
9. ALEXANDER, R. M. (2003). *Principles of Animal Locomotion*. Student edition. Princeton University Press, Princeton.
10. *ALEXANDER, R. M., DIMERY, N. J. & KER, R. F. (1985). Elastic structures in the back and their role in galloping in some mammals. *Journal of Zoology* **207**, 467–482.
11. ALEXANDER, R. M., JAYES, A. S., MALOIY, G. M. O. & WATHUTA, E. M. (1981). Allometry of the leg muscles of mammals. *Journal of Zoology* **194**, 539–552.
12. *ALEXANDER, R. M., MALOIY, G. M. O., KER, R. F., JAYES, A. S. & WARUI, C. N. (1982). The role of tendon elasticity in the locomotion of the camel (*Camelus dromedarius*). *Journal of Zoology* **198**, 293–313.
13. ALLEN, V., ELSEY, R. M., JONES, N., WRIGHT, J. & HUTCHINSON, J. R. (2010). Functional specialization and ontogenetic scaling of limb anatomy in *Alligator mississippiensis*. *Journal of Anatomy* **216**, 423–445.
14. ALLEN, V., MOLNAR, J., PARKER, W., POLLARD, A., NOLAN, G. & HUTCHINSON, J. R. (2014). Comparative architectural properties of limb muscles in Crocodylidae and Alligatoridae and their relevance to divergent use of asymmetrical gaits in extant Crocodylia. *Journal of Anatomy* **225**, 569–582.
15. ALLEN, V. R., KILBOURNE, B. M. & HUTCHINSON, J. R. (2021). The evolution of pelvic limb muscle moment arms in bird-line archosaurs. *Science Advances* **7**, eabe2778.
16. *AN, K. N., HUI, F. C., MORREY, B. F., LINSCHEID, R. L. & CHAO, E. Y. (1981). Muscles across the elbow joint: a biomechanical analysis. *Journal of Biomechanics* **14**, 659–669.
17. *ANAPOL, F. & BARRY, K. (1996). Fibre architecture of the extensors of the hindlimb in semiterrestrial and arboreal guenons. *American Journal of Physical Anthropology* **99**, 429–447.
18. ANAPOL, F. & GRAY, J. P. (2003). Fiber architecture of the intrinsic muscles of the shoulder and arm in semiterrestrial and arboreal guenons. *American Journal of Physical Anthropology* **122**, 51–65.
19. *ANAPOL, F., SHAHNOOR, N. & ROSS, C. F. (2008). Scaling of reduced physiologic cross-sectional area in primate muscles of mastication. In: *Primate Craniofacial Function and Biology* (eds C. VINYARD, M. J. RAVOSA and C. WALL). Springer, Boston.
20. *ANAPOL, F. C. & JUNGERS, W. L. (1986). Architectural and histochemical diversity within the quadriceps femoris of the brown lemur (*Lemur fulvus*). *American Journal of Physical Anthropology* **69**, 355–375.
21. *ANTÓN, S. C. (1999). Macaque masseter muscle: internal architecture, fibre length and cross-sectional area. *International Journal of Primatology* **20**, 441–462.
22. *ANTÓN, S. C. (2000). Macaque pterygoid muscles: internal architecture, fibre length, and cross-sectional area. *International Journal of Primatology* **21**, 131–156.
23. *AZIZI, E., BRAINERD, E. L. & ROBERTS, T. J. (2008). Variable gearing in pennate muscles. *Proceedings of the National Academy of Sciences of the United States of America* **105**, 1745–1750.
24. ARNOLD, E. M., WARD, S. R., LIEBER, R. L. & DELP, S. L. (2010). A model of the lower limb for analysis of human movement. *Annals of Biomedical Engineering* **38**, 269–279.
25. ASKEW, G. N. & MARSH, R. L. (1997). The effects of length trajectory on the mechanical power output of mouse skeletal muscles. *Journal of Experimental Biology* **200**, 3119–3131.
26. BAKER, J. H. & HALL-CRAGGS, E. C. B. (1978). Changes in length of sarcomeres following tenotomy of rat soleus muscle. *Anatomical Record* **192**, 55–58.
27. BARBER, L., BARRETT, R. & LICHTWARK, G. (2009). Validation of a freehand 3D ultrasound system for morphological measures of the medial gastrocnemius muscle. *Journal of Biomechanics* **42**, 1313–1319.
28. BARRETT, B. (1962). The length and mode of termination of individual muscle fibres in the human sartorius and posterior femoral muscles. *Acta Anatomica (Basel)* **48**, 242–257.
29. *BASSETT, R. W., BROWNE, A. O., MORREY, B. F. & AN, K. N. (1990). Glenohumeral muscle force and moment mechanics in a position of shoulder instability. *Journal of Biomechanics* **23**, 405–415.
30. BATES, K. T. & FALKINGHAM, P. L. (2012). Estimating maximum bite performance in *Tyrannosaurus rex* using multi-body dynamics. *Biology Letters* **8**, 660–664.
31. BATES, K. T. & FALKINGHAM, P. L. (2018). The importance of muscle architecture in biomechanical reconstructions of extinct animals: a case study using *Tyrannosaurus rex*. *Journal of Anatomy* **233**, 625–635.
32. BATES, K. T., FALKINGHAM, P. L., RARITY, F., HODGETTS, D., PURSLOW, A. & MANNING, P. L. (2010a). Application of high-resolution laser scanning and photogrammetric techniques to data acquisition, analysis and interpretation in palaeontology. *Proceedings of the ISPRS Commission V Mid-Term Symposium Close Range Image Measurement Techniques* **38**, 68–73.
33. BATES, K. T., MANNING, P. L., MARGETTS, L. & SELLERS, W. I. (2010b). Sensitivity analysis in evolutionary robotic simulations of bipedal dinosaur running. *Journal of Vertebrate Paleontology* **30**, 458–466.
34. BATES, K. T. & SCHACHNER, E. R. (2012). Disparity and convergence in bipedal archosaur locomotion. *Journal of the Royal Society Interface* **9**, 1339–1353.
35. BECERRA, F., ECHEVERRIA, A., VASSALLO, A. I. & CASINOS, A. (2011). Bite force and jaw biomechanics in the subterranean rodent Talas tuco-tuco (*Ctenomys talarum*) (Caviomorpha: Octodontoidea). *Canadian Journal of Zoology* **89**, 334–342.

36. *Becerra, F., Echeverría, A. I., Casinos, A. & Vassallo, A. I. (2014). Another one bites the dust: bite force and ecology in three caviomorph rodents (Rodentia, Hystricognathi). *Journal of Experimental Zoology Part A: Ecological Genetics and Physiology* **321**, 220–232.

37. *Benninghoff, A. & Rollhäuser, H. (1952). Zur inneren Mechanik des gefiederten Muskels. *Pflüger's Archiv für die gesamte Physiologie des Menschen und der Tiere* **254**, 527–548.

38. *Bergmann, P. J. & Hare-Drubka, M. (2015). Hindlimb muscle anatomical mechanical advantage differs among joints and stride phases in basilisk lizards. *Zoology* **118**, 291–298.

39. *Biewener, A. A. & Blickhan, R. (1988). Kangaroo rat locomotion: design for elastic energy storage or acceleration? *Journal of Experimental Biology* **140**, 243–255.

40. *Biewener, A. A. & Roberts, T. J. (2000). Muscle and tendon contributions to force, work, and elastic energy savings: a comparative perspective. *Exercise and Sports Science Reviews* **28**, 99–107.

41. *Biewener, A. A. (1998). Muscle-tendon stresses and elastic energy storage during locomotion in the horse. *Comparative Biochemistry and Physiology Part B: Biochemistry and Molecular Biology* **120**, 73–87.

42. *Biewener, A. A., Corning, W. R. & Tobalske, B. W. (1998a). *In vivo* pectoralis muscle force-length during level flight in pigeons (*Columba livia*). *Journal of Experimental Biology* **201**, 3293–3307.

43. *Biewener, A. A., Konieczynski, D. D. & Baudinette, R. V. (1998b). *In vivo* muscle force-length behavior during steady-speed hopping in tammar wallabies. *Journal of Experimental Biology* **201**, 1681–1694.

44. *Biewener, A. A., Mcgowan, C., Card, G. M. & Baudinette, R. V. (2004). Dynamics of leg muscle function in tammar wallabies (*M. eugenii*) during level versus incline hopping. *Journal of Experimental Biology* **207**, 211–223.

45. Bishop, P. J., Falisse, A., De Groote, F. & Hutchinson, J. R. (2021a). Predictive simulations of musculoskeletal function and jumping performance in a generalized bird. *Integrative Organismal Biology* **3**, obab006.

46. Bishop, P. J., Michel, K. B., Falisse, A., Cuff, A. R., Allen, V. R., De Groote, F. & Hutchinson, J. R. (2021b). Computational modelling of muscle fibre operating ranges in the hindlimb of a small ground bird (*Eudromia elegans*), with implications for modelling locomotion in extinct species. *PLoS Computational Biology* **17**, e1008843.

47. Bodine, S. C., Roy, R. R., Meadows, D. A., Zernicke, R. F., Sacks, R. D., Fournier, M. & Edgerton, V. R. (1982). Architectural, histochemical, and contractile characteristics of a unique biarticular muscle: the cat semitendinosus. *Journal of Neurophysiolgy* **48**, 192–201.

48. *Boettcher, M. L., Leonard, K. C., Dickinson, E., Aujard, F., Herrel, A. & Hartstone-Rose, A. (2020). The forearm musculature of the gray mouse lemur (*Microcebus murinus*): An ontogenetic study. *The Anatomical Record* **303**, 1354–1363.

49. Bohmer, C., Fabre, A. C., Herbin, M., Peigne, S. & Herrel, A. (2018). Anatomical basis of differences in locomotor behavior in martens: a comparison of the forelimb musculature between two sympatric species of *Martes*. *Anatomical Record* **301**, 449–472.

50. Bohmer, C., Fabre, A. C., Taverne, M., Herbin, M., Peigne, S. & Herrel, A. (2019). Functional relationship between myology and ecology in carnivores: do forelimb muscles reflect adaptations to prehension? *Biological Journal of the Linnean Society* **127**, 661–680.

51. Bolsterlee, B., D'Souza, A. & Herbert, R. D. (2019). Reliability and robustness of muscle architecture measurements obtained using diffusion tensor imaging with anatomically constrained tractography. *Journal of Biomechanics* **86**, 71–78.

52. Bolsterlee, B., Finni, T., D'Souza, A., Eguchi, J., Clarke, E. C. & Herbert, R. D. (2018). Three-dimensional architecture of the whole human soleus muscle in vivo. *PeerJ* **6**, e4610.

53. Bolsterlee, B., Veeger, H. E., van der Helm, F. C., Gandevia, S. C. & Herbert, R. D. (2015). Comparison of measurements of medial gastrocnemius architectural parameters from ultrasound and diffusion tensor images. *Journal of Biomechanics* **48**, 1133–1140.

54. *Brainerd, E. L. & Azizi, E. (2005). Muscle fibre angle, segment bulging and architectural gear ratio in segmented musculature. *Journal of Experimental Biology* **208**, 3249–3261.

55. Bramble, D. M. & Lieberman, D. E. (2004). Endurance running and the evolution of *Homo*. *Nature* **432**, 345–352.

56. *Brand, P. W., Beach, R. B. & Thompson, D. E. (1981). Relative tension and potential excursion of muscles in the forearm and hand. *Journal of Hand Surgery* **6**, 209–219.

57. *Breteler, M. D. K., Spoor, C. W. & Van Der Helm, F. C. (1999). Measuring muscle and joint geometry parameters of a shoulder for modeling purposes. *Journal of Biomechanics* **32**, 1191–1197.

58. *Busbey Iii, A. B. (1989). Form and function of the feeding apparatus of *Alligator mississippiensis*. *Journal of Morphology* **202**, 99–127.

59. Bribiesca-Contreras, F., Parslew, B. & Sellers, W. I. (2019). A quantitative and comparative analysis of the muscle architecture of the forelimb myology of diurnal birds of prey (order Accipitriformes and Falconiformes). *Anatomical Record-Advances in Integrative Anatomy and Evolutionary Biology* **302**, 1808–1823.

60. *Brown, N. A., Kawcak, C. E., McIlwraith, C. W. & Pandy, M. G. (2003). Architectural properties of distal forelimb muscles in horses, *Equus caballus*. *Journal of Morphology* **258**, 106–114.

61. Broyde, S., Dempsey, M., Wang, L. J., Cox, P. G., Fagan, M. & Bates, K. T. (2021). Evolutionary biomechanics: hard tissues and soft evidence? *Proceedings of the Royal Society B-Biological Sciences* **288**, 20202809.

62. Bulat, M., Korkmaz Can, N., Arslan, Y. Z. & Herzog, W. (2019). Musculoskeletal simulation tools for understanding mechanisms of lower-limb sports injuries. *Current Sports Medicine Reports* **18**, 210–216.

63. Burkholder, T. J., Fingado, B., Baron, S. & Lieber, R. L. (1994). Relationship between muscle fiber types and sizes and muscle architectural properties in the mouse hindlimb. *Journal of Morphology* **221**, 177–190.

64. Butcher, M. T., Chase, P. B., Hermanson, J. W., Clark, A. N., Brunet, N. M. & Bertram, J. E. A. (2010). Contractile properties of muscle fibers from the deep and superficial digital flexors of horses. *American Journal of Physiology-Regulatory Integrative and Comparative Physiology* **299**, R996–R1005.

65. Butcher, M. T., Rose, J. A., Glenn, Z. D., Tatomirovich, N. M., Russo, G. A., Foster, A. D., Smith, G. A. & Young, J. W. (2019). Ontogenetic allometry and architectural properties of the paravertebral and hindlimb musculature in Eastern cottontail rabbits (*Sylvilagus floridanus*): functional implications for developmental changes in locomotor performance. *Journal of Anatomy* **235**, 106–123.

66. Button, D. J., Barrett, P. M. & Rayfield, E. J. (2016). Comparative cranial myology and biomechanics of *Plateosaurus* and *Camarasaurus* and evolution of the sauropod feeding apparatus. *Palaeontology* **59**, 887–913.

67. Carlson, K. J. (2006). Muscle architecture of the common chimpanzee (Pan troglodytes): perspectives for investigating chimpanzee behavior. *Primates* **47**, 218–229.

68. Chambi-Trowell, S. A. V., Whiteside, D. I., Benton, M. J. & Rayfield, E. J. (2020). Biomechanical properties of the jaws of two species of Clevosaurus and a reanalysis of rhynchocephalian dentary morphospace. *Palaeontology* **63**, 919–939.

69. Channon, S. B., Young, I. S., Cordner, B. & Swann, N. (2019). Ontogenetic scaling of pelvic limb muscles, tendons and locomotor economy in the ostrich (*Struthio camelus*). *Journal of Experimental Biology* **222**, jeb182741.

70. Charles, J. P., Cappellari, O. & Hutchinson, J. R. (2018). A dynamic simulation of musculoskeletal function in the mouse hindlimb during trotting locomotion. *Frontiers in Bioengineering and Biotechnology* **6**, 61. https://doi.org/10.3389/fbioe.2018.00061

71. Charles, J. P., Cappellari, O., Spence, A. J., Hutchinson, J. R. & Wells, D. J. (2016a). Musculoskeletal geometry, muscle architecture and functional specialisations of the mouse hindlimb. *PLoS One* **11**, e0147669.

72. Charles, J. P., Cappellari, O., Spence, A. J., Wells, D. J. & Hutchinson, J. R. (2016b). Muscle moment arms and sensitivity analysis of a mouse hindlimb musculoskeletal model. *Journal of Anatomy* **229**, 514–535.

73. Charles, J. P., Fu, F. H. & Anderst, W. J. (2021). Predictions of anterior cruciate ligament dynamics from subject-specific musculoskeletal models and dynamic biplane radiography. *Journal of Biomechanical Engineering* **143**, 031006.

74. Charles, J. P., Grant, B., D'Aout, K. & Bates, K. T. (2020). Subject-specific muscle properties from diffusion tensor imaging significantly improve the accuracy of musculoskeletal models. *Journal of Anatomy* **237**, 941–959.

75. Charles, J. P., Moon, C. H. & Anderst, W. (2019a). Determining subject-specific lower-limb muscle architecture data for musculoskeletal models using diffusion tensor MRI. *Journal of Biomechanical Engineering* **141**, 060905.

76. Charles, J. P., Suntaxi, F. & Anderst, W. J. (2019b). In vivo human lower limb muscle architecture dataset obtained using diffusion tensor imaging. *PLoS One* **14**, e0223531.

77. *Cheng, E. J. & Scott, S. H. (2000). Morphometry of *Macaca mulatta* forelimb. I. Shoulder and elbow muscles and segment inertial parameters. *Journal of Morphology* **245**, 206–224.

78. Close, R. (1969). Dynamic properties of fast and slow skeletal muscles of rat after nerve cross-union. *Journal of Physiology* **204**, 331–346.

79. Close, R. I. (1972). Relations between sarcomere length and characteristics of isometric twitch contractions of frog sartorius muscle. *Journal of Physiology-London* **220**, 745–762.

80. Collings, A. J. & Richards, C. T. (2019). Digital dissection of the pelvis and hindlimb of the red-legged running frog, *Phlyctimantis maculatus*, using Diffusible Iodine Contrast Enhanced computed microtomography (DICE mu CT). *PeerJ* **7**, e7003.

81. Cost, I. N., Middleton, K. M., Sellers, K. C., Echols, M. S., Witmer, L. M., Davis, J. L. & Holliday, C. M. (2020). Palatal

biomechanics and its significance for cranial kinesis in *Tyrannosaurus rex*. *Anatomical Record-Advances in Integrative Anatomy and Evolutionary Biology* **303**, 999–1017.

82. *Cox, P. G. & Baverstock, H. (2016). Masticatory muscle anatomy and feeding efficiency of the American beaver, *Castor canadensis* (Rodentia, Castoridae). *Journal of Mammalian Evolution* **23**, 191–200.

83. Crompton, R. H., Pataky, T. C., Savage, R., D'Aout, K., Bennett, M. R., Day, M. H., Bates, K., Morse, S. & Sellers, W. I. (2012). Human-like external function of the foot, and fully upright gait, confirmed in the 3.66 million year old Laetoli hominin footprints by topographic statistics, experimental footprint-formation and computer simulation. *Journal of the Royal Society Interface* **9**, 707–719.

84. Crook, T. C., Cruickshank, S. E., McGowan, C. M., Stubbs, N., Wakeling, J. M., Wilson, A. M. & Payne, R. C. (2008). Comparative anatomy and muscle architecture of selected hind limb muscles in the Quarter Horse and Arab. *Journal of Anatomy* **212**, 144–152.

85. Crow, M. T. & Kushmerick, M. J. (1982). Chemical energetics of slow-twitch and fast-twitch muscles of the mouse. *Journal of General Physiology* **79**, 147–166.

86. Cuff, A. R., Sparkes, E. L., Randau, M., Pierce, S. E., Kitchener, A. C., Goswami, A. & Hutchinson, J. R. (2016a). The scaling of postcranial muscles in cats (Felidae) I: forelimb, cervical, and thoracic muscles. *Journal of Anatomy* **229**, 128–141.

87. *Cuff, A. R., Sparkes, E. L., Randau, M., Pierce, S. E., Kitchener, A. C., Goswami, A. & Hutchinson, J. R. (2016b). The scaling of postcranial muscles in cats (Felidae) II: hindlimb and lumbosacral muscles. *Journal of Anatomy* **229**, 142–152.

88. *Curtin, N. A. & Edman, K. A. (1994). Force-velocity relation for frog muscle fibres: effects of moderate fatigue and of intracellular acidification. *The Journal of Physiology* **475**, 483–494.

89. *Curtin, N. A. & Woledge, R. C. (1988). Power output and force-velocity relationship of live fibres from white myotomal muscle of the dogfish, *Scyliorhinus canicula*. *Journal of Experimental Biology* **140**, 187–197.

90. Curtis, N., Jones, M. E. H., Evans, S. E., Shi, J. F., O'Higgins, P. & Fagan, M. J. (2010). Predicting muscle activation patterns from motion and anatomy: modelling the skull of Sphenodon (Diapsida: Rhynchocephalia). *Journal of the Royal Society Interface* **7**, 153–160.

91. Cutts, A. (1988). The range of sarcomere lengths in the muscles of the human lower limb. *Journal of Anatomy* **160**, 79–88.

92. *Cutts, A., Alexander, R. M. & Ker, R. F. (1991). Ratios of cross-sectional areas of muscles and their tendons in a healthy human forearm. *Journal of Anatomy* **176**, 133–137.

93. D'Souza, A., Bolsterlee, B., Lancaster, A. & Herbert, R. D. (2019). Muscle architecture in children with cerebral palsy and ankle contractures: an investigation using diffusion tensor imaging. *Clinical Biomechanics* **68**, 205–211.

94. Daley, M. A., Felix, G. & Biewener, A. A. (2007). Running stability is enhanced by a proximo-distal gradient in joint neuromechanical control. *Journal of Experimental Biology* **210**, 383–394.

95. Damon, B. M., Froeling, M., Buck, A. K., Oudeman, J., Ding, Z., Nederveen, A. J., Bush, E. C. & Strijkers, G. J. (2016). Skeletal muscle diffusion tensor-MRI fiber tracking: rationale, data acquisition and analysis methods, applications and future directions. *NMR in Biomedicine* **30**, e3563. https://doi.org/10.1002/nbm.3563

96. Damsgaard, M., Rasmussen, J., Christensen, S. T., Surma, E. & de Zee, M. (2006). Analysis of musculoskeletal systems in the AnyBody Modeling System. *Simulation Modelling Practice and Theory* **14**, 1100–1111.

97. *Davis, J. L., Santana, S. E., Dumont, E. R. & Grosse, I. R. (2010). Predicting bite force in mammals: two-dimensional versus three-dimensional lever models. *Journal of Experimental Biology* **213**, 1844–1851.

98. De Ruiter, C. J., De Haan, A. & Sargeant, A. J. (1995). Physiological characteristics of two extreme muscle compartments in gastrocnemius medialis of the anaesthetized rat. *Acta Physiologica Scandinavica* **153**, 313–324.

99. *De Souza Junior, P., Santos, L. M. R. P. D., Viotto-Souza, W., De Carvalho, N. D. C., Souza, E. C., Kasper, C. B., Abidu-Figueiredo, M. & Santos, A. L. Q. (2018). Functional myology of the thoracic limb in Pampas fox (*Lycalopex gymnocercus*): a descriptive and comparative analysis. *Journal of Anatomy* **233**, 783–806.

100. Dick, T. J. M., Biewener, A. A. & Wakeling, J. M. (2017). Comparison of human gastrocnemius forces predicted by Hill-type muscle models and estimated from ultrasound images. *Journal of Experimental Biology* **220**, 1643–1653.

101. *Dick, T. J. & Clemente, C. J. (2016). How to build your dragon: scaling of muscle architecture from the world's smallest to the world's largest monitor lizard. *Frontiers in Zoology* **13**, 8.

102. *Dickinson, E., Basham, C., Rana, A. & Hartstone-Rose, A. (2019). Visualization and quantification of digitally dissected muscle fascicles in the masticatory muscles of *Callithrix jacchus* using nondestructive diceCT. *The Anatomical Record* **302**, 1891–1900.

103. Dickinson, E., Stark, H. & Kupczik, K. (2018). Non-destructive determination of muscle architectural variables through the use of DiceCT. *Anatomical Record-Advances in Integrative Anatomy and Evolutionary Biology* **301**, 363–377.

104. *Edman, K. A. P., Elzinga, G. & Noble, M. I. (1978). Enhancement of mechanical performance by stretch during tetanic contractions of vertebrate skeletal muscle fibres. *The Journal of Physiology* **281**, 139–155.

105. *Edman, K. A. P. & Mattiazzi, A. R. (1981). Effects of fatigue and altered pH on isometric force and velocity of shortening at zero load in frog muscle fibres. *Journal of Muscle Research & Cell Motility* **2**, 321–334.

106. Ellis, R. G., Rankin, J. W. & Hutchinson, J. R. (2018). Limb kinematics, kinetics and muscle dynamics during the sit-to-stand transition in greyhounds. *Frontiers in Bioengineering and Biotechnology* **6**, 162. https://doi.org/10.3389/fbioe.2018.00162

107. Eng, C. M., Smallwood, L. H., Rainiero, M. P., Lahey, M., Ward, S. R. & Lieber, R. L. (2008). Scaling of muscle architecture and fiber types in the rat hindlimb. *Journal of Experimental Biology* **211**, 2336–2345.

108. *Ettema, G. J. & Huijing, P. A. (1989). Properties of the tendinous structures and series elastic component of EDL muscle-tendon complex of the rat. *Journal of Biomechanics* **22**, 1209–1215.

109. *Fabre, P. H., Herrel, A., Fitriana, Y., Meslin, L. & Hautier, L. (2017). Masticatory muscle architecture in a water-rat from Australasia (Murinae, *Hydromys*) and its implication for the evolution of carnivory in rodents. *Journal of Anatomy* **231**, 380–397.

110. Fahn-Lai, P., Biewener, A. A. & Pierce, S. E. (2020). Broad similarities in shoulder muscle architecture and organization across two amniotes: implications for reconstructing non-mammalian synapsids. *PeerJ* **8**, e8556.

111. *Falkingham, P. (2012). Acquisition of high resolution three-dimensional models using free, open-source, photogrammetric software. *Palaeontologia Electronica* **15**, 1T:15p.

112. *Felder, A., Ward, S. R. & Lieber, R. L. (2005). Sarcomere length measurement permits high resolution normalization of muscle fibre length in architectural studies. *Journal of Experimental Biology* **208**, 3275–3279.

113. *Franklin, C. E. & Johnston, I. A. (1997). Muscle power output during escape responses in an Antarctic fish. *Journal of Experimental Biology* **200**, 703–712.

114. *Freeman, J. B. & Dale, R. (2013). Assessing bimodality to detect the presence of a dual cognitive process. *Behavior Research Methods* **45**, 83–97. https://doi.org/10.3758/s13428-012-0225-x

115. *Fridén, J. & Lieber, R. L. (2001). Quantitative evaluation of the posterior deltoid to triceps tendon transfer based on muscle architectural properties. *The Journal of Hand Surgery* **26**, 147–155.

116. Friederich, J. A. & Brand, R. A. (1990). Muscle fiber architecture in the human lower limb. *Journal of Biomechanics* **23**, 91–95.

117. Froeling, M., Nederveen, A. J., Heijtel, D. F., Lataster, A., Bos, C., Nicolay, K., Maas, M., Drost, M. R. & Strijkers, G. J. (2012). Diffusion-tensor MRI reveals the complex muscle architecture of the human forearm. *Journal of Magnetic Resonance Imaging* **36**, 237–248.

118. Froeling, M., Oudeman, J., Strijkers, G. J., Maas, M., Drost, M. R., Nicolay, K. & Nederveen, A. J. (2015). Muscle changes detected with diffusion-tensor imaging after long-distance running. *Radiology* **274**, 548–562.

119. *Fukunaga, T., Ichinose, Y., Ito, M., Kawakami, Y. & Fukashiro, S. (1997). Determination of fascicle length and pennation in a contracting human muscle *in vivo*. *Journal of Applied Physiology* **82**, 354–358.

120. *Furuuchi, K., Koyabu, D., Mori, K. & Endo, H. (2013). Physiological cross-sectional area of the masticatory muscles in the giraffe (*Giraffa camelopardalis*). *Mammal Study* **38**, 67–71.

121. *Gans, C., Loeb, G. E. & De Vree, F. (1989). Architecture and consequent physiological properties of the semitendinosus muscle in domestic goats. *Journal of Morphology* **199**, 287–297.

122. Gatesy, S. M. (1990). Caudofemoral musculature and the evolution of theropod locomotion. *Paleobiology* **16**, 170–186.

123. Gatesy, S. M. (1991a). Hind-limb movements of the American alligator (Alligator-mississippiensis) and postural grades. *Journal of Zoology* **224**, 577–588.

124. Gatesy, S. M. (1991b). Hind-limb scaling in birds and other theropods - implications for terrestrial locomotion. *Journal of Morphology* **209**, 83–96.

125. *Gellman, K. S., Bertram, J. E. A. & Hermanson, J. W. (2002). Morphology, histochemistry, and function of epaxial cervical musculature in the horse (*Equus caballus*). *Journal of Morphology* **251**, 182–194.

126. *Gewaily, M. S., Fayed, M. H. & Farrag, F. A. (2017). The architectural and functional specifications of intrinsic muscles of the fore limb of the Egyptian Baladi goats (*Capra hircus*). *Alexandria Journal of Veterinary Sciences* **55**, 110–124.

127. Gignac, P. M. & Erickson, G. M. (2017). The biomechanics behind extreme osteophagy in *Tyrannosaurus rex*. *Integrative and Comparative Biology* **57**, E272.

128. Gignac, P. M., Kley, N. J., Clarke, J. A., Colbert, M. W., Morhardt, A. C., Cerio, D., Cost, I. N., Cox, P. G., Daza, J. D., Early, C. M., Echols, M. S., Henkelman, R. M., Herdina, A. N.,

HOLLIDAY, C. M., LI, Z., et al. (2016). Diffusible iodine-based contrast-enhanced computed tomography (diceCT): an emerging tool for rapid, high-resolution, 3-D imaging of metazoan soft tissues. *Journal of Anatomy* **228**, 889–909.

129. GINOT, S., HERREL, A., CLAUDE, J. & HAUTIER, L. (2018). Skull size and biomechanics are good estimators of in vivo bite force in murid rodents. *Anatomical Record-Advances in Integrative Anatomy and Evolutionary Biology* **301**, 256–266.

130. *GLENN, Z. D., FOSTER, A. D., YOUNG, J. W., SMITH, G. A. & BUTCHER, M. T. (2015). Ontogeny of locomotor performance in Eastern cottontail rabbits: muscle architecture and fibre type of the vertebral extensor muscles. *Integrative Comparative Biology* **55**, E236.

131. *GOETZ, J. E., DERRICK, T. R., PEDERSEN, D. R., ROBINSON, D. A., CONZEMIUS, M. G., BAER, T. E. & BROWN, T. D. (2008). Hip joint contact force in the emu (*Dromaius novaehollandiae*) during normal level walking. *Journal of Biomechanics* **41**, 770–778.

132. *GOH, C., BLANCHARD, M. L., CROMPTON, R. H., GUNTHER, M. M., MACAULAY, S. & BATES, K. T. (2017). A 3D musculoskeletal model of the western lowland gorilla hind limb: moment arms and torque of the hip, knee and ankle. *Journal of Anatomy* **231**, 568–584.

133. GOLLNICK, P. D., TIMSON, B. F., MOORE, R. L. & RIEDY, M. (1981). Muscular enlargement and number of fibers in skeletal muscles of rats. *Journal of Applied Physiology: Respiratory, Environmental and Exercise Physiology* **50**, 936–943.

134. GONZALES, J. M., GALPIN, A. J., MONTGOMERY, M. M. & PAMUKOFF, D. N. (2019). Comparison of lower limb muscle architecture and geometry in distance runners with rearfoot and forefoot strike pattern. *Journal of Sports Sciences* **37**, 2184–2190.

135. GRABKE, E. P., MASANI, K. & ANDRYSEK, J. (2019). Lower limb assistive device design optimization using musculoskeletal modeling: a review. *Journal of Medical Devices-Transactions of the Asme* **13**, 040801. https://doi.org/10.1115/1.4044739

136. GRONING, F., JONES, M. E., CURTIS, N., HERREL, A., O'HIGGINS, P., EVANS, S. E. & FAGAN, M. J. (2013). The importance of accurate muscle modelling for biomechanical analyses: a case study with a lizard skull. *Journal of the Royal Society Interface* **10**, 20130216.

137. *HARTIGAN, P. M. (1985). Computation of the dip statistic to test for unimodality. *Journal of the Royal Statistical Society Series C-Applied Statistics* **34**, 320–325.

138. HARTSTONE-ROSE, A., DEUTSCH, A. R., LEISCHNER, C. L. & PASTOR, F. (2018). Dietary correlates of primate masticatory muscle fiber architecture. *Anatomical Record-Advances in Integrative Anatomy and Evolutionary Biology* **301**, 311–324.

139. HARTSTONE-ROSE, A., HERTZIG, I. & DICKINSON, E. (2019). Bite force and masticatory muscle architecture adaptations in the dietarily diverse Musteloidea (Carnivora). *Anatomical Record-Advances in Integrative Anatomy and Evolutionary Biology* **302**, 2287–2299.

140. HARTSTONE-ROSE, A., PERRY, J. M. G. & MORROW, C. J. (2012). Bite force estimation and the fiber architecture of felid masticatory muscles. *Anatomical Record-Advances in Integrative Anatomy and Evolutionary Biology* **295**, 1336–1351.

141. HENRIKSSON-LARSEN, K. B., LEXELL, J. & SJOSTROM, M. (1983). Distribution of different fibre types in human skeletal muscles. I. Method for the preparation and analysis of cross-sections of whole tibialis anterior. *The Histochemical Journal* **15**, 167–178.

142. *HERMANSON, J. W. & COBB, M. A. (1992). Four forearm flexor muscles of the horse, *Equus caballus*: anatomy and histochemistry. *Journal of Morphology* **212**, 269–280.

143. HERMANSON, J. W. & HURLEY, K. J. (1990). Architectural and histochemical analysis of the biceps brachii muscle of the horse. *Acta Anatomica* **137**, 146–156.

144. HERREL, A., DE SMET, A., AGUIRRE, L. F. & AERTS, P. (2008). Morphological and mechanical determinants of bite force in bats: do muscles matter? *Journal of Experimental Biology* **211**, 86–91.

145. HILL, A. V. (1938). The heat of shortening and the dynamic constants of muscle. *Proceedings of the Royal Society Series B-Biological Sciences* **126**, 136–195.

146. *HORSMAN, M. K., KOOPMAN, H. F., VAN DER HELM, F. C., PROSÉ, L. P. & VEEGER, H. E. J. (2007). Morphological muscle and joint parameters for musculoskeletal modelling of the lower extremity. *Clinical Biomechanics* **22**, 239–247.

147. HOSSEINI NASAB, S. H., SMITH, C. R., SCHUTZ, P., DAMM, P., TREPCZYNSKI, A., LIST, R. & TAYLOR, W. R. (2020). Length-change patterns of the collateral ligaments during functional activities after total knee arthroplasty. *Annals of Biomedical Engineering* **48**, 1396–1406.

148. *HUBER, D. R., DEAN, M. N. & SUMMERS, A. P. (2008). Hard prey, soft jaws and the ontogeny of feeding mechanics in the spotted ratfish *Hydrolagus colliei*. *Journal of the Royal Society Interface* **5**, 941–953.

149. HUDSON, P. E., CORR, S. A., PAYNE-DAVIS, R. C., CLANCY, S. N., LANE, E. & WILSON, A. M. (2011a). Functional anatomy of the cheetah (*Acinonyx jubatus*) forelimb. *Journal of Anatomy* **218**, 375–385.

150. HUDSON, P. E., CORR, S. A., PAYNE-DAVIS, R. C., CLANCY, S. N., LANE, E. & WILSON, A. M. (2011b). Functional anatomy of the cheetah (*Acinonyx jubatus*) hindlimb. *Journal of Anatomy* **218**, 363–374.

151. *HUQ, E., WALL, C. E. & TAYLOR, A. B. (2015). Epaxial muscle fibre architecture favors enhanced excursion and power in the leaper *Galago senegalensis*. *Journal of Anatomy* **227**, 524–540.

152. *HUTCHINSON, J. R. (2004a). Biomechanical modeling and sensitivity analysis of bipedal running ability. I. Extant taxa. *Journal of Morphology* **262**, 421–440.

153. HUTCHINSON, J. R. (2004b). Biomechanical modeling and sensitivity analysis of bipedal running ability. II. Extinct taxa. *Journal of Morphology* **262**, 441–461.

154. HUTCHINSON, J. R. & GATESY, S. M. (2000). Adductors, abductors, and the evolution of archosaur locomotion. *Paleobiology* **26**, 734–751.

155. *JACOBSON, M. D., RAAB, R., FAZELI, B. M., ABRAMS, R. A., BOTTE, M. J. & LIEBER, R. L. (1992). Architectural design of the human intrinsic hand muscles. *The Journal of Hand Surgery* **17**, 804–809.

156. JAMES, R. S., ALTRINGHAM, J. D. & GOLDSPINK, D. F. (1995). The mechanical properties of fast and slow skeletal muscles of the mouse in relation to their locomotory function. *Journal of Experimental Biology* **198**, 491–502.

157. *JAYES, A. S. & ALEXANDER, R. M. (1982). Estimates of mechanical stresses in leg muscles of galloping Greyhounds (*Canis familiaris*). *Journal of Zoology* **198**, 315–328.

158. JENKINS, T. & BRYANT, M. (2019). Variable stiffness soft robotics using pennate muscle architecture. *Bioinspiration, Biomimetics, and Bioreplication IX* **10965**, 1096505. https://doi.org/10.1117/12.2514265

159. *JUUL-KRISTENSEN, B., BOJSEN-MØLLER, F., FINSEN, L., ERIKSSON, J., JOHANSSON, G., STÅHLBERG, F. & EKDAHL, C. (2000). Muscle sizes and moment arms of rotator cuff muscles determined by magnetic resonance imaging. *Cells, Tissues, Organs* **167**, 214–222.

160. *KAMIBAYASHI, L. K. & RICHMOND, F. J. (1998). Morphometry of human neck muscles. *Spine* **23**, 1314–1323.

161. *KAWAKAMI, Y., ABE, T., KUNO, S. Y. & FUKUNAGA, T. (1995). Training-induced changes in muscle architecture and specific tension. *European Journal of Applied Physiology and Occupational Physiology* **72**, 37–43.

162. *KEATING, J. F., WATERWORTH, P., SHAW-DUNN, J. & CROSSAN, J. (1993). The relative strengths of rotator cuff muscles. A cadaver study. *Journal of Bone and Joint Surgery* **75**, 137–140.

163. *KER, R. F., ALEXANDER, R. M. & BENNETT, M. B. (1988). Why are mammalian tendons so thick? *Journal of Zoology* **216**, 309–324.

164. *KIKUCHI, Y. (2009). Quantitative analysis of variation in muscle internal parameters in crab-eating macaques (*Macaca fascicularis*). *Anthropological Science* **118**, 9–21.

165. *KIKUCHI, Y. (2010). Comparative analysis of muscle architecture in primate arm and forearm. *Anatomia, Histologia, Embryologia* **39**, 93–106.

166. KIM, S. Y., BOYNTON, E. L., RAVICHANDIRAN, K., FUNG, L. Y., BLEAKNEY, R. & AGUR, A. M. (2007). Three-dimensional study of the musculotendinous architecture of supraspinatus and its functional correlations. *Clinical Anatomy* **20**, 648–655.

167. KISSANE, R. W. P., EGGINTON, S. & ASKEW, G. N. (2018). Regional variation in the mechanical properties and fibre-type composition of the rat extensor digitorum longus muscle. *Experimental Physiology* **103**, 111–124.

168. KUPCZIK, K., STARK, H., MUNDRY, R., NEININGER, F. T., HEIDLAUF, T. & ROHRLE, O. (2015). Reconstruction of muscle fascicle architecture from iodine-enhanced microCT images: a combined texture mapping and streamline approach. *Journal of Theoretical Biology* **382**, 34–43.

169. LAI, A. K. M., BIEWENER, A. A. & WAKELING, J. M. (2019). Muscle-specific indices to characterise the functional behaviour of human lower-limb muscles during locomotion. *Journal of Biomechanics* **89**, 134–138.

170. LAMAS, L. P., MAIN, R. P. & HUTCHINSON, J. R. (2014). Ontogenetic scaling patterns and functional anatomy of the pelvic limb musculature in emus (*Dromaius novaehollandiae*). *PeerJ* **2**, e716.

171. LANGENBACH, G. E. & WEIJS, W. A. (1990). Growth patterns of the rabbit masticatory muscles. *Journal of Dental Research* **69**, 20–25.

172. *LANGENDERFER, J. E., CARPENTER, J. E., JOHNSON, M. E., AN, K. N. & HUGHES, R. E. (2006). A probabilistic model of glenohumeral external rotation strength for healthy normals and rotator cuff tear cases. *Annals of Biomedical Engineering* **34**, 465–476.

173. *LANGENDERFER, J., JERABEK, S. A., THANGAMANI, V. B., KUHN, J. E. & HUGHES, R. E. (2004). Musculoskeletal parameters of muscles crossing the shoulder and elbow and the effect of sarcomere length sample size on estimation of optimal muscle length. *Clinical Biomechanics* **19**, 664–670.

174. LEISCHNER, C. L., CROUCH, M., ALLEN, K. L., MARCHI, D., PASTOR, F. & HARTSTONE-ROSE, A. (2018). Scaling of primate forearm muscle architecture as it relates to locomotion and posture. *Anatomical Record-Advances in Integrative Anatomy and Evolutionary Biology* **301**, 484–495.

175. *LEONARD, K. C., BOETTCHER, M. L., DICKINSON, E., MALHOTRA, N., AUJARD, F., HERREL, A. & HARTSTONE-ROSE, A. (2020). The ontogeny of

masticatory muscle architecture in *Microcebus murinus*. *The Anatomical Record* **303**, 1364–1373.

176. LEXELL, J., DOWNHAM, D. & SJOSTROM, M. (1986). Distribution of different fibre types in human skeletal muscles. Fibre type arrangement in m. vastus lateralis from three groups of healthy men between 15 and 83 years. *Journal of the Neurological Sciences* **72**, 211–222.

177. *LICHTWARK, G. A., BOUGOULIAS, K. & WILSON, A. M. (2007). Muscle fascicle and series elastic element length changes along the length of the human gastrocnemius during walking and running. *Journal of Biomechanics* **40**, 157–164.

178. LICHTWARK, G. A., FARRIS, D. J., CHEN, X., HODGES, P. W. & DELP, S. L. (2018). Microendoscopy reveals positive correlation in multiscale length changes and variable sarcomere lengths across different regions of human muscle. *Journal of Applied Physiology* **125**, 1812–1820.

179. *LICHTWARK, G. A. & WILSON, A. M. (2006). Interactions between the human gastrocnemius muscle and the Achilles tendon during incline, level and decline locomotion. *Journal of Experimental Biology* **209**, 4379–4388.

180. LIEBER, R. L. & BLEVINS, F. T. (1989). Skeletal muscle architecture of the rabbit hindlimb: functional implications of muscle design. *Journal of Morphology* **199**, 93–101.

181. *LIEBER, R. L. & BOAKES, J. L. (1988). Sarcomere length and joint kinematics during torque production in frog hindlimb. *American Journal of Physiology-Cell Physiology* **254**, C759–C768.

182. LIEBER, R. L. & BROWN, C. G. (1992). Sarcomere length-joint angle relationships of seven frog hindlimb muscles. *Acta Anatomica* **145**, 289–295.

183. LIEBER, R. L., FAZELI, B. M. & BOTTE, M. J. (1990). Architecture of selected wrist flexor and extensor muscles. *Journal of Hand Surgery-American Volume* **15a**, 244–250.

184. LIEBER, R. L. & FRIDÉN, J. (2000). Functional and clinical significance of skeletal muscle architecture. *Muscle & Nerve* **23**, 1647–1666.

185. *LIEBER, R. L., JACOBSON, M. D., FAZELI, B. M., ABRAMS, R. A. & BOTTE, M. J. (1992). Architecture of selected muscles of the arm and forearm: anatomy and implications for tendon transfer. *The Journal of Hand Surgery* **17**, 787–798.

186. LIEBER, R. L. & SHOEMAKER, S. D. (1992). Muscle, joint, and tendon contributions to the torque profile of frog hip-joint. *American Journal of Physiology* **263**, R586–R590.

187. LOEB, G. E., PRATT, C. A., CHANAUD, C. M. & RICHMOND, F. J. R. (1987). Distribution and innervation of short, interdigitated muscle-fibers in parallel-fibered muscles of the cat hindlimb. *Journal of Morphology* **191**, 1–15.

188. LOMBARDI, V. & PIAZZESI, G. (1990). The contractile response during steady lengthening of stimulated frog-muscle fibers. *Journal of Physiology-London* **431**, 141–171.

189. *LOWIE, A., GILLET, E., VANHOOYDONCK, B., IRSCHICK, D. J., LOSOS, J. B. & HERREL, A. (2019). Do the relationships between hindlimb anatomy and sprint speed variation differ between sexes in Anolis lizards? *Journal of Experimental Biology* **222**, jeb188805.

190. LUFF, A. R. (1981). Dynamic properties of the inferior rectus, extensor digitorum longus, diaphragm and soleus muscles of the mouse. *Journal of Physiology-London* **313**, 161–171.

191. *MACLAREN, J. A. & MCHORSE, B. K. (2020). Comparative forelimb myology and muscular architecture of a juvenile Malayan tapir (*Tapirus indicus*). *Journal of Anatomy* **236**, 85–97.

192. *MAGANARIS, C. N., BALTZOPOULOS, V. & SARGEANT, A. J. (1998). *In vivo* measurements of the triceps surae complex architecture in man: implications for muscle function. *The Journal of Physiology* **512**, 603–614.

193. MALOIY, G. M. O., ALEXANDER, R. M., NJAU, R. & JAYES, A. S. (1979). Allometry of the legs of running birds. *Journal of Zoology* **187**, 161–167.

194. MANAL, K. & BUCHANAN, T. (2004). Subject-specific estimates of tendon slack length: a numerical method. *Journal of Applied Biomechanics* **20**, 195–203.

195. *MARCHI, D., LEISCHNER, C. L., PASTOR, F. & HARTSTONE-ROSE, A. (2018). Leg muscle architecture in primates and its correlation with locomotion patterns. *The Anatomical Record* **301**, 515–527.

196. *MARTIN, D. C., MEDRI, M. K., CHOW, R. S., OXORN, V., LEEKAM, R. N., AGUR, A. M. & MCKEE, N. H. (2001). Comparing human skeletal muscle architectural parameters of cadavers with *in vivo* ultrasonographic measurements. *Journal of Anatomy* **199**, 429–434.

197. *MARTIN, M. L., WARBURTON, N. M., TRAVOUILLON, K. J. & FLEMING, P. A. (2019). Mechanical similarity across ontogeny of digging muscles in an Australian marsupial (*Isoodon fusciventer*). *Journal of Morphology* **280**, 423–435.

198. *MATHEWSON, M. A., CHAPMAN, M. A., HENTZEN, E. R., FRIDÉN, J. & LIEBER, R. L. (2012). Anatomical, architectural, and biochemical diversity of the murine forelimb muscles. *Journal of Anatomy* **221**, 443–451.

199. *MATHEWSON, M. A., KWAN, A., ENG, C. M., LIEBER, R. L. & WARD, S. R. (2014). Comparison of rotator cuff muscle architecture between humans and other selected vertebrate species. *Journal of Experimental Biology* **217**, 261–273.

200. *MAXWELL, L. C., FAULKNER, J. A. & HYATT, G. J. (1974). Estimation of number of fibres in Guinea pig skeletal muscles. *Journal of Applied Physiology* **37**, 259–264.

201. *MCCLEARN, D. (1985). Anatomy of raccoon (*Procyon lotor*) and coati (*Nasua narica* and *N. nasua*) forearm and leg muscles: relations between fibre length, moment-arm length, and joint-angle excursion. *Journal of Morphology* **183**, 87–115.

202. *MEDLER, S. (2002). Comparative trends in shortening velocity and force production in skeletal muscles. *American Journal of Physiology- Regulatory, Integrative and Comparative Physiology* **283**, R368–R378.

203. MEYERS, J. J., NISHIKAWA, K. C. & HERREL, A. (2018). The evolution of bite force in horned lizards: the influence of dietary specialization. *Journal of Anatomy* **232**, 214–226.

204. *MICHILSENS, F., VEREECKE, E. E., D'AOÛT, K. & AERTS, P. (2009). Functional anatomy of the gibbon forelimb: adaptations to a brachiating lifestyle. *Journal of Anatomy* **215**, 335–354.

205. *MOORE, A. L. (2011). *Functional Specialization in the Intrinsic Forelimb Musculature of the American Badger (Taxidea taxus)*. Youngstown State University, Youngstown, OH, pp. 75.

206. *MOORE, A. L., BUDNY, J. E., RUSSELL, A. P. & BUTCHER, M. T. (2013). Architectural specialization of the intrinsic thoracic limb musculature of the American badger (*Taxidea taxus*). *Journal of Morphology* **274**, 35–48.

207. MYATT, J. P., CROMPTON, R. H., PAYNE-DAVIS, R. C., VEREECKE, E. E., ISLER, K., SAVAGE, R., D'AOUT, K., GUNTHER, M. M. & THORPE, S. K. S. (2012). Functional adaptations in the forelimb muscles of non-human great apes. *Journal of Anatomy* **220**, 13–28.

208. MYATT, J. P., CROMPTON, R. H. & THORPE, S. K. S. (2011). Hindlimb muscle architecture in non-human great apes and a comparison of methods for analysing inter-species variation. *Journal of Anatomy* **219**, 150–166.

209. *NARICI, M. V., BINZONI, T., HILTBRAND, E., FASEL, J., TERRIER, F. & CERRETELLI, P. (1996). In vivo human gastrocnemius architecture with changing joint angle at rest and during graded isometric contraction. *The Journal of Physiology* **496**, 287–297.

210. *NARICI, M. V., MAGANARIS, C. N., REEVES, N. D. & CAPODAGLIO, P. (2003). Effect of aging on human muscle architecture. *Journal of Applied Physiology* **95**, 2229–2234.

211. *NELSON, F. E., GABALDÓN, A. M. & ROBERTS, T. J. (2004). Force–velocity properties of two avian hindlimb muscles. *Comparative Biochemistry and Physiology Part A: Molecular & Integrative Physiology* **137**, 711–721.

212. NOORKOIV, M., NOSAKA, K. & BLAZEVICH, A. J. (2010). Assessment of quadriceps muscle cross-sectional area by ultrasound extended-field-of-view imaging. *European Journal of Applied Physiology* **109**, 631–639.

213. NYAKATURA, J. A., BAUMGARTEN, R., BAUM, D., STARK, H. & YOULATOS, D. (2019). Muscle internal structure revealed by contrast-enhanced mu CT and fibre recognition: the hindlimb extensors of an arboreal and a fossorial squirrel. *Mammalian Biology* **99**, 71–80.

214. *NYAKATURA, J. A. & STARK, H. (2015). Aberrant back muscle function correlates with intramuscular architecture of dorsovertebral muscles in two-toed sloths. *Mammalian Biology* **80**, 114–121.

215. O'BRIEN, K. M., JOYCE, W., CROCKETT, E. L., AXELSSON, M., EGGINTON, S. & FARRELL, A. P. (2021). Resilience of cardiac performance in Antarctic notothenioid fishes in a warming climate. *Journal of Experimental Biology* **224**, jeb220129.

216. *OGIHARA, N., KUNAI, T. & NAKATSUKASA, M. (2005). Muscle dimensions in the chimpanzee hand. *Primates* **46**, 275–280.

217. *OISHI, M., OGIHARA, N., ENDO, H. & ASARI, M. (2008). Muscle architecture of the upper limb in the orangutan. *Primates* **49**, 204–209.

218. *OISHI, M., OGIHARA, N., ENDO, H., ICHIHARA, N. & ASARI, M. (2009). Dimensions of forelimb muscles in orangutans and chimpanzees. *Journal of Anatomy* **215**, 373–382.

219. *OLSON, R. A., GLENN, Z. D., CLIFFE, R. N. & BUTCHER, M. T. (2018). Architectural properties of sloth forelimb muscles (Pilosa: Bradypodidae). *Journal of Mammalian Evolution* **25**, 573–588.

220. *OLSON, R. A., WOMBLE, M. D., THOMAS, D. R., GLENN, Z. D. & BUTCHER, M. T. (2016). Functional morphology of the forelimb of the nine-banded armadillo (*Dasypus novemcinctus*): comparative perspectives on the myology of Dasypodidae. *Journal of Mammalian Evolution* **23**, 49–69.

221. O'NEILL, M. C., LEE, L. F., LARSON, S. G., DEMES, B., STERN, J. T. & UMBERGER, B. R. (2013). A three-dimensional musculoskeletal model of the chimpanzee (*Pan troglodytes*) pelvis and hind limb. *Journal of Experimental Biology* **216**, 3709–3723.

222. *OUNJIAN, M., ROY, R. R., ELDRED, E., GARFINKEL, A., PAYNE, J. R., ARMSTRONG, A., TOGA, A. W. & EDGERTON, V. R. (1991). Physiological and developmental implications of motor unit anatomy. *Journal of Neurobiology* **22**, 547–559.

223. Padilla, C. J., Harrigan, M. E., Harris, H., Schwab, J. M., Rutkove, S. B., Rich, M. M., Clark, B. C. & Arnold, W. D. (2021). Profiling age-related muscle weakness and wasting: neuromuscular junction transmission as a driver of age-related physical decline. *Geroscience* **43**, 1265–1281.

224. *Pasi, B. M. & Carrier, D. R. (2003). Functional trade-offs in the limb muscles of dogs selected for running vs. fighting. *Journal of Evolutionary Biology* **16**, 324–332.

225. Pate, E., Bhimani, M., Franksskiba, K. & Cooke, R. (1995). Reduced effect of pH on skinned rabbit psoas muscle mechanics at high-temperatures - implications for fatigue. *Journal of Physiology-London* **486**, 689–694.

226. Paxton, H., Anthony, N. B., Corr, S. A. & Hutchinson, J. R. (2010). The effects of selective breeding on the architectural properties of the pelvic limb in broiler chickens: a comparative study across modern and ancestral populations. *Journal of Anatomy* **217**, 153–166.

227. Paxton, H., Tickle, P. G., Rankin, J. W., Codd, J. R. & Hutchinson, J. R. (2014). Anatomical and biomechanical traits of broiler chickens across ontogeny. Part II. Body segment inertial properties and muscle architecture of the pelvic limb. *PeerJ* **2**, e473.

228. Payne, R. C., Crompton, R. H., Isler, K., Savage, R., Vereecke, E. E., Gunther, M. M., Thorpe, S. K. S. & D'Aout, K. (2006). Morphological analysis of the hindlimb in apes and humans. I. Muscle architecture. *Journal of Anatomy* **208**, 709–724.

229. Payne, R. C., Hutchinson, J. R., Robilliard, J. J., Smith, N. C. & Wilson, A. M. (2005a). Functional specialisation of pelvic limb anatomy in horses (*Equus caballus*). *Journal of Anatomy* **206**, 557–574.

230. *Payne, R. C., Veenman, P. & Wilson, A. M. (2005b). The role of the extrinsic thoracic limb muscles in equine locomotion. *Journal of Anatomy* **206**, 193–204.

231. Pellegrino, M. A., Canepari, M., Rossi, R., D'Antona, G., Reggiani, C. & Bottinelli, R. (2003). Orthologous myosin isoforms and scaling of shortening velocity with body size in mouse, rat, rabbit and human muscles. *Journal of Physiology-London* **546**, 677–689.

232. Perry, J. M. G., Hartstone-Rose, A. & Wall, C. E. (2011). The jaw adductors of Strepsirrhines in relation to body size, diet, and ingested food size. *Anatomical Record-Advances in Integrative Anatomy and Evolutionary Biology* **294**, 712–728.

233. *Perry, J. M., St Clair, E. M. & Hartstone-Rose, A. (2015). Craniomandibular signals of diet in adapids. *American Journal of Physical Anthropology* **158**, 646–662.

234. *Pfister, R., Schwarz, K. A., Janczyk, M., Daleand, R. & Freeman, J. B. (2013). Good things peak in pairs: a note on the bimodality coefficient. *Frontiers in Psychology* **4**, 700. https://doi.org/10.3389/fpsyg.2013.00700

235. *Pierrynowski, M. R. (1995). Human kinetics. In: *Three-Dimensional Analysis of Human Movement* (eds P. Allard, I. A. F. Stokes and J. Blanchi), pp. 215–256. Human Kinetics Publishers, Champaign.

236. Plüss, M., Schellenberg, F., Taylor, W. R. & Lorenzetti, S. (2018). Towards subject-specific strength training design through predictive use of musculoskeletal models. *Applied Bionics and Biomechanics* **2018**, 9721079.

237. *Pollock, C. M. & Shadwick, R. E. (1994). Allometry of muscle, tendon, and elastic energy storage capacity in mammals. *American Journal of Physiology-Regulatory, Integrative and Comparative Physiology* **266**, R1022–R1031.

238. *Porro, L. B., Holliday, C. M., Anapol, F., Ontiveros, L. C., Ontiveros, L. T. & Ross, C. F. (2011). Free body analysis, beam mechanics, and finite element modeling of the mandible of *Alligator mississippiensis*. *Journal of Morphology* **272**, 910–937.

239. *Powell, P. L., Roy, R. R., Kanim, P. A. U. L. A., Bello, M. A. & Edgerton, V. R. (1984). Predictability of skeletal muscle tension from architectural determinations in Guinea pig hindlimbs. *Journal of Applied Physiology* **57**, 1715–1721.

240. Qiao, M. & Jindrich, D. L. (2016). Leg joint function during walking acceleration and deceleration. *Journal of Biomechanics* **49**, 66–72.

241. Rack, P. M. & Westbury, D. R. (1969). The effects of length and stimulus rate on tension in the isometric cat soleus muscle. *Journal of Physiology* **204**, 443–460.

242. Rajagopal, A., Dembia, C. L., DeMers, M. S., Delp, D. D., Hicks, J. L. & Delp, S. L. (2016). Full-body musculoskeletal model for muscle-driven simulation of human gait. *IEEE Transactions on Biomedical Engineering* **63**, 2068–2079.

243. Randhawa, A., Jackman, M. E. & Wakeling, J. M. (2013). Muscle gearing during isotonic and isokinetic movements in the ankle plantarflexors. *European Journal of Applied Physiology* **113**, 437–447.

244. Rankin, J., Rubenson, J. & Hutchinson, J. (2016). Inferring muscle functional roles of the ostrich pelvic limb during walking and running using computer optimization. *Journal of the Royal Society Interface* **13**, 20160035.

245. Reeves, N. D. & Narici, M. V. (2003). Behavior of human muscle fascicles during shortening and lengthening contractions in vivo. *Journal of Applied Physiology* **95**, 1090–1096.

246. Richards, R. E., Andersen, M. S., Harlaar, J. & van den Noort, J. C. (2018). Relationship between knee joint contact forces and external knee joint moments in patients with medial knee osteoarthritis: effects of gait modifications. *Osteoarthritis and Cartilage* **26**, 1203–1214.

247. *Roberts, T. J., Chen, M. S. & Taylor, C. R. (1998). Energetics of bipedal running. II. Limb design and running mechanics. *Journal of Experimental Biology* **201**, 2753–2762.

248. Roberts, T. J., Marsh, R. L., Weyand, P. G. & Taylor, C. R. (1997). Muscular force in running turkeys: the economy of minimizing work. *Science* **275**, 1113–1115.

249. *Roh, M. S., Wang, V. M., April, E. W., Pollock, R. G., Bigliani, L. U. & Flatow, E. L. (2000). Anterior and posterior musculotendinous anatomy of the supraspinatus. *Journal of Shoulder and Elbow Surgery* **9**, 436–440.

250. Rojas-Martinez, M., Serna, L. Y., Jordanic, M., Marateb, H. R., Merletti, R. & Mananas, M. A. (2020). High-density surface electromyography signals during isometric contractions of elbow muscles of healthy humans. *Scientific Data* **7**, 397.

251. Rosatelli, A. L., Ravichandiran, K. & Agur, A. M. (2008). Three-dimensional study of the musculotendinous architecture of lumbar multifidus and its functional implications. *Clinical Anatomy* **21**, 539–546.

252. *Rose, J. A. (2014). *Hindlimb Morphology in Eastern Cottontail Rabbits (Sylvilagus floridanus): Correlation of Muscle Achitecture and MHC Isform Content with Ontogeny*. Youngstown State University, Youngstown, OH, pp. 81.

253. *Rose, J. A., Sandefur, M., Huskey, S., Demler, J. L. & Butcher, M. T. (2013). Muscle architecture and out-force potential of the thoracic limb in the eastern mole (*Scalopus aquaticus*). *Journal of Morphology* **274**, 1277–1287.

254. Rose, K. A., Bates, K. T., Nudds, R. L. & Codd, J. R. (2016a). Ontogeny of sex differences in the energetics and kinematics of terrestrial locomotion in leghorn chickens (*Gallus gallus domesticus*). *Scientific Reports* **6**, 24292.

255. Rose, K. A., Nudds, R. L. & Codd, J. R. (2016b). Variety, sex and ontogenetic differences in the pelvic limb muscle architectural properties of leghorn chickens (*Gallus gallus domesticus*) and their links with locomotor performance. *Journal of Anatomy* **228**, 952–964.

256. Rosin, S. & Nyakatura, J. A. (2017). Hind limb extensor muscle architecture reflects locomotor specialisations of a jumping and a striding quadrupedal caviomorph rodent. *Zoomorphology* **136**, 267–277.

257. Roy, R. R., Baldwin, K. M., Martin, T. P., Chimarusti, S. P. & Edgerton, V. R. (1985). Biochemical and physiological-changes in overloaded rat fast-twitch and slow-twitch ankle extensors. *Journal of Applied Physiology* **59**, 639–646.

258. *Roy, R. R., Bello, M. A., Powell, P. L. & Simpson, D. R. (1984a). Architectural design and fibre-type distribution of the major elbow flexors and extensors of the monkey (cynomolgus). *American Journal of Anatomy* **171**, 285–293.

259. *Roy, R. R., Bodine-Fowler, S. C., Kim, J., Haque, N., De Leon, D., Rudolph, W. & Edgerton, V. R. (1991). Architectural and fibre type distribution properties of selected rhesus leg muscles: feasibility of multiple independent biopsies. *Cells, Tissues, Organs* **140**, 350–356.

260. *Roy, R. R., Powell, P. L., Kanim, P. & Simpson, D. R. (1984b). Architectural and histochemical analysis of the semitendinousus muscle in mice, rats, Guinea pigs, and rabbits. *Journal of Morphology* **181**, 155–160.

261. *Roy, R. R., Sacks, R. D., Baldwin, K. M., Short, M. & Edgerton, V. R. (1984c). Interrelationships of contraction time, Vmax, and myosin ATPase after spinal transection. *Journal of Applied Physiology* **56**, 1594–1601.

262. Rubenson, J., Lloyd, D. G., Heliams, D. B., Besier, T. F. & Fournier, P. A. (2011). Adaptations for economical bipedal running: the effect of limb structure on three-dimensional joint mechanics. *Journal of the Royal Society Interface* **8**, 740–755.

263. *Rupert, J. E., Rose, J. A., Organ, J. M. & Butcher, M. T. (2015). Forelimb muscle architecture and myosin isoform composition in the groundhog (*Marmota monax*). *Journal of Experimental Biology* **218**, 194–205.

264. *Ryan, J. M., Cobb, M. A. & Hermanson, J. W. (1992). Elbow extensor muscles of the horse: postural and dynamic implications. *Cells, Tissues, Organs* **144**, 71–79.

265. Sacks, R. D. & Roy, R. R. (1982). Architecture of the hind limb muscles of cats: functional significance. *Journal of Morphology* **173**, 185–195.

266. Santana, S. E. (2018). Comparative anatomy of bat jaw musculature via diffusible iodine-based contrast-enhanced computed tomography. *Anatomical Record-Advances in Integrative Anatomy and Evolutionary Biology* **301**, 267–278.

267. Santana, S. E., Dumont, E. R. & Davis, J. L. (2010). Mechanics of bite force production and its relationship to diet in bats. *Functional Ecology* **24**, 776–784.

268. Schache, A. G., Dorn, T. W., Blanch, P. D., Brown, N. A. & Pandy, M. G. (2012). Mechanics of the human hamstring muscles during sprinting. *Medicine & Science in Sports & Exercise* **44**, 647–658.

269. Schenk, P., Siebert, T., Hiepe, P., Gullmar, D., Reichenbach, J. R., Wick, C., Blickhan, R. & Bol, M. (2013). Determination of three-

dimensional muscle architectures: validation of the DTI-based fiber tractography method by manual digitization. *Journal of Anatomy* **223**, 61–68.

270. *Scott, S. H., Engstrom, C. M. & Loeb, G. E. (1993). Morphometry of human thigh muscles. Determination of fascicle architecture by magnetic resonance imaging. *Journal of Anatomy* **182**, 249–257.

271. *Selbie, W. S., Thomson, D. B. & Richmond, F. J. R. (1993). Suboccipital muscles in the cat neck: morphometry and histochemistry of the rectus capitis muscle complex. *Journal of Morphology* **216**, 47–63.

272. Sellers, W. I., Cain, G. M., Wang, W. J. & Crompton, R. H. (2005). Stride lengths, speed and energy costs in walking of *Australopithecus afarensis*: using evolutionary robotics to predict locomotion of early human ancestors. *Journal of the Royal Society Interface* **2**, 431–441.

273. Sellers, W. I., Manning, P. L., Lyson, T., Stevens, K. & Margetts, L. (2009). Virtual palaeontology: gait reconstruction of extinct vertebrates using high performance computing. *Palaeontologia Electronica* **12**, 3.

274. Sellers, W. I., Margetts, L., Coria, R. A. & Manning, P. L. (2013). March of the titans: the locomotor capabilities of sauropod dinosaurs. *PLoS One* **8**, e78733.

275. Seth, A., Hicks, J. L., Uchida, T. K., Habib, A., Dembia, C. L., Dunne, J. J., Ong, C. F., DeMers, M. S., Rajagopal, A., Millard, M., Hamner, S. R., Arnold, E. M., Yong, J. R., Lakshmikanth, S. K., Sherman, M. A., et al. (2018). OpenSim: simulating musculoskeletal dynamics and neuromuscular control to study human and animal movement. *PLoS Computational Biology* **14**, e1006223.

276. Seymour, J. M., Ward, K., Sidhu, P. S., Puthucheary, Z., Steier, J., Jolley, C. J., Rafferty, G., Polkey, M. I. & Moxham, J. (2009). Ultrasound measurement of rectus femoris cross-sectional area and the relationship with quadriceps strength in COPD. *Thorax* **64**, 418–423.

277. *Shahar, R. & Milgram, J. (2001). Morphometric and anatomic study of the hind limb of a dog. *American Journal of Veterinary Research* **62**, 928–933.

278. *Shahar, R. & Milgram, J. (2005). Morphometric and anatomic study of the forelimb of the dog. *Journal of Morphology* **263**, 107–117.

279. *Sharir, A., Milgram, J. & Shahar, R. (2006). Structural and functional anatomy of the neck musculature of the dog (*Canis familiaris*). *Journal of Anatomy* **208**, 331–351.

280. Sharples, S. A. & Miles, G. B. (2021). Maturation of persistent and hyperpolarization-activated inward currents shapes the differential activation of motoneuron subtypes during postnatal development. *Elife* **10**, e71385.

281. Sieben, J. M., van Otten, I., Lataster, A., Froeling, M., Nederveen, A. J., Strijkers, G. J. & Drost, M. R. (2016). In vivo reconstruction of lumbar erector spinae architecture using diffusion tensor MRI. *Clinical Spine Surgery* **29**, E139–E145.

282. *Siebert, T., Leichsenring, K., Rode, C., Wick, C., Stutzig, N., Schubert, H., Blickhan, R. & Böl, M. (2015). Three-dimensional muscle architecture and comprehensive dynamic properties of rabbit gastrocnemius, plantaris and soleus: input for simulation studies. *PLoS One* **10**, e0130985.

283. *Sinclair, A. G. & Alexander, R. M. (1987). Estimated forces exerted by the jaw muscles of some reptiles. *Journal of Zoology* **213**, 107–115.

284. Smith, N. C., Wilson, A. M., Jespers, K. J. & Payne, R. C. (2006). Muscle architecture and functional anatomy of the pelvic limb of the ostrich (*Struthio camelus*). *Journal of Anatomy* **209**, 765–779.

285. *Sopher, R. S., Amis, A. A., Davies, D. C. & Jeffers, J. R. (2017). The influence of muscle pennation angle and cross-sectional area on contact forces in the ankle joint. *The Journal of Strain Analysis for Engineering Design* **52**, 12–23.

286. *Spector, S. A., Gardiner, P. F., Zernicke, R. F., Roy, R. R. & Edgerton, V. R. (1980). Muscle architecture and force-velocity characteristics of cat soleus and medial gastrocnemius: implications for motor control. *Journal of Neurophysiology* **44**, 951–960.

287. Stark, H., Fischer, M. S., Hunt, A., Young, F., Quinn, R. & Andrada, E. (2021). A three-dimensional musculoskeletal model of the dog. *Scientific Reports* **11**, 11335.

288. *Stark, H., Fröber, R. & Schilling, N. (2013). Intramuscular architecture of the autochthonous back muscles in humans. *Journal of Anatomy* **222**, 214–222.

289. Steele, K. M., Seth, A., Hicks, J. L., Schwartz, M. S. & Delp, S. L. (2010). Muscle contributions to support and progression during single-limb stance in crouch gait. *Journal of Biomechanics* **43**, 2099–2105.

290. Steele, K. M., van der Krogt, M. M., Schwartz, M. H. & Delp, S. L. (2012). How much muscle strength is required to walk in a crouch gait? *Journal of Biomechanics* **45**, 2564–2569.

291. Strait, D. S., Grosse, I. R., Dechow, P. C., Smith, A. L., Wang, Q., Weber, G. W., Neubauer, S., Slice, D. E., Chalk, J., Richmond, B. G., Lucas, P. W., Spencer, M. A., Schrein, C., Wright, B. W., Byfton, C., et al. (2010). The structural rigidity of the cranium of Australopithecus africanus: implications for diet, dietary adaptations, and the allometry of feeding biomechanics. *Anatomical Record-Advances in Integrative Anatomy and Evolutionary Biology* **293**, 583–593.

292. Strait, D. S., Weber, G. W., Neubauer, S., Chalk, J., Richmond, B. G., Lucas, P. W., Spencer, M. A., Schrein, C., Dechow, P. C., Ross, C. F., Grosse, I. R., Wright, B. W., Constantino, P., Wood, B. A., Lawn, B., et al. (2009). The feeding biomechanics and dietary ecology of *Australopithecus africanus*. *Proceedings of the National Academy of Sciences of the United States of America* **106**, 2124–2129.

293. Sullivan, S. P., McGechie, F. R., Middleton, K. M. & Holliday, C. M. (2019). 3D muscle architecture of the pectoral muscles of European starling (*Sturnus vulgaris*). *Integrative Organismal Biology* **1**, oby010.

294. *Sustaita, D. (2008). Musculoskeletal underpinnings to differences in killing behavior between North American accipiters (Falconiformes: Accipitridae) and falcons (Falconidae). *Journal of Morphology* **269**, 283–301.

295. *Tallis, J., James, R. S., Little, A. G., Cox, V. M., Duncan, M. J. & Seebacher, F. (2014). Early effects of ageing on the mechanical performance of isolated locomotory (EDL) and respiratory (diaphragm) skeletal muscle using the work-loop technique. *American Journal of Physiology-Regulatory, Integrative and Comparative Physiology* **307**, R670–R684.

296. Talmadge, R. J., Roy, R. R., Caiozzo, V. J. & Edgerton, V. R. (2002). Mechanical properties of rat soleus after long-term spinal cord transection. *Journal of Applied Physiology* **93**, 1487–1497.

297. Taverne, M., Fabre, A. C., Herbin, M., Herrel, A., Peigne, S., Lacroux, C., Lowie, A., Pages, F., Theil, J. C. & Bohmer, C. (2018). Convergence in the functional properties of forelimb muscles in carnivorans: adaptations to an arboreal lifestyle? *Biological Journal of the Linnean Society* **125**, 250–263.

298. Taylor, A. B., Eng, C. M., Anapol, F. C. & Vinyard, C. J. (2009). The functional correlates of jaw-muscle fiber architecture in tree-gouging and nongouging callitrichid monkeys. *American Journal of Physical Anthropology* **139**, 353–367.

299. *Taylor, A. B. & Vinyard, C. J. (2004). Comparative analysis of masseter fibre architecture in tree-gouging (*Callithrix jacchus*) and nongouging (*Saguinus oedipus*) callitrichids. *Journal of Morphology* **261**, 276–285.

300. Taylor, A. B., Vinyard, C. J. & Payseur, B. A. (2008). Variation in masseter muscle fiber architecture in five strains of inbred mice: implications for heritability of fiber architecture. *American Journal of Physical Anthropology Supplement* **46**, 204–205.

301. *Ter Keurs, H. E. D. J., Luff, A. R. & Luff, S. E. (1984). Force–sarcomere-length relation and filament length in rat extensor digitorum muscle. In: *Contractile Mechanisms in Muscle*, pp. 511–525. Springer, Boston.

302. *Thorpe, S. K., Crompton, R. H., Guenther, M. M., Ker, R. F. & Alexander, R. M. (1999). Dimensions and moment arms of the hind-and forelimb muscles of common chimpanzees (*Pan troglodytes*). *American Journal of Physical Anthropology* **110**, 179–199.

303. *Tickle, P. G., Paxton, H., Rankin, J. W., Hutchinson, J. R. & Codd, J. R. (2014). Anatomical and biomechanical traits of broiler chickens across ontogeny. Part I. Anatomy of the musculoskeletal respiratory apparatus and changes in organ size. *PeerJ* **2**, e432.

304. Valente, G., Crimi, G., Vanella, N., Schileo, E. & Taddei, F. (2017). nmsBuilder: freeware to create subject-specific musculoskeletal models for OpenSim. *Computer Methods and Programs in Biomedicine* **152**, 85–92.

305. *Van Daele, P. A. A. G., Herrel, A. & Adriaens, D. (2009). Biting performance in teeth-digging African mole-rats (Fukomys, Bathyergidae, Rodentia). *Physiological and Biochemical Zoology* **82**, 40–50.

306. *Van Der Meij, M. A. A. & Bout, R. G. (2004). Scaling of jaw muscle size and maximal bite force in finches. *Journal of Experimental Biology* **207**, 2745–2753.

307. *Van Eijden, T. M. G. J., Koolstra, J. H. & Brugman, P. (1995). Architecture of the human pterygoid muscles. *Journal of Dental Research* **74**, 1489–1495.

308. *Van Eijden, T. M. G. J., Koolstra, J. H. & Brugman, P. (1996). Three-dimensional structure of the human temporalis muscle. *The Anatomical Record* **246**, 565–572.

309. *Van Eijden, T. M. G. J., Korfage, J. A. M. & Brugman, P. (1997). Architecture of the human jaw-closing and jaw-opening muscles. *The Anatomical Record* **248**, 464–474.

310. *Van Eijden, T. M. G. J. & Raadsheer, M. C. (1992). Heterogeneity of fibre and sarcomere length in the human masseter muscle. *The Anatomical Record* **232**, 78–84.

311. Vickerton, P., Jarvis, J. & Jeffery, N. (2013). Concentration-dependent specimen shrinkage in iodine-enhanced microCT. *Journal of Anatomy* **223**, 185–193.

312. Vigotsky, A. D., Rouse, E. J. & Lee, S. S. M. (2020). Mapping the relationships between joint stiffness, modeled muscle stiffness, and shear wave velocity. *Journal of Applied Physiology* **129**, 483–491.

313. Vinyard, C. J. & Payseur, B. A. (2008). Of "mice" and mammals: utilizing classical inbred mice to study the genetic architecture of function and performance in mammals. *Integrative and Comparative Biology* **48**, 324–337.

314. *Walmsley, B. & Proske, U. (1981). Comparison of stiffness of soleus and medial gastrocnemius muscles in cats. *Journal of Neurophysiology* **46**, 250–259.

315. Ward, S. R., Eng, C. M., Smallwood, L. H. & Lieber, R. L. (2009). Are current measurements of lower extremity muscle architecture accurate? *Clinical Orthopaedics and Related Research* **467**, 1074–1082.

316. Wareing, K., Tickle, P. G., Stokkan, K. A., Codd, J. R. & Sellers, W. I. (2011). The musculoskeletal anatomy of the reindeer (*Rangifer tarandus*): fore- and hindlimb. *Polar Biology* **34**, 1571–1578.

317. *Watson, J. C. & Wilson, A. M. (2007). Muscle architecture of biceps brachii, triceps brachii and supraspinatus in the horse. *Journal of Anatomy* **210**, 32–40.

318. Watson, P. J., Groning, F., Curtis, N., Fitton, L. C., Herrel, A., McCormack, S. W. & Fagan, M. J. (2014). Masticatory biomechanics in the rabbit: a multi-body dynamics analysis. *Journal of the Royal Society Interface* **11**, 20140564.

319. Webster, E. L., Hudson, P. E. & Channon, S. B. (2014). Comparative functional anatomy of the epaxial musculature of dogs (*Canis familiaris*) bred for sprinting vs. fighting. *Journal of Anatomy* **225**, 317–327.

320. *Weijs, W. A., Brugman, P. & Klok, E. M. (1987). The growth of the skull and jaw muscles and its functional consequences in the New Zealand rabbit (*Oryctolagus cuniculus*). *Journal of Morphology* **194**, 143–161.

321. *Weijs, W. A. & Dantuma, R. (1981). Functional anatomy of the masticatory apparatus in the rabbit (*Oryctolagus cuniculus* L.). *Netherlands Journal of Zoology* **31**, 99–147.

322. *Weijs, W. A. & Hillen, B. (1984). Relationship between the physiological cross-section of the human jaw muscles and their cross-sectional area in computer tomograms. *Cells, Tissues, Organs* **118**, 129–138.

323. Wickiewicz, T. L., Roy, R. R., Powell, P. L. & Edgerton, V. R. (1983). Muscle architecture of the human lower limb. *Clinical Orthopaedics and Related Research* **179**, 275–283.

324. Wickiewicz, T. L., Roy, R. R., Powell, P. L., Perrine, J. J. & Edgerton, V. R. (1984). Muscle architecture and force-velocity relationships in humans. *Journal of Applied Physiology: Respiratory, Environmental and Exercise Physiology* **57**, 435–443.

325. Wilkinson, D. J., Piasecki, M. & Atherton, P. J. (2018). The age-related loss of skeletal muscle mass and function: measurement and physiology of muscle fibre atrophy and muscle fibre loss in humans. *Ageing Research Reviews* **47**, 123–132.

326. *Williams, P. E. & Goldspink, G. (1971). Longitudinal growth of striated muscle fibres. *Journal of Cell Science* **9**, 751–767.

327. Williams, S. B., Payne, R. C. & Wilson, A. M. (2007a). Functional specialisation of the pelvic limb of the hare (*Lepus europeus*). *Journal of Anatomy* **210**, 472–490.

328. Williams, S. B., Wilson, A. M., Daynes, J., Peckham, K. & Payne, R. C. (2008a). Functional anatomy and muscle moment arms of the thoracic limb of an elite sprinting athlete: the racing greyhound (*Canis familiaris*). *Journal of Anatomy* **213**, 373–382.

329. *Williams, S. B., Wilson, A. M. & Payne, R. C. (2007b). Functional specialisation of the thoracic limb of the hare (*Lepus europeus*). *Journal of Anatomy* **210**, 491–505.

330. Williams, S. B., Wilson, A. M., Rhodes, L., Andrews, J. & Payne, R. C. (2008b). Functional anatomy and muscle moment arms of the pelvic limb of an elite sprinting athlete: the racing greyhound (*Canis familiaris*). *Journal of Anatomy* **213**, 361–372.

331. Witmer, L. M. (1995). The extant phylogenetic bracket and the importance of reconstructing soft tissues in fossils. In: *Functional Morphology in Vertebrate Paleontology*. Cambridge University Press, Cambridge.

332. Woittiez, R. D., Heerkens, Y. F., Huijing, P. A., Rijnsburger, W. H. & Rozendal, R. H. (1986). Functional-morphology of the m-gastrocnemius medialis of the rat during growth. *Journal of Morphology* **187**, 247–258.

333. *Woittiez, R. D., Huijing, P. A., Boom, H. B. K. & Rozendal, R. H. (1984). A three-dimensional muscle model: a quantified relation between form and function of skeletal muscles. *Journal of Morphology* **182**, 95–113.

334. *Yang, Y., Wang, H. & Zhang, Z. (2015). Muscle architecture of the forelimb of the Golden Pheasant (*Chrysolophus pictus*)(Aves: Phasianidae) and its implications for functional capacity in flight. *Avian Research* **6**, 3. https://doi.org/10.1186/s40657-015-0013-2

335. *Yeh, F. C., Verstynen, T. D., Wang, Y., Fernandez-Miranda, J. C. & Tseng, W. Y. (2013). Deterministic diffusion fiber tracking improved by quantitative anisotropy. *PLoS One* **8**, e80713.

336. Young, R. P., Scott, S. H. & Loeb, G. E. (1993). The distal hindlimb musculature of the cat: multiaxis moment arms at the ankle joint. *Experimental Brain Research* **96**, 141–151.

337. *Zaaf, A., Herrel, A., Aerts, P. & De Vree, F. (1999). Morphology and morphometrics of the appendicular musculature in geckoes with different locomotor habits (Lepidosauria). *Zoomorphology* **119**, 9–22.

338. Zajac, F. E. (1989). Muscle and tendon: properties, models, scaling, and application to biomechanics and motor control. *Critical Reviews in Biomedical Engineering* **17**, 359–411.

339. *Zuurbier, C. J. & Huijing, P. A. (1992). Influence of muscle geometry on shortening speed of fibre, aponeurosis and muscle. *Journal of Biomechanics* **25**, 1017–1026.

## VII. Supporting information

Additional supporting information may be found online in the Supporting Information section at the end of the article.

**Appendix S1.** Additional information on methods.
**Table S1.** Details of the methods used in studies measuring vertebrate muscle architecture, specifically detailing the number of muscle fibres measured to obtain muscle fibre length.
**Table S2.** Study participant information.
**Tables S3–S12.** Fibre architecture and distributions of the individual study subjects.
**Table S13.** Mean and median fibre length ($L_f$) and physiological cross-sectional area (PCSA) values averaged across all 10 subjects.
**Table S14.** All-subject averages in absolute and percentage differences in fibre length and physiological cross-sectional area (PCSA) between the mean and median values of the full sample of fibres and the maximum and minimum possible mean and median values from random subsamples of 5 fibres.
**Tables S15–S24.** The percentage of randomly generated mean fibre length values in subsamples of 5, 10, 50, 100, 250, 500, 1000 and 2000 fibres falling in each 'accuracy bin' relative to the mean value from the full sample of >3000 fibres in 25 lower limb muscles from the individual study subjects.
**Table S25.** All-subject averaged percentages of randomly generated mean fibre length values in subsample of 5, 10, 50, 100, 250, 500, 1000 and 2000 fibres falling in each 'accuracy bin' relative to the mean value from the full sample of >3000 fibres in 25 lower limb muscles, and these values averaged across all muscles for all subjects.
**Table S26.** Root mean squared errors (RMSEs) of fibre lengths and forces as predicted by musculoskeletal models containing mean (Model$^{mean}$) fibre lengths as well as maximum (Model$^{max5}$) and minimum (Model$^{min5}$) possible fibre lengths from samples of 5 fibres relative to a model containing median fibre lengths (Model$^{median}$) during walking and vertical jumping.
**Table S27.** Variations in possible estimates of optimal fibre length possible from using different sarcomere length values from various literature sources.